Travail de fin d'études

Auteur : Ndayizeye, Tony
Promoteur(s) : Demonceau, Jean-François
Faculté : Faculté des Sciences appliquées
Diplôme : Master en ingénieur civil des constructions, à finalité spécialisée en "civil engineering"
Année académique : 2024-2025
URI/URL : http://hdl.handle.net/2268.2/23190

UNIVERSITY OF LIÈGE
FACULTY OF APPLIED SCIENCES

Innovative Bolted Joint Solutions for Demountable Modular Structures

Graduation Studies conducted for obtaining the Master's degree in
Civil Engineering

by

Tony Robert Ndayizeye

MEMBERS OF THE JURY

Jean-François Demonceau
Tudor Golea
Boyan Mihaylov
Tung Nguyen

SUPERVISOR

Jean-François Demonceau

Academic year 2024-2025

Contents

Abstract

Understanding the mechanical behaviour of metallic connections within structural frameworks is essential for ensuring overall stability and safety. These connections often govern the global response of the system under various loading conditions. Accurate characterization enables reliable predictions of structural performance, particularly in seismic or high-stress environments. Without such analysis, design assumptions may lead to unsafe or overly conservative constructions. Therefore, studying joint behaviour plays a critical role in optimizing structural efficiency and integrity.

This research focuses on a roof assembly that connects structural elements not commonly encountered in conventional design, thus requiring a tailored scientific approach. The analysis is grounded in Eurocode principles, ensuring regulatory compliance and structural safety. Emphasis is placed on the component method, enabling a detailed evaluation of individual component behaviours. Given the atypical configuration, specific adaptations of standard design procedures are proposed. The objective is to develop a robust analytical framework that bridges theoretical rigour and practical applicability.

The adopted methodology involves performing a preliminary design of the assembly in order to approach a specific target. This initial step serves as a foundation for a subsequent optimization phase. The optimized assembly is then integrated into a finite element model that encompasses the entire global structure. This approach enables iterative refinement to balance performance and design constraints. It also ensures compatibility within the overall structural system.

The main findings of this research demonstrate that, given the specific configuration of a modular construction, there exists a range of assembly classes, in terms of stiffness and strength, that are preferable to adopt. This work provides an analytical approach for an in-depth study on the characterization of a joint in a modular structure, as well as its impact on the global structural response.

Acknowledgements

I would like to express my sincere and heartfelt gratitude to my research supervisor, Prof. Jean-François Demonceau, for granting me the invaluable opportunity to conduct this study under his expert guidance. The successful completion of this work would not have been possible without his unwavering support, insightful advice, and constructive feedback throughout the entire research process.

I would like to emphasize the remarkable assistance provided by Mr. Tudor Golea, my supervisor's assistant, throughout the course of this work. His corrections and insightful comments have been invaluable to the development of this project.

I would also like to express my sincere gratitude to Dr. Loris Saufnay for his considerable contributions, which were instrumental in the optimization of the project.

Finally, I extend my heartfelt thanks to my family for their unconditional support, and in particular, to my parents, who gave me the opportunity to pursue my education.

Chapter 1 — Introduction

1.1 Context

In collaboration with companies such as DEGOTTE, GDTech, and CRM, the University of Liège is engaged in a sustainable development project led by the Service Public Wallon (SPW), focusing on modular construction.

DEGOTTE S.A., founded in 1987, is the leader of this project. This privately owned construction company is based within the province of Liège, Belgium. The firm has established itself as a specialist in the design, manufacture, and installation of prefabricated modular buildings for both temporary and permanent applications. Sustainability is central to DEGOTTE's operations, with a strong emphasis on environmental responsibility and circular economy principles. The company actively promotes efficient material use and waste reduction practices throughout its projects. Therefore, based on its extensive experience in manufacturing and on-site installation, DEGOTTE is responsible for selecting the most suitable materials and for designing and drafting the assembly systems.

The University of Liège is responsible for the development and validation of design procedures in alignment with the design philosophy outlined in the Eurocodes. Due to the innovative nature of these solutions, often falling outside the scope of conventional calculation methods prescribed by the Eurocodes, the development process will involve the formulation of tailored computational approaches. These approaches will be grounded in a detailed understanding of the underlying physical phenomena associated with the new designs.

1.2 Objectives

The objective of this master's thesis is to design and characterize an innovative beam to column joint for the modules developed by the company DEGOTTE. This study focuses exclusively on the roof assembly. In addition, the research investigates the impact of this assembly on the overall behaviour of the structure, with the aim of optimizing its performance.

The structural elements, such as beams, columns, and bracing, are predefined in terms of their geometry and mechanical properties. Therefore, the optimization will be focused solely

on the assembly. It is important to emphasize that this thesis is conducted simultaneously with modifications being made to the structure itself. However, the assembly configurations serve as a starting point for identifying certain design challenges. More importantly, this thesis provides a detailed calculation sheet for the studied configurations, which will aid in their future adaptation.

1.3 Thesis Outline

The structure of this Master's thesis is organized into four chapters.

First, Chapter 1 serves as an introduction, outlining the objectives of this research and the key parties involved.

Next, Chapter 2 provides a detailed overview of the fundamental concepts related to metallic assemblies, which are often poorly understood. In this chapter, the reader will find a series of definitions and concepts based on Eurocode 3, which serves as the regulatory framework for the design of steel joints.

Chapter 3 addresses the design and sizing of three different joint configurations. This chapter includes the full calculation note for the design of the first assembly configuration. The two remaining configurations are briefly discussed, with their results presented, while the complete calculation notes for these configurations can be found in Annexes A and B. This approach is justified by the repetitive nature of the sizing process, despite certain variations in specific aspects. It is therefore recommended to refer to the annexes for a more comprehensive understanding of the results summarized in this chapter.

Chapter 4 focuses on the optimization of one of the three assembly configurations. The optimization process is conducted using the FineLg finite element software, where the selected assembly is analyzed within the frame of modular structures. By the end of this chapter, the optimized assembly configuration suitable for the structure will be clearly identified.

Finally, the conclusion serves to summarize the findings of the research, while also offering suggestions for potential improvements.

Chapter 2 — Fundamental Concepts

This chapter aims to revisit and clarify the theoretical foundations underpinning the analytical procedures involved in applying the component method and joint characterisation.

To begin, the key mechanical properties that characterize the stiffness and strength of structural connections are introduced with a concise overview, establishing a basis for the subsequent discussion. Following this, the chapter details the principles and steps of the component method, a widely recognized approach in structural engineering for evaluating the behaviour of a joint. This method breaks down complex connections into simpler, idealized components, facilitating a more precise and modular analysis of joint behaviour.

2.1 Steel Joints

Traditionally, the design process of steel building structures follows a sequence of well-established stages:

- Modelling of the structural frame, assuming either rigid or pinned joints[1];
- Preliminary sizing of beams and columns;
- Determination of internal forces and moments for each load combination under ultimate limit state (ULS) and serviceability limit state (SLS) conditions;
- Verification of compliance with ULS and SLS design criteria;
- Iterative adjustment of member sizes until all design checks are met;
- Design of joints capable of withstanding either the computed member-end forces or the maximum forces transferable by the connected members.

Hence, the design process is conducted in alignment with the initial assumptions regarding joint stiffness adopted during the modelling phase. One key benefit of this approach lies in the separation of responsibilities: joint design is addressed independently from member design. In fact, until fairly recently, and in some instances still today, connection calculations are frequently assigned to other engineers or subcontracted to specialised firms.

[1] Rigid and pinned joints are defined in Section 2.2.

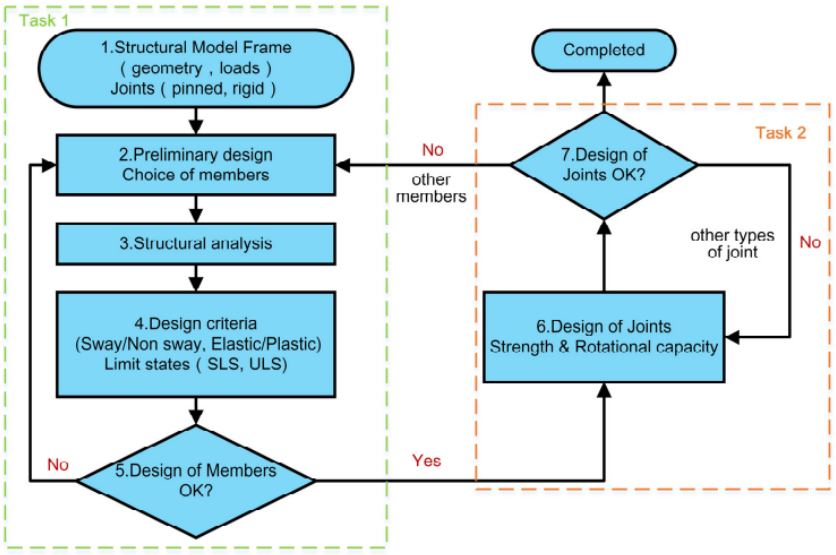

Figure 2.1: Traditional design flowchart for steel frames (Tulong Yin, 2022)

It is widely acknowledged that the behaviour of most structural joints falls between the two extremes of ideal pinned and rigid connections. In response to this reality, EN 1993-1-8 introduces provisions for a semi-rigid modelling approach, which enables the incorporation of joint flexibility into structural analysis and design. This refined consideration of joint behaviour can contribute to more accurate predictions of structural performance and, ultimately, to more economical and efficient design solutions.

By the end of this work, the semi-rigid design methodology is identified as the most suitable option regarding the conception of modular structure.

2.2 Classification of Steel Joints

Before examining the joint behaviour, it is essential to clarify the distinction between two terms that often lead to confusion: *connection* and *joint*. A *connection* refers to the set of physical components that serve to mechanically secure the connected elements. This term typically relates to the specific location where the fastening occurs, such as at the interface between a beam and column in a major axis beam-to-column connection. In contrast, when both the connection and the corresponding interaction zone between the connected members are considered as a whole, the term *joint* is employed.

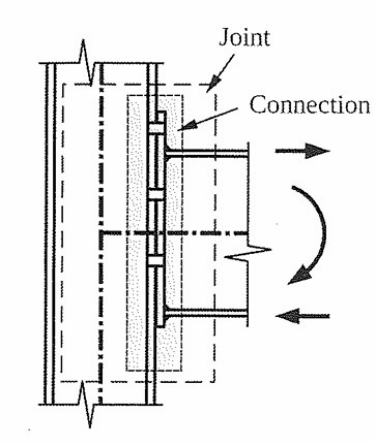

Figure 2.2: Typical double sided beam-to-column joint (Jaspart and Weynand, 2016)

The mechanical behaviour of joints significantly influences the global response of structural frames. Consequently, joints must be explicitly represented in structural analysis and design, in the same way as other structural components. According to *NBN EN 1993-1-8:2024*, joint modelling is typically categorized based on two main criteria:

- *By moment resistance:* rigid, semi-rigid, and pinned;
- *By rotational stiffness:* full-strength, partial-strength, and pinned.

From a theoretical standpoint, the term *rigid* implies that no relative rotation occurs between connected members under any applied moment, whereas *pinned* denotes an idealized frictionless hinge allowing free rotation. In practice, however, the standard permits a range of stiffness values within which a joint may be classified as either *rigid* (Zone 1) or *pinned* (Zone 2), as illustrated in Figure 2.3. Joints that fall between these two extremes are considered *semi-rigid* (Zone 3).

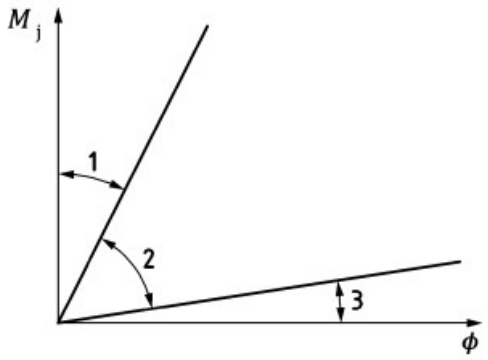

Figure 2.3: Classification of joints other than column bases by rotational stiffness

The stiffness-based classification defined in *NBN EN 1993-1-8:2024* specifies that a joint may be regarded as *rigid* if its initial rotational stiffness $S_{j,ini}$ satisfies the following conditions:

- $S_{j,ini} \geq 8EI_b/L_b$ for frames equipped with a bracing system that reduces lateral displacement by at least 80%;

- $S_{j,ini} \geq 25EI_b/L_b$ for unbraced frames or those without effective lateral restraint.

Conversely, a joint is considered *pinned* if its initial rotational stiffness is less than half the flexural stiffness of the connected beam, i.e., $S_{j,ini} \leq 0.5EI_b/L_b$.

Joints falling within the intermediate range — that is, satisfying $0.5EI_b/L_b \leq S_{j,ini} \leq 8EI_b/L_b$ for braced frames and $0.5EI_b/L_b \leq S_{j,ini} \leq 25EI_b/L_b$ for unbraced ones — are classified as *semi-rigid*.

Strength-based classification is determined by comparing the design moment resistance of the joint, $M_{j,Rd}$, to that of the adjoining members. A joint is deemed *full-strength* if its design moment resistance is at least equal to that of the connected members. In contrast, a joint is considered nominally *pinned* if $M_{j,Rd}$ does not exceed 25% of the moment resistance required for a *full-strength* joint. Once again, joints that fall within the intermediate range are classified as *partial-strength* joints.

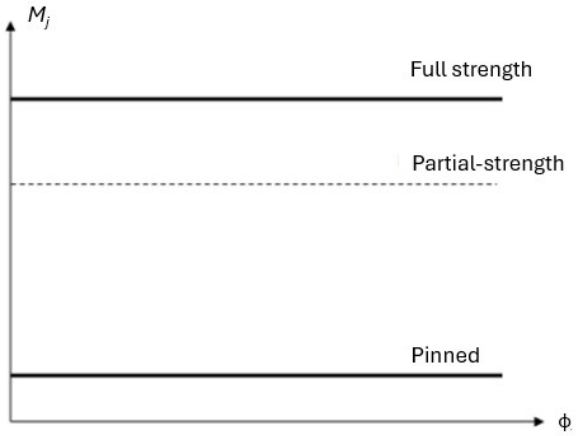

Figure 2.4: Classification of joints by strength

To facilitate practical design and analysis, Eurocode 3 introduces a classification system encompassing three idealized joint models, as outlined in Table 2.1. These models provide a simplified representation of joint behaviour based on their ability to transmit rotational effects between connected members. The classifications are defined as follows:

- *Continuous:* the joint provides full rotational continuity, effectively allowing moment transfer as if the members were monolithically connected;
- *Semi-continuous:* the joint offers limited rotational continuity, permitting partial moment transfer between members;
- *Simple:* the joint offers no rotational continuity, behaving as a hinge and transmitting only axial and shear forces.

STIFFNESS	**RESISTANCE**		
	Full-strength	**Partial-strength**	**Pinned**
Rigid	Continuous	Semicontinuous	*
Semi-rigid	Semicontinuous	Semicontinuous	*
Pinned	*	*	Simple
** : Without meaning*			

Table 2.1: Classification of joint modelling according to stiffness and resistance

The interpretation of the terms related to joint behaviour is inherently linked to the type of structural analysis being undertaken. For example, in an elastic global frame analysis, the modelling of joints primarily relies on their stiffness characteristics. Conversely, in a rigid-plastic analysis, the focus shifts toward the joint's resistance capacity. In analyses that do not fall strictly within these two categories, both stiffness and resistance properties must be considered simultaneously, as they collectively influence the appropriate modelling approach for the joints.

The inherently non-linear behaviour of an isolated flexural spring, which characterizes the realistic response of a structural joint, poses challenges for routine design applications. To facilitate practical analysis and design, the moment-rotation (M-ϕ) response is often simplified through idealization, typically without substantial compromise in accuracy.

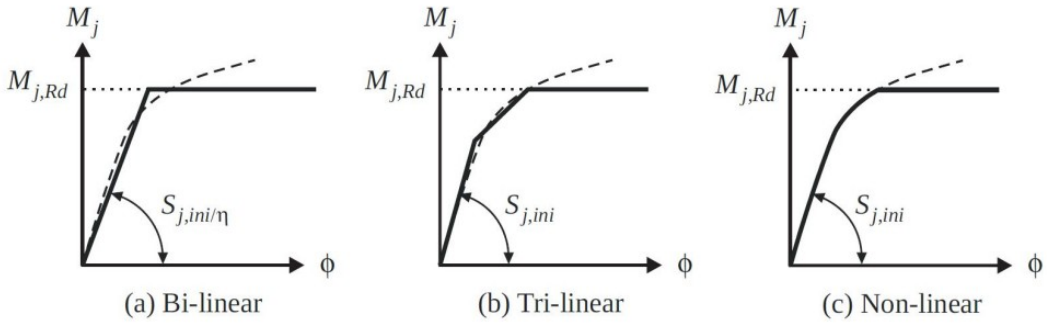

Figure 2.5: Non-linear representations of a $M - \phi$ curve (Jaspart and Weynand, 2016)

In a global structure modelling, the value of the constant stiffness $S_{j,ini}$ depends on the type of frame analysis which is contemplated [2]. Eurocode 3 outlines three distinct idealisation approaches to accommodate the various structural analysis methods commonly used in design practice. These include:

- *Elastic idealisation*, for an elastic analysis;
- *Rigid-plastic idealisation*, for a rigid-plastic analysis;
- *Non-linear idealisation* used for elastic–plastic analysis, with possible idealisations illustrated in Figure 2.5.

[2]The types of frame analysis considered in this work are discussed in Chapter 4.

For moment-resisting joints, the moment–rotation (M–ϕ) relationship typically exhibits a bi-linear behaviour. The initial stiffness, denoted as $S_{j,\mathrm{ini}}$, represents the joint's elastic response. Beyond this phase, yielding begins progressively in one or more joint components, leading up to the design moment resistance, $M_{j,\mathrm{Rd}}$. When a structural frame undergoes loading, the formation of plastic hinges and the consequent redistribution of internal forces necessitate that the affected joints possess sufficient rotational capacity. In essence, ductility is a critical requirement to enable this force redistribution.

Based on the joint's rotational capacity and moment resistance characteristics, three ductility classes are defined:

- *Class 1 joints:* These joints can achieve $M_{j,\mathrm{Rd}}$ through full plastic redistribution of internal forces and exhibit ample rotational capacity. As a result, plastic analysis and design of the frame can be conducted without special limitations.
- *Class 2 joints:* While these joints also reach $M_{j,\mathrm{Rd}}$ via complete plastic redistribution, their rotation capacity is more restricted. In such cases, an elastic frame analysis is typically required, possibly supplemented by a plastic verification of the joints. A plastic frame analysis remains permissible, provided that the demanded rotational capacity does not exceed what the joints can actually offer. Therefore, the available and required rotations must be compared to ensure the validity of the analysis.
- *Class 3 joints:* These joints experience brittle failure or instability before full moment redistribution can occur, thereby limiting their moment resistance. An elastic verification of such joints is mandatory unless it can be demonstrated that no plastic hinge will develop at their location.

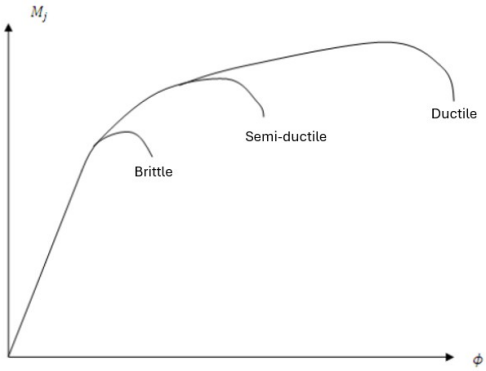

Figure 2.6: Joint classification based on ductility

In this master thesis, a bilinear moment–rotation relationship, similar to the one illustrated in Figure 2.5.a, is adopted to represent the joint behaviour. In this idealization, the moment at which yielding initiates, denoted $M_{j,Rd}$, is referred to as the *design moment resistance* in Eurocode 3. It represents a pseudo-plastic resistance of the joint, omitting the influence of strain-hardening and any additional membrane actions. These simplifications account for the discrepancy observed in Figure 2.5 between the actual moment-rotation relationship and the idealized yield plateau.

In this idealisation, according to Eurocode 3, when the design moment M_{Ed} is less than $\frac{2}{3}M_{j,Rd}$, the initial stiffness $S_{j,ini}$ is used as rotation stiffness of the joint in the global model. For moments exceeding this threshold, i.e., $M_{j,Ed} \geq \frac{2}{3}M_{j,Rd}$, the rotational stiffness is reduced and calculated as $\frac{S_{j,ini}}{\eta}$, where $\eta = 2$ for beam-to-column joints. This value of $\frac{2}{3}M_{j,Rd}$ can be interpreted as the elastic moment resistance of the joint prior to the formation of any plastic hinges.

2.3 Introduction to the Component Method

The component method involves characterizing the stiffness and strength of individual elements to determine the overall mechanical behaviour of the joint. This method offers a more detailed understanding of joint behaviour. For instance, in the case of the extended end-plate connection subjected to bending, as depicted in Figure 2.7, the joint can be decomposed into the following active components:

- Tension in the bolts;
- Bending in the end-plate;
- Tension in the column web;
- Compression in the column web;
- Shear in the column web panel.
- Bending in the column flange;
- Compression in the beam flange and web;
- Tension in the beam web;

Each component exhibits specific mechanical properties, such as stiffness and strength. Notably, the column web is often simultaneously subjected to compression, tension, and shear, resulting in complex stress interactions. These overlapping effects can compromise the individual capacity of each component. Some components are characterized in Eurocode 1993-1-8.

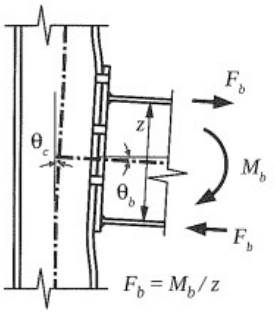

Figure 2.7: Single-sided joint under bending moment

Applying the component method involves the following key stages:

1. Identifying all active components in the joint under consideration;

2. Determining the mechanical properties of each component, such as initial stiffness and resistance;

3. Assembling the components into a comprehensive joint model and evaluating its global mechanical response, including stiffness and resistance, based on the interaction of the parts.

This assembly process requires translating the external forces applied to the joint into internal forces acting on each component. This distribution must satisfy static equilibrium and align with the mechanical behaviour of the individual elements. Through this systematic approach, the global response of the joint can be accurately estimated from the behaviour of its constituents.

2.4 Conclusion

The theoretical foundations outlined in this document highlight the critical role of joint behaviour in structural design, emphasizing the spectrum between rigid and pinned connections. The semi-rigid approach, as per EN 1993-1-8, offers a balanced solution for modular structures by accounting for joint flexibility. Key classifications, based on stiffness (rigid, semi-rigid, pinned) and strength (full-strength, partial-strength,pinned), guide accurate modelling and analysis. The component method further enhances precision by decomposing joints into active components, each contributing to overall stiffness and resistance. Simplified representations, such as the bilinear moment-rotation relationship, provide a practical means for structural modelling and design. Ultimately, integrating these principles enables efficient, economical, and reliable structural solutions.

Chapter 3 — Overview and Design of Possible Technical Solutions

3.1 Overview of Possible Joint Solutions

The beam-to-column joints designed by DEGOTTE within the framework of modular construction consist of a component comprising a sleeve that serves as a connector between beams and columns. This sleeve is made from a $SHS90/4$ steel profile and is inserted into the top of the column. Subsequently, a beam is connected to the same connector element. This system is implemented at each of the four corners of the module.

A major advantage of this technique is the ability to assemble the floor or roof system at ground level and then position it atop the four columns. The steel sleeve used in this connection is illustrated in the figure below. In Figure 3.1, the steel sleeve is shown in purple, the main roof beam in red, a secondary beam in blue, and the column in yellow. This roof or floor assembly is placed on top of a support welded to the column, which is composed of an SHS 80/5 profile.

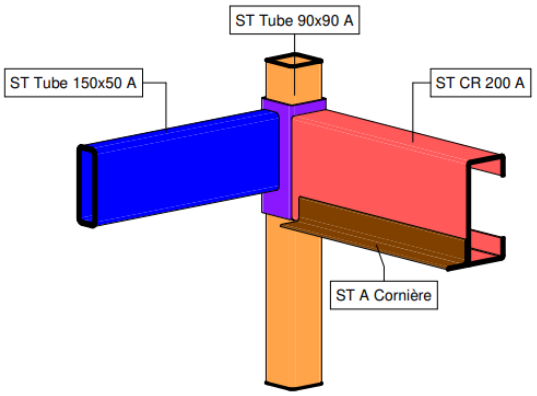

Figure 3.1: Beam-to-column junction (DEGOTTE)

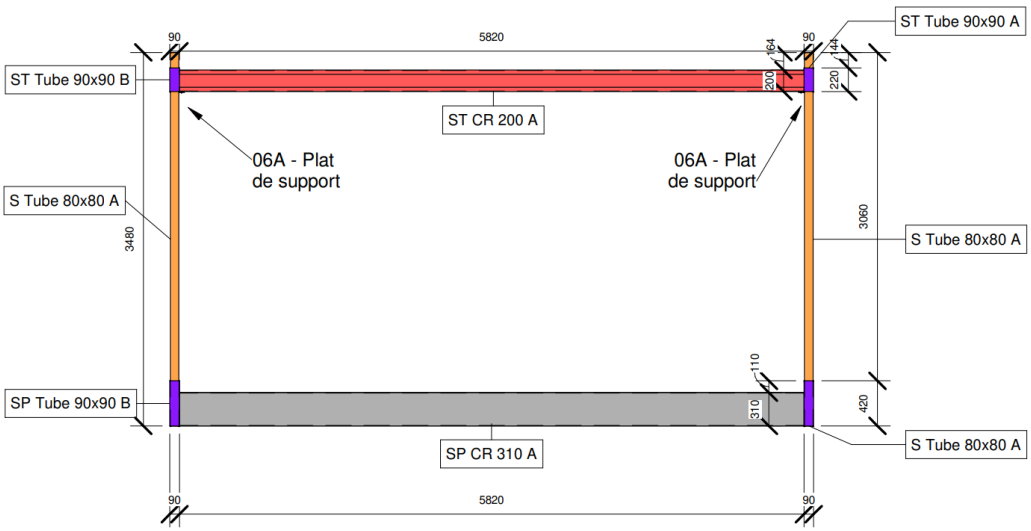

Figure 3.2: Elevation view of the modular construction (DEGOTTE)

The objective of this master's thesis is to develop an effective method for connecting this sleeve to the roof beams, which are C-shaped profiles requiring a specific joint configuration. Three connection configurations have been investigated:

- *Option 1-A*: This configuration entails the attachment of three individual plates welded to the sleeve, with a single row of M20 bolts employed to secure the connection to the beam flanges.
- *Option 1-B*: In this configuration, three individual plates are welded to the sleeve, with two rows of M12 bolts utilized to establish the connection to the beam flanges.
- *Option 2*: This alternative features a C-shaped profile welded to the sleeve, which is subsequently bolted to the beam flanges using a single row of bolts, with M20 bolts initially considered for the connection.

The various geometric characteristics of the columns and beams are presented in Chapter 4.

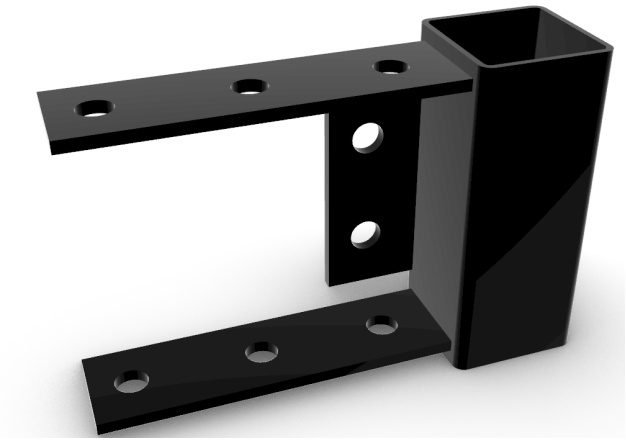

Figure 3.3: *Option 1-A* and *Option 1-B* configuration

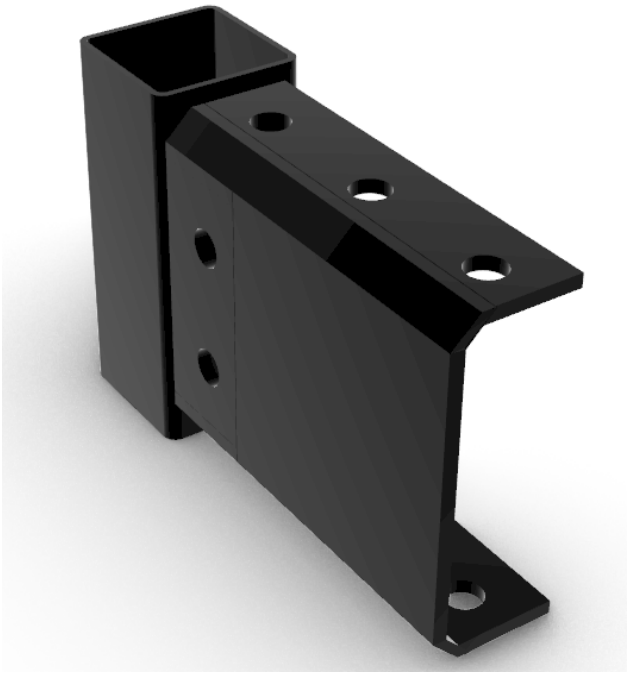

Figure 3.4: *Option 2* joint configuration

3.2 Defining the Requirements for a Fully Resistant joint

The company DEGOTTE initially requested a joint with a resistance greater than that of the connected beam. This section presents the design criterion for ensuring that the joint achieves a higher moment resistance than the beam, i.e.,

$$M_{j,Rd} \geq M_{b,Rd} \tag{3.1}$$

To this end, the plastic moment resistance of the roof beam is considered. For strong-axis bending, this value is known to be 29.6 kN·m. This moment is decomposed into tensile and compressive forces using a rotational equilibrium assumption within the beam's cross-section.

Consequently, the force to be transmitted through the plates connected to the beam flanges can be expressed as:

$$F_t = \frac{M_{b,Rd}}{Z} \tag{3.2}$$

where Z is the lever arm measured between the centroids of plates 1 and 2. Indeed, the tensile force transmitted through the plates is assumed to act at the mid-thickness of each plate. It is therefore inappropriate to consider the lever arm measured at the mid-thickness of the beam flanges, as this would underestimate the axial force required to achieve a fully resistant joint relative to the beam.

Thus, the effective lever arm is computed as:

$$\begin{aligned} Z &= h_b - 2 \cdot t_f - t_p \\ &= 200 - 2 \cdot 4 - 8 = 184 \text{ mm} \end{aligned}$$

With:

- h_b is the beam height: 200 mm
- t_f is the beam flange thickness: 4 mm
- t_p is the plate thickness: 8 mm

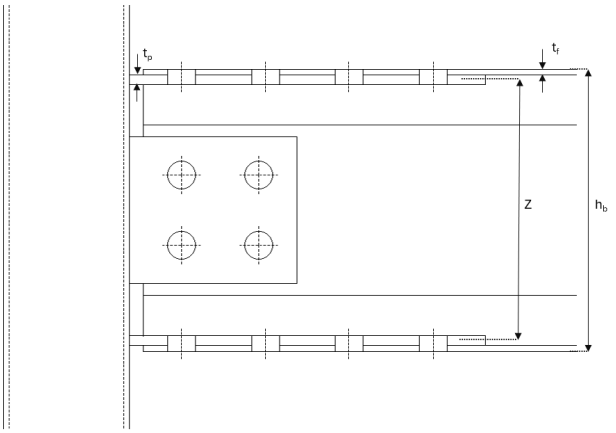

Figure 3.5: Elevation view of the joint

Using equation 3.2, the compression and tension forces transmetted to the plates connected to the beam flange are equal to 160 kN. [1]

3.3 Component Identification

For a rigid or semi-rigid beam-to-column connection, in the vicinity of the joint, the distribution of axial stresses due to beam bending is such that the top beam flange is subjected to tension, while the bottom flange experiences compression. The forces developed in the beam flanges are transmitted to the top and bottom plates by engaging the bolts in shear, and causing bearing stresses in both the beam flanges and the plates. These mechanisms constitute the first three components.

Subsequently, the forces are transferred into the top and bottom plates, respectively inducing tension and compression in them. The next two components are therefore the top plate in tension and the bottom plate in compression.

[1] This value is certainly conservative as the bolt's shear plan is at the interface between the plates and the beam flange.

When either the plates or the beam flanges are subjected to tension, block tearing may occur and must be verified. This is not truly a component, but rather a failure mechanism that may occur when a plate is subjected to tensile stress.

Finally, the top and bottom plates transfer the tensile and compressive forces to the rectangular hollow section (RHS) steel sleeve. This type of section requires additional verifications. The transmission of tension from the top plate to the RHS wall can lead to chord plastification and chord punching shear. Under compressive forces, similar failure modes may also need to be checked.

While the top and bottom plates primarily resist the effects of beam bending, the intermediate plate ensures the transmission of shear forces to the column. This plate must be designed considering again the bolts in shear, bearing in the plate and beam web, and potential block tearing of the plate.

The components in the three configurations analyzed, namely *Option 1-A*, *Option 1-B*, and *Option 2*, exhibit significant similarities. However, the treatment of block tearing may differ across these configurations. In certain instances, the risk of block tearing is negligible.[2]

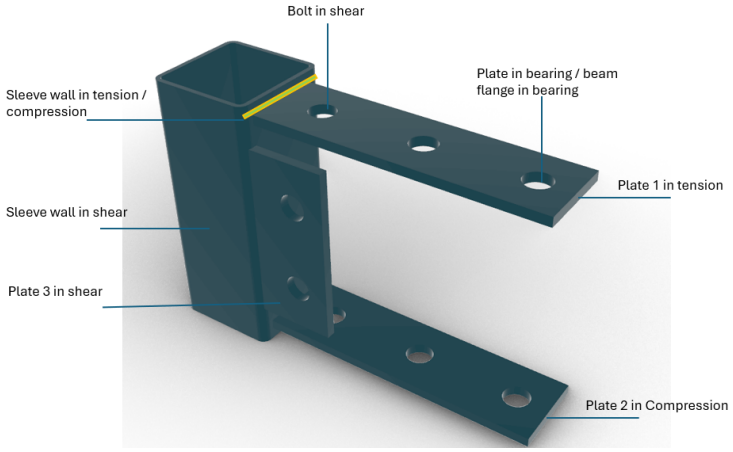

Figure 3.6: Illustration of some components in case of *Option 1-A* and *Option 1-B*

3.4 Option 1-A

The first proposed configuration consists of three individual plates welded directly to a steel sleeve, as illustrated in Figure 3.7. Plates 1 and 2 are designed to connect to the beam flanges, while Plate 3 interfaces with the beam web [3]. For this option, M20 bolts of class 10.9 have been selected as fasteners, ensuring high strength and reliability. Plan, elevation, and perspective views of

[2]Annexes A and B provide detailed design calculations for *Option 1-B* and *Option 2*, respectively, in which the risk of block tearing is addressed in the relevant sections.

[3]Plate 1 represents the upper plate, whereas Plate 2 denotes the lower plate. Both plates serve as connecting elements between the sleeve and the beam flange. Plate 3 functions as the intermediate plate, establishing a link between the sleeve and the beam web.

the proposed connection are presented below to provide a comprehensive understanding of the assembly.

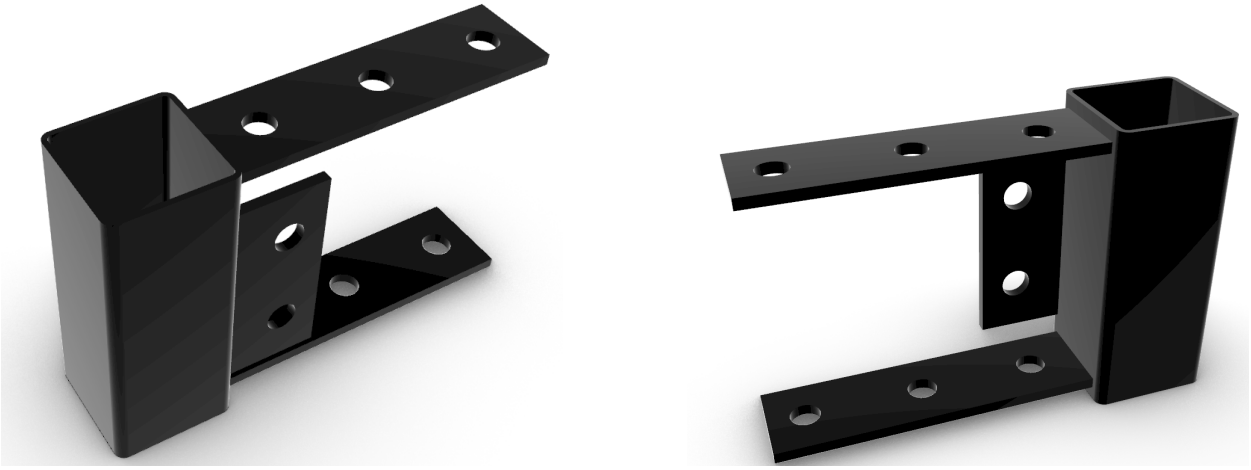

Figure 3.7: Individual plate configuration welded on RHS steel sleeve

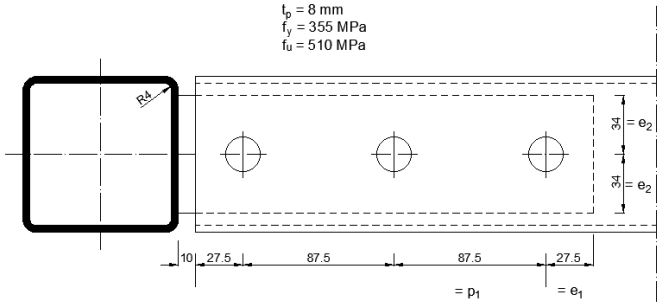

Figure 3.8: Beam flange-Plate 1 and 2 connection

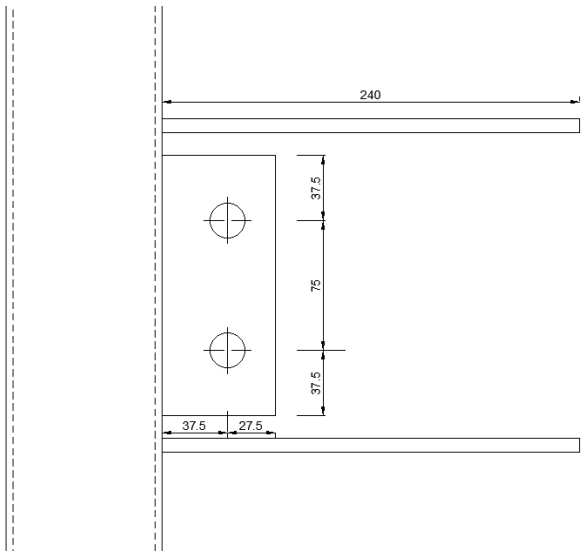

Figure 3.9: Beam web-Plate 3 geometry

In the following sections, each component mentioned in Section 3.3 will be characterized in terms of both resistance and stiffness.

3.4.1 Bolt in shear - Beam flange/ Plate 1 and 2 connection

a) Resistance

Option 1-A proposes a single row of three M20 bolts, grade 10.9. The shear resistance of a single M20 bolt is calculated using the following expression:

$$F_{v,Rd} = \frac{\alpha_v \cdot f_{ub} \cdot A_s}{\gamma_{M2}} \tag{3.3}$$

where:

- $\alpha_v = 0.5$, as recommended for grade 10.9 bolts. This factor reflect the low capacity of deformation of that grade. Class 10.9 corresponds to an ultimate strength of $f_{ub} = 1000$ MPa.
- A_s is the tensile stress area of the bolt, taken in the threaded portion[4], with a value of 245 mm^2.
- $\gamma_{M2} = 1.25$, the partial safety factor for bolt resistance, as specified in the NBN EN 1993 Part 1-8.

Substituting the values into the equation 3.3 gives:

$$F_{v,Rd} = \frac{0.5 \cdot 1000 \cdot 245}{1.25} = 98 \text{ kN}$$

The total shear resistance of the connection is then calculated by:

$$F_{tot,Rd} = n \cdot m \cdot F_{v,Rd}$$

with:

- $n = 3$, the number of bolts involved in shear,
- $m = 1$, the number of shear planes in the connection (see figure 3.10).

Hence:

$$F_{tot,Rd} = 3 \cdot 1 \cdot 98 = 294 \text{ kN}$$

[4]This is a conservative assumption: the threaded section is considered the critical area.

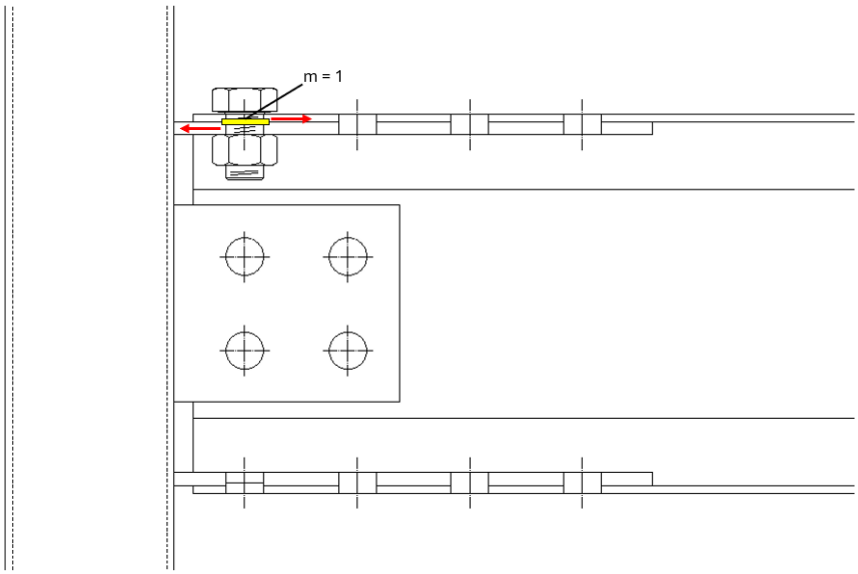

Figure 3.10: Shear plan illustration

This value is taken as the design shear resistance of the bolt rows, under the assumption of equal force distribution between all bolts. Such an assumption implies sufficient ductility in the system to allow for plastic redistribution of internal forces.[5] When adequate deformation occurs in each bolt zone, a complete plastic redistribution of forces can take place. In contrast, failure arises due to insufficient ductility, resulting in a lower maximum external force being transferred compared to the force associated with full plastic redistribution.

To ensure that this resistance can be achieved, it is also necessary to ensure that the distance between the rows of bolts is not too large, as this could result in the risk of the end bolts breaking before any redistribution occurs due to their intrinsic lack of ductility. This latter condition is satisfied because:

$$p_1 \leq 15 \cdot d$$

$$87.5 \leq 15 \cdot 22 = 330\ mm$$

b) Stiffness

The shear stiffness coefficient of bolts, denoted as k_{BS}, for a single bolt row, shall be determined using the following expression:

- For bolt rows in bearing-type connections:

$$k_{\mathrm{v}} = \frac{8 n_{\mathrm{b}} d^2 f_{\mathrm{ub}}}{E\, d_{\mathrm{M16}}} \tag{3.4}$$

where:

[5] In certain cases where the distance between the two outermost rows of bolts is relatively large, the shear resistance of the bolts, denoted as $F_{v,\mathrm{Rd}}$, may be reached prior to achieving a complete redistribution of internal forces, provided that there is ductility.

- d, 20 mm, is the bolt diameter,
- d_{M16}, 16 mm, is the nominal diameter of an M16 bolt,
- f_{ub}, 1000 MPa, is the ultimate tensile strength of the bolt,
- E, 210 GPa, is the Young's modulus of elasticity,
- n_b, 3 bolt, is the number of bolt rows (each consisting of two bolts per row).

Hence, the shear stiffness coefficient of the top flange connection is 2.86mm. By multiplying this coefficient by the Young's modulus, a shear stiffness of 600 kN/mm is obtained.

c) Deformation capacity

The load-displacement curve is illustrated in figure 3.11. According to the methods outlined in the Eurocode, the shear stiffness of a bolt is derived based on a maximum allowable deformation approach.[6]

It will therefore be crucial to ensure that this component does not govern the strength of the assembly.

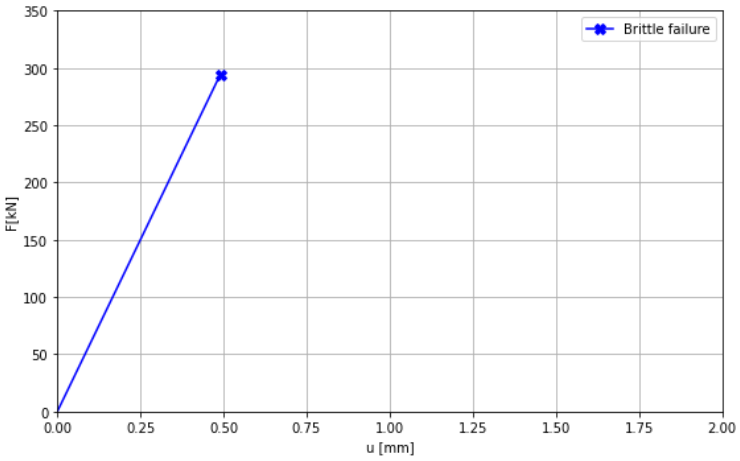

Figure 3.11: Load–Deformation Behaviour for Three Rows of Bolts in Shear

3.4.2 Plate 1 and 2 in bearing

a) Resistance

The bearing resistance of the plates is determined using the Belgian Standard, NBN EN 1993-1-8:2024[7]. The resistance is given by the following equation:

$$F_{b,Rd} = \frac{k_m \alpha_b f_u dt}{\gamma_{M2}} \tag{3.5}$$

Where:

[6] However, in practice, for bearing-type connections, it is often observed that larger deformations may occur prior to failure.

[7] NBN EN 1993-1-8:2024 provides enhanced bearing resistance.

- For end fasteners:

$$\alpha_{\text{b,end bolt}} = \min\left(\frac{e_1}{d_0}; 3\cdot\frac{f_{\text{ub}}}{f_{\text{u}}}; 3\right) = \min\left(\frac{27.5}{20+2}; 3\cdot\frac{1000}{490}; 3\right) = 1.25$$

- For inner fasteners:

$$\alpha_{\text{b,inner bolt}} = \min\left(\frac{p_1}{d_0} - \frac{1}{2}; 3\cdot\frac{f_{\text{ub}}}{f_{\text{u}}}; 3\right) = \min\left(\frac{87.5}{20+2} - 0.5; 3\cdot\frac{1000}{490}; 3\right) = 3$$

- $k_m = 1$, as the elastic resistance of the plates is 355 MPa, so that $f_y \leq 460$ MPa. The ultimate resistance f_u of the plates is 510 MPa.

In Figure 3.8, the geometry of Plates 1 and 2 is presented, from which e_1 and p_1 can be extracted. In this configuration, there are two internal bolts (in green) and one external bolt (in red), as illustrated in Figure 3.12.

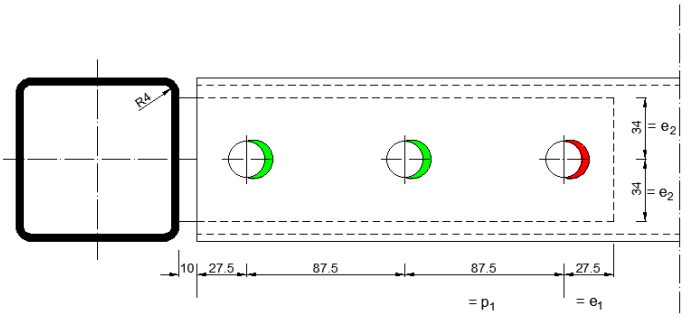

Figure 3.12: Plate 1 and 2 in bearing : Inner bolt (in green) and End bolt (in red)

Using Equation 3.5, the resistance of the inner and external bolts can be calculated as follows:

- For the inner bolts:

$$F_{b,\text{Rd,inner bolt}} = 2\cdot\frac{k_m\cdot\alpha_{\text{b,inner bolt}}\cdot f_u\cdot d\cdot t}{\gamma_{\text{M2}}} = 2\cdot\frac{1\cdot 3\cdot 510\cdot 20\cdot 8}{1.25\cdot 1000} = 391.6\,\text{kN}$$

- For the end bolt:

$$F_{b,\text{Rd,end bolt}} = 1\cdot\frac{k_m\cdot\alpha_{\text{b,end bolt}}\cdot f_u\cdot d\cdot t}{\gamma_{\text{M2}}} = 1\cdot\frac{1\cdot 1.25\cdot 510\cdot 20\cdot 8}{1.25\cdot 1000} = 81.6\,\text{kN}$$

Therefore, the total bearing resistance of plates 1 and 2 is:

$$F_{\text{b,Rd,tot}} = F_{b,\text{Rd,inner bolt}} + F_{b,\text{Rd,end bolt}}$$

$$F_{\text{b,Rd,tot}} = 391.6 + 81.6 = 473.2\,\text{kN}$$

b) Stiffness

For bolt in bearing, it is important to represent the deformation behaviour especially in this project where the joint must be reused.Two models are proposed in the Eurocode :

- Linear behaviour proposed by Professor Jaspart
- Non-linear behaviour proposed by Primož Može .[7].

The first model provides an elastic stiffness that depends on the position of the bolt from the edge or from other bolts. This model is used to predict the yield deformation and is not able to accurately describe the bolt embedment. The elastic stiffness for bearing for a single bolt hole is given by :

$$k_{\mathrm{PB}} = \frac{12 \cdot n_{\mathrm{b}} \cdot k_{\mathrm{d}} \cdot k_{\mathrm{t}} \cdot d \cdot f_{\mathrm{u}}}{E} \tag{3.6}$$

Where:

- n_{b}, is the number of bolt rows [8]
- $k_d = min(k_{d1}, k_{d2}) = min(0.84; 1.25) = 0.84$
- $k_{d1} = min(0.25 \cdot \frac{e_1}{d} + 0.5; 1.25) = min(0.25 \cdot \frac{27.5}{20} + 0.5; 1.25) = 0.84$
- $k_{d2} = min(0.25 \cdot \frac{p_1}{d} + 0.375; 1.25) = min(0.25 \cdot \frac{87.5}{20} + 0.375; 1.25) = 1.25$
- $k_t = min(1.5 \cdot \frac{t_j}{d_{M16}}; 2.5) = min(1.5 \cdot \frac{8}{16}; 2.5) = 0.75$
  with t_{j}, the thickness of the steel plate on which the bolt bears.

Replacing the different parameters in equation 3.6, the stiffness coefficient is

$$k_{\mathrm{b}} = \frac{12 \cdot 1 \cdot 0.84 \cdot 0.75 \cdot 20 \cdot 510}{210000} = 0.37\ mm$$

This stiffness coefficient is related to one bolt hole. This first model doesn't distinguish end bolt hole from inner bolt hole which can have a significative impact on the deformation behaviour. However, the main of taking the minimum between k_{d1} and k_{d2} is to assimilate the joint to an equivalent one retaining the most conservative case. Then, the stiffness is multiplied by the number of bolt hole to modelize the total stiffness of the top plates in bearing. Thus, the stiffness coefficient, k_b, is equal to $3 \cdot 0.74 = 1.1$mm. Thus, the elasto-plastic behaviour curve is derived. This curve is illustrated in figure 3.13.

[8] In this first configuration, n_{b} is differently defined from the Eurocode as there is only one bolt per bolt row. The version of equation 3.6 presented in eurocde only cover the cases where a bolt row is composed by two bolts. Indeed, the factor 24 from equation 3.6 became 12.

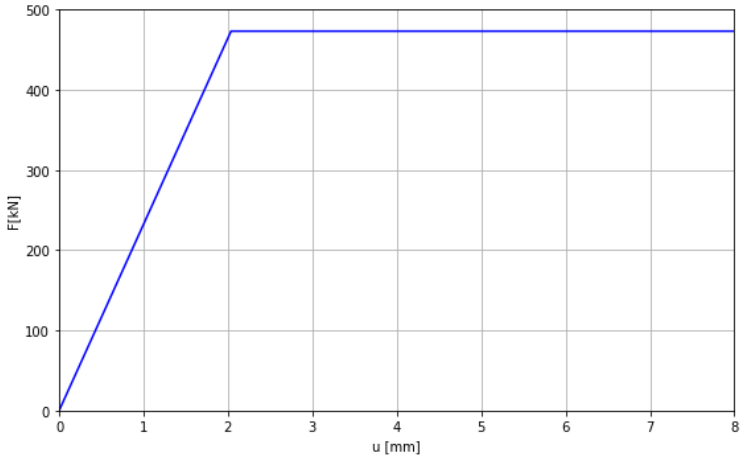

Figure 3.13: Load-deformation behaviour of the plate in bearing

The second model, developed by Primož Mož, focuses on the mechanical interaction between the bolt and the surrounding material, specifically addressing the embedment effects. This approach offers a more refined representation, as the bolt's embedment leads to progressive deformation and elongation of the bolt hole. The resulting non-linear response is predominantly driven by this localised contact, which initiates yielding in the plate material beyond the bolt hole region.

This model suggest a bearing stiffness coefficient given by

$$k_{PB} = \frac{\bar{S_b} \cdot n_b \cdot t_j \cdot f_u}{E} \tag{3.7}$$

where the relative bearing stiffness $\bar{S_b}$ is obtained from the ratio between the relative bearing stress and the relative bolt hole elongation, $\bar{S_b}(u) = \frac{\bar{\sigma}_{b,Ed}}{\bar{u}}$.
The relative load-deformation behaviour for bearing is the simplest way to present the behaviour. Indeed, the relative behaviour is prefered to compare the effects of plate thicknesses, edge distances, bolt diameter or steel grades.
The non-dimensional average bearing stress, $\bar{\sigma}_{b,Ed} = \frac{F_{b,Ed}}{d \cdot t_j \cdot f_u}$, with $F_{b,Ed}$ design bearing force at bolt hole.
The non-dimensional bolt hole elongation at design non-dimensional average bearing stress is given by $\bar{u} = \left(\frac{\sqrt{30} + \sqrt{\frac{126}{\bar{\sigma}_{b,Ed}}}}{\frac{126}{\bar{\sigma}_{b,Ed}} - 30} \right)$.
The bearing mechanism can be described in three successive phases. *Phase I* involves the initial interaction between the bolt and the plate, where slight plasticity is observed near the bolt hole with minimal displacement. In *Phase II*, the plastic zone extends across the plate area ahead of the bolt, resulting in a gradual increase in load-carrying capacity, though the load–deformation curve remains relatively smooth. *Phase III* is characterised by extensive plastic flow, during which the structure mobilises its residual strength and significant elongation of the bolt hole occurs.

The bolt embedment curve is found by incrementing the design bearing force, $F_{b,Ed}$, till reaching

80% of the bearing resistance of a bolt hole. This represent a certain elongation at bolt hole, u, and will be connected with a solid line to the lower limit of the bolt elongation at ultimate resistance, u_u, given by

$$u_u = min\left(\frac{\alpha_b}{3}; 1\right) \cdot d$$

where α_b varies between the end bolts and the inner bolts (cf. resistance in bearing computation).

As seen in the previous section, the bearing resistances for one inner bolt and one end bolt are, respectively:

$$F_{b,Rd,innerbolt} = \frac{391.6}{2} = 195.5\ kN$$

$$F_{b,Rd,endbolt} = 81.6\ kN$$

and 80% of their capacity corresponds to 156.7 kN and 65.8 kN, respectively.

$F_{b,Ed}[kN]$	0.00	19.58	39.17	58.75	78.34	97.92	117.50	137.09	156.67
$\sigma_{b,Ed}[-]$	0.00	0.24	0.48	0.72	0.96	1.20	1.44	1.68	1.92
u [-]	0.00	0.00	0.01	0.02	0.03	0.04	0.07	0.10	0.15
S_b	0.00	72.96	55.21	43.26	34.32	27.30	21.64	17.02	13.22
$k_b[mm]$	0.00	1.42	1.07	0.84	0.67	0.53	0.42	0.33	0.26
u[mm]	0.00	0.07	0.17	0.33	0.56	0.88	1.33	1.97	2.91

Table 3.1: Characteristic points of the embedment curve for inner bolt hole

From those characteristic points given in table 3.1, graph illustrated in figure 3.14 is obtained.

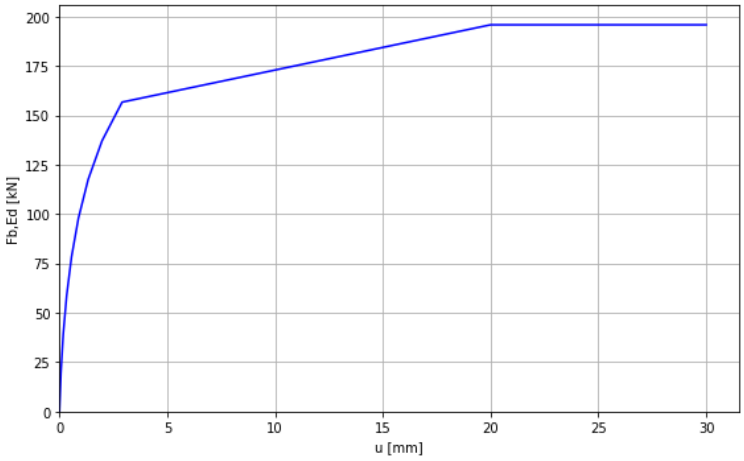

Figure 3.14: Load-Deformation behaviour for one inner bolt hole

The same methodology is applied for the end bolt hole where caracteristic point are given in table 3.2 and their graph presented in figure 3.15.

$F_{b,Ed}[kN]$	0.00	8.16	16.32	24.48	32.64	40.80	48.96	57.12	65.28
$\sigma_{b,Ed,endbolt}$ [-]	0.00	0.10	0.20	0.30	0.40	0.50	0.60	0.70	0.80
$u_{endbolt}$ [-]	0.00	0.00	0.00	0.00	0.01	0.01	0.01	0.02	0.02
$S_{b,endbolt}$	0.00	90.12	77.01	67.65	60.23	54.05	48.75	44.12	40.02
$k_{b,endbolt}$ [mm]	0.00	1.75	1.50	1.31	1.17	1.05	0.95	0.86	0.78
$u_{endbolt}$ [mm]	0.00	0.02	0.05	0.09	0.13	0.19	0.25	0.32	0.40

Table 3.2: Characteristic points of the embedment curve for end bolt hole

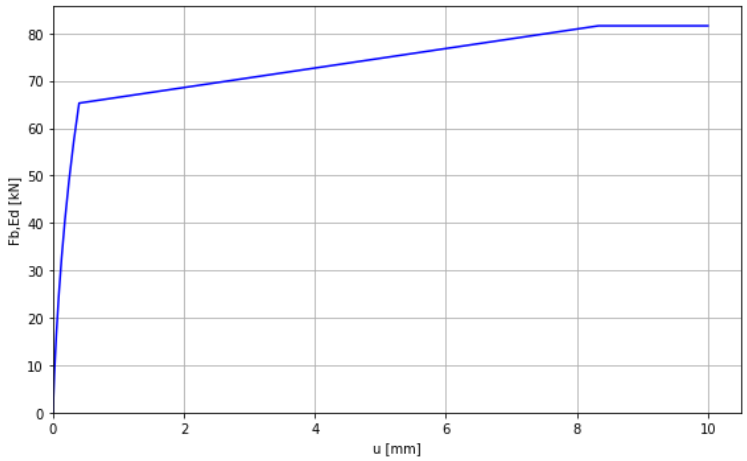

Figure 3.15: Load-Deformation behaviour for one end bolt hole

As this model distinguish end bolt and inner bolt behaviour, knowing that the joint has two inner bolt and one end bolt, the equivalent bearing stiffness coefficient is obtainted by puting them in series. Hence,

$$\frac{1}{k_{b,eq}} = \frac{1}{k_{b,endbolt}} + \frac{1}{2 \cdot k_{b,innerbolt}}$$

This equivalent bearing stiffness coefficient depends on the applied for at each bolt hole. Later, an even distribution of loads between bolt rows will be assumed [9].

Finally, for one bolt hole, a comparison of the first and second model can be done as illustrated in figure 3.16. In this figure, it is evident that the initial portion of the curve, along with Model 1 and Model 2, result in closely aligned values for the end bolts. Indeed, since the model considers the most unfavourable case between the end bolts and the inner bolts, it tends to inaccurately capture the behaviour of the neglected case, which in this instance corresponds to the inner bolts. However, Model 1 provides a stiffness value without requiring knowledge of the load applied at the bolt hole, thereby avoiding the need for an iterative approach.

[9] In bearing-type connections, forces are transferred through the contact between the bolt and the bolt hole's wall. The distribution of these forces among all bolts in the connection relies on the steel's ductility, which enables the bolt to embed. The embedding of the bolt plays a key role in ensuring a uniform distribution of forces.

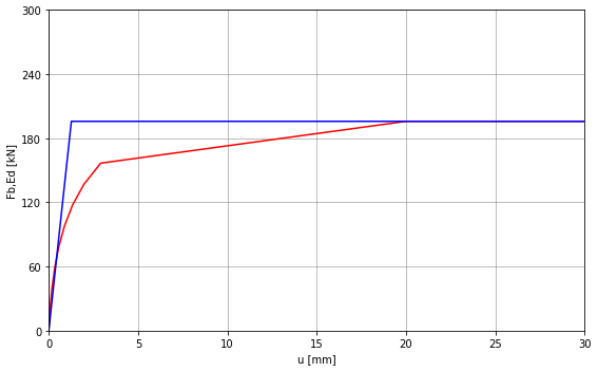

(a) Comparison at the inner bolt

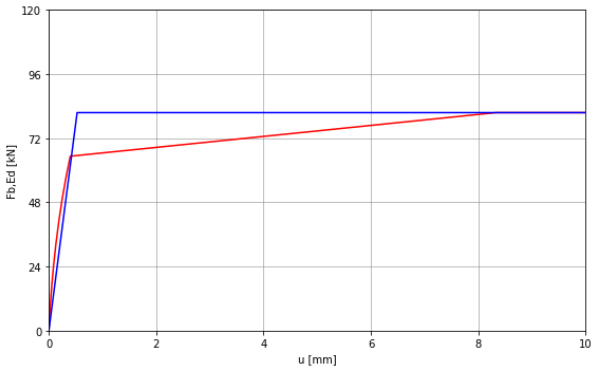

(b) Comparison at the end bolt

Figure 3.16: Comparison between Jaspart's model and Primoz's model at different bolt locations

c) Deformation capacity

Plates in bearing are is recognized as ductile.

3.4.3 Beam flange in bearing

a) Resistance

The bearing resistance of the beam flange is determined in the same manner as for the plates in bearing. The only differences to consider are the beam flange thickness, which is 4 mm, and the steel grade, with a yield strength of $f_y = 235\,\text{MPa}$ and an ultimate tensile strength of $f_u = 360\,\text{MPa}$. As with the plates 1 and 2 on bearing, there are two internal bolts and one external bolt involved in the connection.

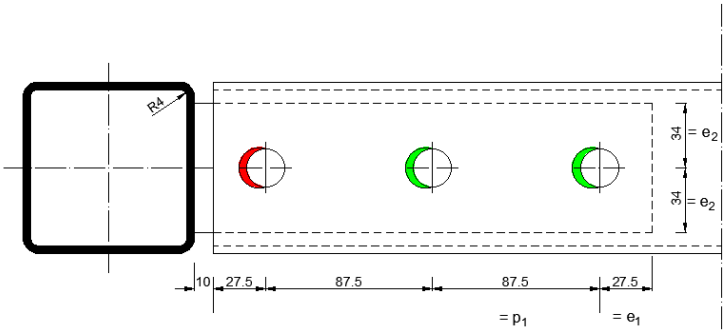

Figure 3.17: Beam flange in bearing : Inner bolts (in red) and End bolt (in green)

Using Equation 3.5, the resistance for both the internal and external bolts can be calculated as follows:

- For the inner bolts:

$$F_{b,\text{Rd,inner bolt}} = 2 \cdot \frac{k_m \cdot \alpha_{\text{b,inner bolt}} \cdot f_u \cdot d \cdot t}{\gamma_{\text{M2}}} = 2 \cdot \frac{1 \cdot 3 \cdot 360 \cdot 20 \cdot 4}{1.25 \cdot 1000} = 138.2\,\text{kN}$$

- For the end bolt:

$$F_{b,\text{Rd,end bolt}} = 1 \cdot \frac{k_m \cdot \alpha_{\text{b,end bolt}} \cdot f_u \cdot d \cdot t}{\gamma_{\text{M2}}} = 1 \cdot \frac{1 \cdot 1.25 \cdot 360 \cdot 20 \cdot 4}{1.25 \cdot 1000} = 28.8\,\text{kN}$$

Therefore, the total bearing resistance for the beam flange is:

$$F_{\text{b,Rd},tot} = 138.2 + 28.8 = 167.0\,\text{kN}.$$

b) Stiffness

Replacing the different parameters in equation 3.6 (Jaspart's model), the stiffness coefficient for three bolts is

$$k_{\text{FB}} = \frac{12 \cdot 3 \cdot 0.84 \cdot 0.38 \cdot 20 \cdot 360}{210000} = 0.39\,mm$$

with $k_t = min(1.5 \cdot \frac{t_j}{d_{M16}}; 2.5) = min(1.5 \cdot \frac{4}{16}; 2.5) = 0.38$.

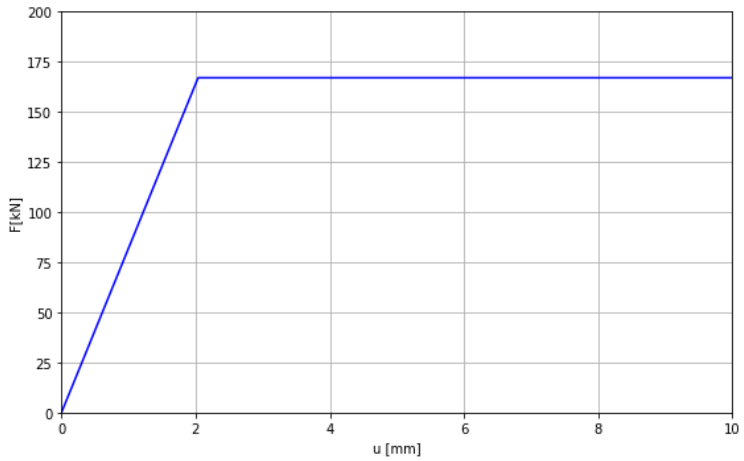

Figure 3.18: Load-deformation behaviour for one bolt hole

The second model offers results presented in tables and graphs below.

$F_{b,Ed}$ [kN]	0.00	6.91	13.82	20.74	27.65	34.56	41.47	48.38	55.30
$\sigma_{b,Ed}$ [-]	0.00	0.24	0.48	0.72	0.96	1.20	1.44	1.68	1.92
u [-]	0.00	0.00	0.01	0.02	0.03	0.04	0.07	0.10	0.15
S_b	0.00	72.96	55.21	43.26	34.32	27.30	21.64	17.02	13.22
k_b[mm]	0.00	0.50	0.38	0.30	0.24	0.19	0.15	0.12	0.09
u[mm]	0.00	0.07	0.17	0.33	0.56	0.88	1.33	1.97	2.91

Table 3.3: Characterstic points of the embedment curve for one inner bolt hole

$F_{b,Ed}$ [kN]	0.00	2.88	5.76	8.64	11.52	14.40	17.28	20.16	23.04
$\sigma_{b,Ed}$ [-]	0.00	0.10	0.20	0.30	0.40	0.50	0.60	0.70	0.80
u [-]	0.00	0.00	0.00	0.00	0.01	0.01	0.01	0.02	0.02
S_b	0.00	90.12	77.01	67.65	60.23	54.05	48.75	44.12	40.02
k_b	0.00	0.62	0.53	0.46	0.41	0.37	0.33	0.30	0.27
u [mm]	0.00	0.02	0.05	0.09	0.13	0.19	0.25	0.32	0.40

Table 3.4: Characterstic points of the embedment curve for one end bolt hole

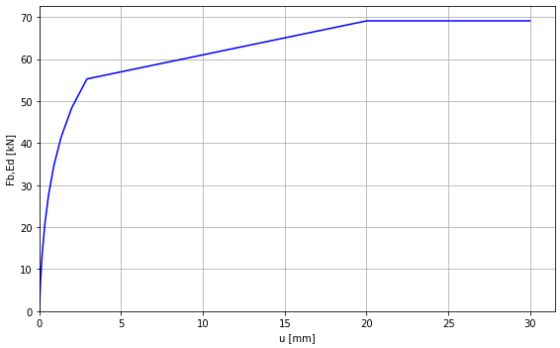

Figure 3.19: Load-Deformation behaviour for one inner bolt hole

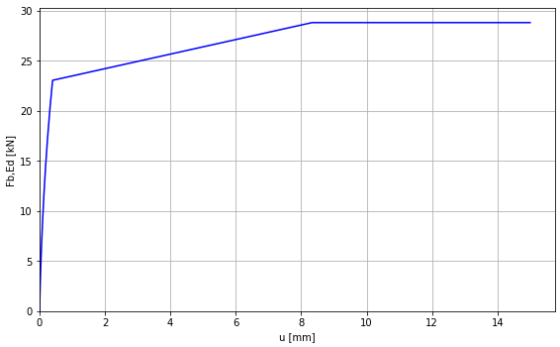

Figure 3.20: Load-Deformation behaviour for one end bolt hole

A comparison of the first and second model is shown in figure 5.20.

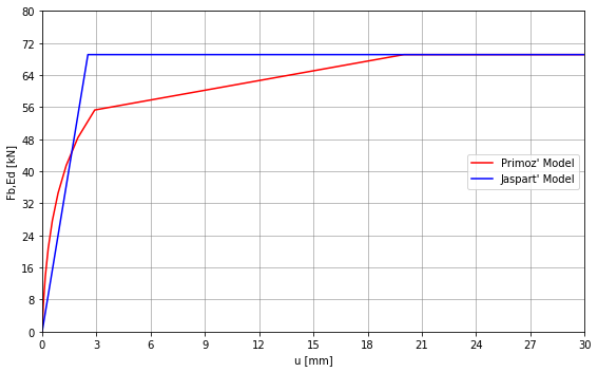

(a) Comparison at the inner bolt

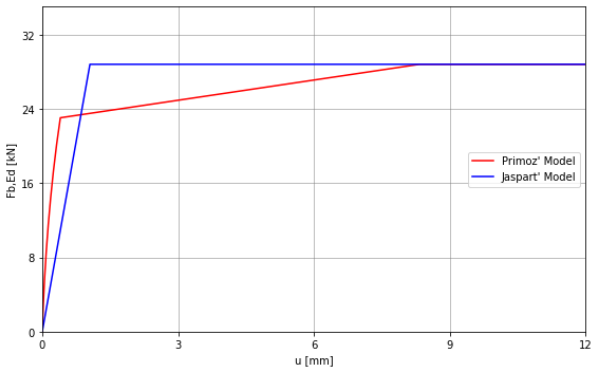

(b) Comparison at the end bolt

Figure 3.21: Comparison between Jaspart's model and Primoz's model for Option 1-b

c) Deformation capacity

Similar to the plate in bearing, the beam flange in bearing is also recognized for its ductile behaviour.

3.4.4 Plate 1 in tension

a) Resistance

Once the bolts resist the applied shear forces, a tensile force is induced in Plate 1. The tensile resistance of the plate is evaluated by considering both the gross and net section capacities. The governing resistance is taken as the lower of the two.

- **Gross Section Resistance:**
  The tensile resistance of the gross cross-section is calculated as:

$$N_{pl,Rd} = \frac{A_p \cdot f_y}{\gamma_{M0}} = \frac{8 \cdot 68 \cdot 355}{1.0 \cdot 1000} = 193.1\,\text{kN}$$

- **Net Section Resistance:**
  The tensile resistance of the net section, accounting for the bolt hole deduction, is given by:

$$N_{u,Rd} = \frac{0.9 \cdot (A_p - d_0 \cdot t) \cdot f_u}{\gamma_{M0}} = \frac{0.9 \cdot (8 \cdot 68 - 22 \cdot 8) \cdot 510}{1.0 \cdot 1000} = 168.9\,\text{kN}$$

Since the net section resistance is lower, it governs the design. This indicates a brittle failure mode, as rupture occurs through the reduced cross-section near the bolt hole.

b) Stiffness

According to the Eurocode 3 Part 1-8, the stiffness coefficient of a plate under tension should be considered infinite.

$$k_t = \infty$$

The deformation of the plate under compression is considered to be accounted for within the beam element deformation, as part of the frame analysis, and therefore does not need to be included again. [10]

c) Deformation capacity

Since the resistance of this component is governed by that of the net section, brittle failure is expected.

3.4.5 Plate 2 in compression

a) Resistance

The design resistance in compression is evaluated in accordance with EN 1993-1-1 of the Eurocode. Since the plate is laterally stabilized through its connection to the beam flange, global instability is not expected to occur. Nevertheless, the plate is classified as Class 3. As a result, the design check is limited to the section capacity, given by the following expression:

$$N_{pl,Rd} = \frac{A_p \cdot f_{y,fp}}{\gamma_{M0}} \tag{3.8}$$

[10] Even if it were considered again, this component has such a high stiffness that its contribution to the equivalent stiffness of the assembly would be negligible. The equivalent stiffness will be shown later.

where A_p is the cross-sectional area of the plate, $f_{y,fp}$ is the yield strength of the fin plate material, and γ_{M1} is the partial safety factor for resistance of cross-sections. Hence,

$$N_{pl,Rd} = \frac{68 \cdot 8 \cdot 355}{1.0 \cdot 1000} = 193.1\,\text{kN}$$

b) Stiffness

Once again, Eurocode 3 Part 1-8 assumes an infinitely stiff coefficient for plates in compression, for same reasons as plate in tension.

$$k_c = \infty$$

c) Deformation capacity

Ample deformation capacity is anticipated, as no instability is expected to arise.

3.4.6 Block tearing resistance - Top beam flange

Due to the tensile forces acting on the top flange of the beam, there is a potential risk of block tearing. This risk is primarily attributed to the lack of double symmetry in the beam section. The presence of the web on only one side results in asymmetric stiffness, which increases the likelihood of block tearing in the outstand flange. Therefore, in addition to verifying the bearing capacity of the beam flange, a separate check must be performed to ensure that block tearing does not govern the failure mode.

According to NBN EN1993-1-8:2024 standard, block tearing is decomposed into two simultaneous failure modes: tension and shear. Given that the beam flange is subjected to uniform tension, it is assumed that the tension is uniformly distributed over the tension area, as illustrated in Figure 3.22.

The beam flange behaves as a cleat, as shown in Figure 3.23.

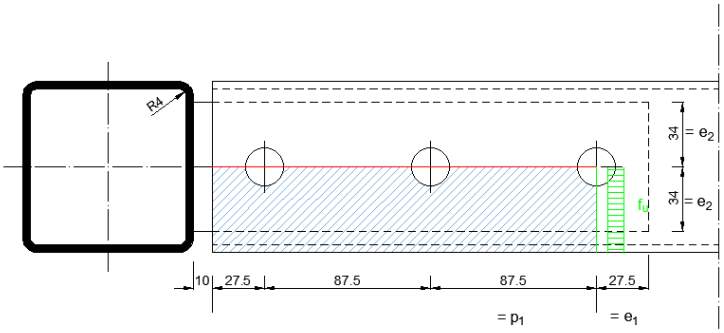

Figure 3.22: Beam flange - Block tearing

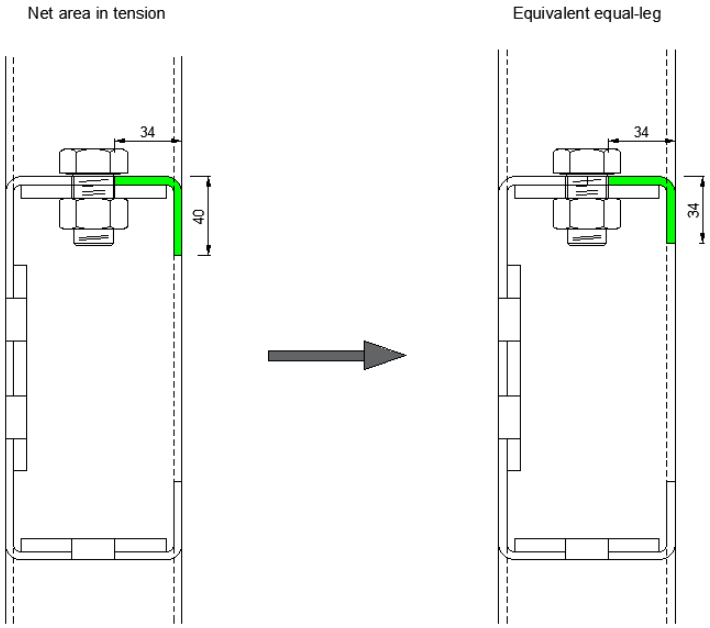

Figure 3.23: Block Tearing: Equivalent Net Tension Area – Elevation View

The net tension area is determined based on an equivalent cleat section, in which the stiffener leg (initially 40 mm) is effectively reduced to $\frac{b-d_0}{2}$. According to Eurocode provisions, an "equivalent equal-leg angle with leg length equal to the smaller leg" should be considered for unequal-leg angle connected by its smaller leg.

This adjustment reflects a conservative assumption that, under tensile loading, stress distribution is limited to the length of the connected leg. Consequently, the net tension area is given by:

$$A_{nt} = \left(\frac{b-d_0}{2}\right) \cdot t_f + \left(\frac{b-d_0}{2} - t_f\right) \cdot t_w$$

$$A_{nt} = \left(\frac{90-22}{2}\right) \cdot 4 + \left(\frac{90-22}{2} - 4\right) \cdot 4 = 256\,\text{mm}^2$$

The gross and net shear areas are calculated as:

$$A_{gv} = (e_1 + 2 \cdot p_1) \cdot t_f = (27.5 + 2 \cdot 87.5) \cdot 4 = 810\,\text{mm}^2$$

$$A_{nv} = (e_1 + 2 \cdot p_1 - 2.5 \cdot d_0) \cdot t_f = (27.5 + 2 \cdot 87.5 - 2.5 \cdot 22) \cdot 4 = 590\,\text{mm}^2$$

Assuming uniform stress distribution within the tension area, the block tearing resistance is evaluated as:

$$V_{eff,1,Rd} = \frac{A_{nt} \cdot f_u + \min\left(\frac{A_{gv} \cdot f_y}{\sqrt{3}}, \frac{A_{nv} \cdot f_u}{\sqrt{3}}\right)}{\gamma_{M2}}$$

$$V_{eff,1,Rd} = \frac{256 \cdot 360 + \min\left(\frac{810 \cdot 235}{\sqrt{3}}, \frac{590 \cdot 360}{\sqrt{3}}\right)}{1.25 \cdot 1000} = 161.7\,\text{kN}$$

3.4.7 Sleeve wall Chord plastification and chord punching shear

This component is associated with the deformation induced in the two plates connected to the beam flanges as they transfer tension or compression to the face of the steel sleeve.

The verification of the connection between a plate in tension (or compression) and a rectangular hollow section (RHS) chord is carried out in accordance with the recommendations of NBN EN 1993-1-8:2024. In this case, the connection is checked for two main failure modes:

- **Chord wall plastification**, which occurs when the transverse force introduced by the plate leads to yielding of the chord wall. This limit state ensures that the local plastic deformation of the chord wall remains within acceptable limits.
- **Chord punching shear**, which refers to the potential failure of the chord wall due to shear around the loaded area. This check ensures that the force transmitted through the plate does not cause local punching failure of the RHS wall.

These checks are essential to ensure the local integrity of the RHS chord and the safe transfer of forces through the connection. The following calculations apply the relevant expressions from the Eurocode, accounting for the geometry and material properties of both the plate and the RHS profile.

The design chord plastification is given by:

$$N_{1,\mathrm{Rd}} = \frac{2.3 \cdot C_{\mathrm{f}} \cdot f_{\mathrm{y0}} \cdot t_0^2 \left(1 + 3\beta^2\right) \cdot \gamma^{0,35} \cdot Q_{\mathrm{f}}}{\gamma_{\mathrm{M5}}} \tag{3.9}$$

where

- the material factor, C_{f}, equal to 1 for $f_y < 355MPa$.
- the chord stress function, Q_f is written as

$$(1 - |n_0|)^{C_1} \geq Q_{min}$$

with $Q_{min} = 0.3$ for transverse plate connected to RHS and exponent C_1 for joint configurations with chords loaded in compression, $C_1 = 0.03\gamma$, and in tension, $C_1 = 0.1$. Note that n_0 is negative in compression and $n_0 \geq 0$ under tension. Under static theorem, the plate is not subjected to bending, then

$$n_0 = \underbrace{\frac{N_{0,\mathrm{Ed}}}{A_0 f_{\mathrm{y0}}}}_{=0 \text{ no compression for roof joint}} \pm \underbrace{\frac{M_{\mathrm{ip,0,Ed}}}{W_{\mathrm{ip,pl,0}} f_{\mathrm{y0}}}}_{=0 \text{ no bending moment in the plate}}$$

$$n_0 = 0$$

Hence, $Q_f = 1.0$.

- The width ratio, β, given by the ratio between the plate width and the connected RHS width, $\frac{b_p}{b_0} = \frac{68}{90} = 0.76$.
- The chord slenderness, γ, given by the RHS geometry, $\frac{b_0}{2t_0} = \frac{90}{2 \cdot 4} = 11.25$.
- The safety factor related to resistance of joints in hollow section lattice girder, $\gamma_{M5} = 1.0$ (cfr. Eurocode 1).

The obtained resistances are:

- **Plate 1 in tension** :

$$N_{1,t,\mathrm{Rd}} = \frac{2.3 \cdot 235 \cdot 4^2 \cdot \left(1 + 3 \cdot 0.76^2\right) \cdot 11.25^{0,35} \cdot 1.0}{1.0 \cdot 1000} = 54.7\,kN$$

- **Plate 2 in compression** :

$$N_{1,c,\mathrm{Rd}} = \frac{2.3 \cdot 235 \cdot 4^2 \cdot \left(1 + 3 \cdot 0.76^2\right) \cdot 11.25^{0,35} \cdot 1.0}{1.0 \cdot 1000} = 54.7\,kN$$

Chord punching shear must be verified when the condition $b_{\mathrm{plate}} \geq b_{\mathrm{sleeve}} - 2t_0$ is not satisfied, where $b_{\mathrm{plate}} = 68$ mm, $b_{\mathrm{sleeve}} = 90$ mm, and $t_0 = 4$ mm. As this condition is partially fulfilled, there is a potential risk of punching shear occurring in specific cases where the following inequality is not satisfied:

$$\frac{N_{1,\mathrm{Ed}}}{A_1} + \frac{M_{\mathrm{ip},1,\mathrm{Ed}}}{W_{\mathrm{ip,el},1}} + \frac{M_{\mathrm{op},1,\mathrm{Ed}}}{W_{\mathrm{op,el},1}} \leq \frac{2}{\sqrt{3}} C_{\mathrm{f}} \frac{f_{\mathrm{y}0}}{\gamma_{\mathrm{M5}}} \frac{t_0}{t_1} \tag{3.10}$$

In the current configuration, both $M_{\mathrm{ip},1,\mathrm{Ed}}$ and $M_{\mathrm{op},1,\mathrm{Ed}}$ are equal to zero, as the plate is not subjected to any bending moment. Consequently, Equation 3.10 simplifies to:

$$N_{1,\mathrm{Ed}} \leq \frac{2}{\sqrt{3}} C_{\mathrm{f}} \frac{f_{\mathrm{y}0}}{\gamma_{\mathrm{M5}}} \frac{t_0}{t_1} A_1 \tag{3.11}$$

In other words, punching shear may occur if the axial force in the plate exceeds the right-hand side of the above expression, which corresponds to a resistance of 73.8 kN.

b) Stiffness

According to reference [8], "A model for the initial stiffness of the face plate component", the stiffness of a face plate loaded in tension or compression by horizontal plate depends on the rotational stiffness provided by the other face plates. This rotational stiffness must differ from the configuration. Figure 3.24a and 3.24b show the deformed shape of the RHS column when its face are subjected, respectively, to tension for the top plate, and to compression for the bottom plate.

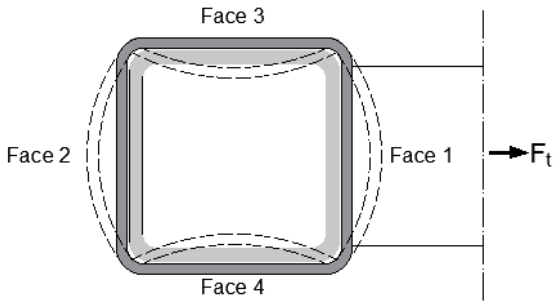

(a) Deformed shape of the RHS sleeve when horizontal plate transmits tension

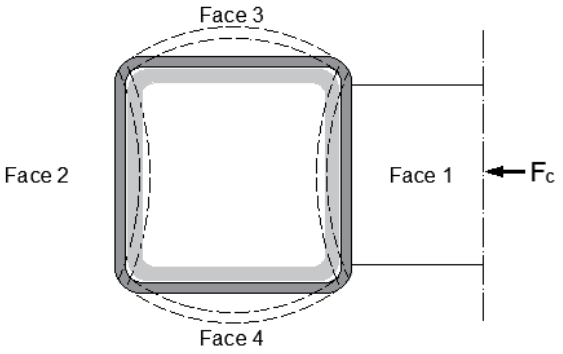

(b) Deformed shape of the RHS sleeve when horizontal plate transmits compression

Figure 3.24: Comparison of deformed shapes under tension and compression

Under tension, Face 1 and Face 2, as shown in Figure 3.24, bend outward from the right-hand side (RHS). In contrast, Face 3 and Face 4 bend inward from the RHS, which is considerably stiffer due to the presence of the inner column inside the steel sleeve. As a result, since Face 3 and Face 4 are restrained by the inner column, their contribution to the rotational stiffness at the edge of Face 1 approaches infinity.[11]. Under these conditions, when the plate transmits tension through Face 1, the rotational stiffness at the edge of this face is assumed to tend to infinity, effectively modeling a fixed configuration.

On the other hand, under compression, Faces 1 and Face 2 bend inward within the steel sleeve. The stiffness of these faces is enhanced by the presence of the inner column. In this case, Face 1 carries half of the compressive force, with the other half being transferred to the face of the inner column. This assumption arises from the fact that there is no continuity between the faces of the two elements[12]. Thus, the stiffness provided by the inner column is sufficient to model the rotational stiffness at the edge of Face 1 as infinite.

Consequently, the sleeve wall may be idealized as a surface with rotational stiffness approaching infinity along its boundary, as illustrated in Figure 5.12.

[11]This assumption is based on the idealization that the stiffness is between a pinned and fixed configuration. A more accurate representation of partial fixity can be obtained through finite element analysis, as demonstrated in reference [2].

[12]If continuity existed between the faces, the load would be transmitted through a thickness equal to the sum of the thicknesses of the two faces.

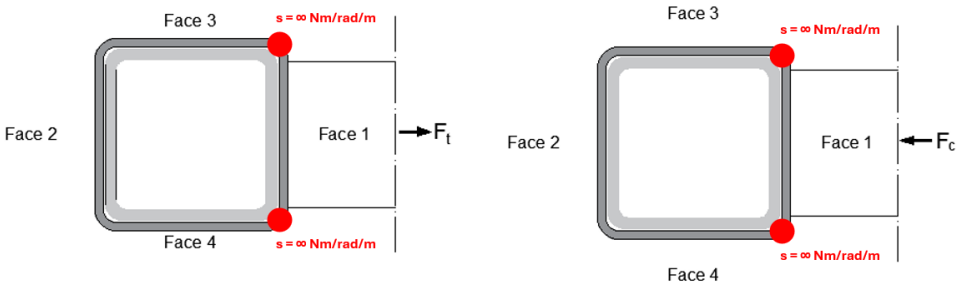

Figure 3.25: Representation of a face with rigid rotational boundary conditions

The analytical approach presented in Reference [2], which assumes a fully fixed-edge condition, can be outlined as follows:

$$K_{D,fixed} = \frac{E}{1-\nu^2}\frac{t^3}{n^3} \tag{3.12}$$

where

ν is the poisson coefficient related to steel, 0.33

t the thickness of the face, 4mm

n the distance of the horizontal plate to the edge of the RHS face, 3mm

The column face stiffness, for both tension and compression, is equal to 558.6 kN/m. The stiffness coefficient of the column face in tension or in compression is equal to 2.7mm ($k_{t,c} = k_{c,c}$).

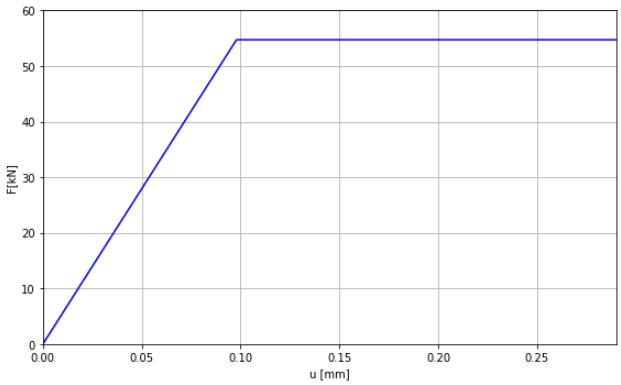

Figure 3.26: Load-Deformation behaviour of the RHS sleeve face

c) Deformation capacity

Since the chord plastification resistance is lower than the punching shear resistance, the governing failure mode of this component is ductile in nature.

3.4.8 Sleeve faces in shear

a) Resistance

The design resistance related to a panel in shear is given by

$$V_{wp,Ed} = \frac{0.9 \cdot f_{y,wc} \cdot A_{v,c}}{\sqrt{3} \cdot \gamma_{M0}} \tag{3.13}$$

in which

- The shear area of the column face is given by: $A_{v,c} = (90 - 2 \cdot 4 - 2 \cdot 4) \cdot 4 = 296mm^2$.
- The design yield strength of the column's steel, $f_{y,wc}$, equals to 235 MPa.
- The partial safety factor, γ_{M0}, is equal to 1.0.

Replacing those factors in equation 3.13, the design resistance in shear for the two panels of the column is $72.3kN$. Indeed, there are two faces resisting to the shear induced, in the column faces, due to top tension and top compression transmitted from Plate 1 and Plate2 to the column.

Note that the equation 3.13 is used only for column web panels that satisfy the following condition[13]:

$$\frac{h_{\mathrm{wc}}}{t_{\mathrm{wc}}} \leq 72 \frac{\varepsilon}{\eta}$$

where

h_{wc} clear depth of the column web measured between the flanges;

t_{wc} column web thickness;

$\varepsilon = \sqrt{\frac{235}{f_{\mathrm{y}}}}$ with f_{y} in $\left[\mathrm{N/mm^2}\right]$

η assumed equal to 1.2.

The panel's slenderness is then $\frac{h_{\mathrm{wc}}}{t_{\mathrm{wc}}} = \frac{90-2\cdot4-2\cdot4}{4} = 18.5$, while the comparative term $72 \cdot \frac{\sqrt{\frac{235}{235}}}{1.2} = 60$. Then, the slenderness limit is respected.

b) Stiffness

The stiffness coefficient of an unstiffened column web panel is provided by the expression:

$$k_{v,c} = \frac{0.38 \cdot A_{vc}}{\beta \cdot z} \tag{3.14}$$

with β equals to 1 as recommended in EN 1993-1-8 for one side column-beam joint configurations and z, the effective length of the column web . Thus, for two faces resisting in shear:

$$k_{v,c} = 2 \cdot \frac{0.38 \cdot 296}{1 \cdot 74} = 3$$

[13]This additional verification serves to ensure that the web is not susceptible to buckle, particularly due to its slenderness.

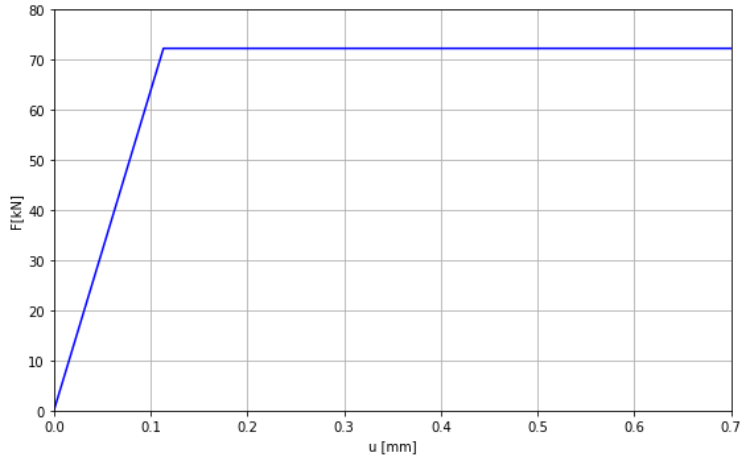

Figure 3.27: Column faces in shear stiffness

c) Deformation capacity

The expected deformation capacity of the steel web is considered sufficiently high to classify this component as ductile. As noted in [3], "the deformation capacity of steel column web panels is recognised as being high". Therefore, plastic redistribution between components requiring ductility can be accommodated by the shear panel without significant risk.

3.4.9 Bolts in Shear – Beam Web / Plate 3

Figure 3.9 illustrates Plate 3, which features two M20 bolts. Bolts of class 10.9 are employed, ensuring consistency with those used in flange connections. Plate 3 possesses similar mechanical properties to Plates 1 and 2. The shear resistance of a single M20 bolt has been determined in Section 3.4.1 as $F_{v,Rd} = 98\,\text{kN}$. Considering one shear plane and two bolts engaged in shear, the total shear resistance is:

$$F_{\text{tot},v,Rd} = n \cdot m \cdot F_{v,Rd} = 2 \cdot 1 \cdot 98 = 196\,\text{kN}$$

At the beginning of this present thesis, the loads applied on the roof were not well known. During this chapter, it is assumed that the shear force supported by the joint is equal to the resistance in shear of the supported beam which is approximately 104 kN.

3.4.10 Plate 3 in Bearing

The methodology for evaluating the bearing resistance of Plate 3 follows that described in Section 3.4.2. The edge distance in the direction of loading is $e_1 = 37.5\,\text{mm}$, and the vertical spacing between bolt rows is $p_1 = 75\,\text{mm}$. The resistance is calculated as follows:

- Material coefficient: $k_m = 1$ (Plate 3 is made of S355 steel).
- End bolts:

$$\alpha_{\text{b,end}} = \min\left(\frac{e_1}{d_0}, 3 \cdot \frac{f_{\text{ub}}}{f_u}, 3\right) = \min\left(\frac{27.5}{22}, 3 \cdot \frac{1000}{490}, 3\right) = 1.7$$

$$F_{b,Rd,\text{end}} = \frac{k_m \cdot \alpha_{\text{b,end}} \cdot f_u \cdot d \cdot t}{\gamma_{\text{M2}}}$$

$$F_{b,Rd,\text{end}} = \frac{1 \cdot 1.7 \cdot 510 \cdot 20 \cdot 8}{1.25 \cdot 1000} = 111\,\text{kN}$$

- Inner bolts:

$$\alpha_{\text{b,inner}} = \min\left(\frac{p_1}{d_0} - 0.5,\, 3 \cdot \frac{f_{\text{ub}}}{f_u},\, 3\right) = \min\left(\frac{75}{22} - 0.5,\, 3 \cdot \frac{1000}{490},\, 3\right) = 2.9$$

$$F_{b,Rd,\text{inner}} = \frac{k_m \cdot \alpha_{\text{b,inner}} \cdot f_u \cdot d \cdot t}{\gamma_{\text{M2}}}$$

$$F_{b,Rd,\text{inner}} = \frac{1 \cdot 2.9 \cdot 510 \cdot 20 \cdot 8}{1.25 \cdot 1000} = 189\,\text{kN}$$

Among the two bolts,one is classified as inner bolt and the other as end bolt (refer to Figure 3.28).

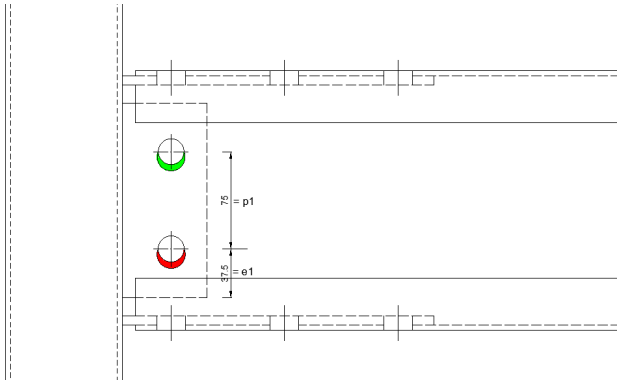

Figure 3.28: Plate 3 in bearing : Inner bolt (in green) and End bolt (in red)

Thus, the total bearing resistance is:

$$F_{b,Rd,\text{tot}} = F_{b,Rd,\text{end}} + F_{b,Rd,\text{inner}} = 111 + 189 = 300\,\text{kN}$$

3.4.11 Beam Web in Bearing

As illustrated in Figure 3.29, the edge distance is $e_1 = 62.5\,\text{mm}$. As the beam is made of S235 steel, the bearing resistance is computed as:

- $k_m = 1$.
- End bolts:

$$\alpha_{\text{b,end}} = \min\left(\frac{e_1}{d_0},\, 3 \cdot \frac{f_{\text{ub}}}{f_u},\, 3\right) = \min\left(\frac{62.5}{22},\, 3 \cdot \frac{1000}{360},\, 3\right) = 2.8$$

$$F_{b,Rd,\text{end}} = \frac{1 \cdot 2.8 \cdot 360 \cdot 20 \cdot 4}{1.25 \cdot 1000} = 64.5\,\text{kN}$$

- Inner bolts:

$$\alpha_{\text{b,inner}} = \min\left(\frac{p_1}{d_0} - 0.5, 3 \cdot \frac{f_{\text{ub}}}{f_u}, 3\right) = \min\left(\frac{75}{22} - 0.5, 3 \cdot \frac{1000}{360}, 3\right) = 2.9$$

$$F_{b,Rd,\text{inner}} = \frac{1 \cdot 2.9 \cdot 360 \cdot 20 \cdot 4}{1.25 \cdot 1000} = 66.8\,\text{kN}$$

Thus, the total bearing resistance of the beam web is:

$$F_{b,Rd,\text{tot}} = 64.5 + 66.8 = 131.3\,\text{kN}$$

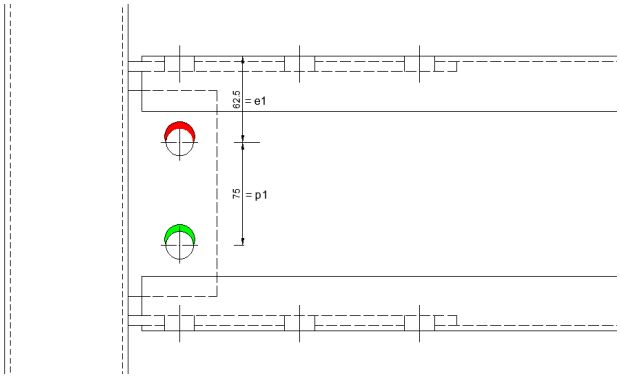

Figure 3.29: Beam web in bearing : Inner bolt (in green) and end bolt (in red)

3.4.12 Plate 3 in Shear

According to the NBN 1993 1-8:2024 Annex C recommendations, the design shear resistance of the fin plate should be taken as the smallest of the following design resistance values: the gross section in shear, the net section in shear, and block tearing.

- **Gross section in shear** :

$$V_{v,p,Rd} = \frac{A_{v,fp} \cdot f_{y,fp}}{1.27 \cdot \sqrt{3} \cdot \gamma_{M0}} \tag{3.15}$$

$$V_{v,p,Rd} = \frac{150 \cdot 8 \cdot 355}{1.27 \cdot \sqrt{3} \cdot 1.0 \cdot 1000} = 193.7\,\text{kN}$$

- **Net section in shear** :

$$V_{u,fp,Rd} = \frac{A_{v,net,fp} \cdot f_{u,fp}}{\sqrt{3} \cdot \gamma_{M2}} \tag{3.16}$$

$$V_{u,fp,Rd} = \frac{(150 - 2 \cdot 22) \cdot 8 \cdot 510}{\sqrt{3} \cdot 1.25 \cdot 1000} = 199.8\,\text{kN}$$

- **Block tearing** : In the presence of shear, block tearing may occur.
  The net tension area is:

$$A_{nt} = (e_2 - 0.5 \cdot d_0) \cdot t_p = (27.5 - 0.5 \cdot 22) \cdot 8 = 132\,\text{mm}^2$$

The gross and net shear areas are:

$$A_{gv} = (e_1 + p_1) \cdot t_p = (37.5 + 75) \cdot 8 = 900\,\text{mm}^2$$

$$A_{nv} = (e_1 + p_1 - 1.5 \cdot d_0) \cdot t_p = (37.5 + 75 - 1.5 \cdot 22) \cdot 8 = 636\,\text{mm}^2$$

Considering a non-uniform distribution of tension in the tensile area, the design block tearing resistance is given by:

$$V_{eff,1,Rd} = \frac{0.5 \cdot A_{nt} \cdot f_u + \min\left(\frac{A_{gv} \cdot f_y}{\sqrt{3}}, \frac{A_{nv} \cdot f_u}{\sqrt{3}}\right)}{\gamma_{M2}} = 174.5\,\text{kN}$$

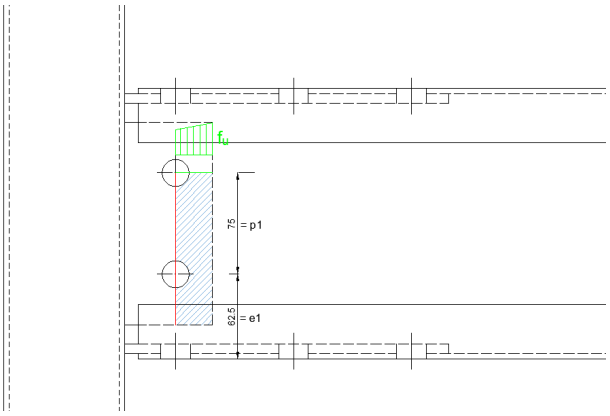

Figure 3.30: Plate 3 - Block tearing

3.4.13 Assembling of the components

The joint resistance is determined by the components contributing in the bending resistance. Those are enumerated in the table 3.7.

Component	Resistance [kN]
Bolt in shear (beam flange)	294.0
Plate 1 and 2 in bearing	473.3
Beam flange in bearing	167.0
Plate 1 in tension	168.9
Plate 2 in compression	193.1
Block tearing-Beam flange	161.6
Sleeve face in tension	54.7
Sleeve face in compression	54.7
Sleeve face in shear	72.29

Table 3.5: Computed Results for Bending-Resisting Components

The bending resistance of the joint is determined using the following expression:

$$M_{j,Rd} = z \cdot \min(F_{Rd})$$

In this equation, z denotes the lever arm, which is equal to 192 mm. The minimum component resistance, $\min(F_{Rd})$, is found to be 56.8 kN, corresponding to the plastification of the column face under either tension or compression. Substituting these values into the equation gives:

$$M_{j,Rd} = 192 \cdot 10^{-3} \cdot 54.7 = 10.6\,\text{kNm}$$

Hence, the design moment resistance of the joint is calculated to be 10.5 kNm.

As a reminder, the design objective in terms of resistance is to achieve a joint with a higher moment resistance than that of the connected beam, i.e. 29.6 kNm. As discussed in Section 3.2, this requirement is satisfied when the weakest component of the joint reaches a resistance of 160 kN. However, in the present case, the weakest component only reaches 54.7 kN.

While it is theoretically possible to enhance the mechanical properties of this component to meet the target resistance, the required modifications are not practically viable. Specifically, it would be necessary to upgrade the sleeve's steel grade to S355 and increase the thickness to the maximum value tolerable by DEGOTTE for bending operations, i.e. 6 mm. With these modifications, the resistance of the chord plastification component would reach 161 kN. In this case, the risk of punching shear on the sleeve's face can be disregarded, as it would require an axial force exceeding 167 kN. However, by modifying the wall thickness of the sleeve, the SHS90/5 section currently employed for the sleeve can no longer be fitted over the column. The required clearance of 1 mm between the sleeve and the column would no longer be achieved. A possible improvement would be to replace the current section with an SHS100/8 profile, thereby increasing the sleeve's capacity. Nevertheless, this would significantly complicate the assembly process with the column[14]. If, however, an alternative viable connection method were to be identified, the resistance of this component could increase to 223 kN.

In conclusion, achieving a joint moment resistance higher than that of the beam, is not feasible without altering either the mechanical and geometric properties of the steel sleeve[15].

From the Eurocode perspective, this roof joint can be classified as fully-strength joint, as its moment resistance exceeds that of at least one of the connected members. In this case, the joint moment resistance is greater than the bending resistance of the column SHS80/5, which is equal to 9.3 kNm.

3.4.14 Rotational stiffness

The stiffness coefficients of the various components contributing to the overall rotational stiffness have been calculated in the preceding sections. Final results are recapitulated in table 3.6.

[14] At present, the connection between the sleeve and the column is intended to be made using a full penetration weld.

[15] It is worth recalling that the sleeve is of type SHS90/4 with steel grade S235.

Section	Component	Stiffness [mm]
3.4.1	Bolt in shear (beam flange)	$k_v = 2.86$
3.4.2	Plate 1 and 2 in bearing [16]	$k_{PB} = 1.1$
3.4.3	Beam flange in bearing [17]	$k_{FB} = 0.39$
3.4.4	Plate 1 in tension	$k_t = \infty$
3.4.5	Plate 2 in compression	$k_c = \infty$
3.4.7	Sleeve face in tension	$k_{t,c} = 2.7$
3.4.7	Sleeve face in compression	$k_{c,c} = 2.7$
3.4.8	Sleeve face in shear	$k_{v,c} = 3$

Table 3.6: Elastic stiffnesses of the components involved in bending flexibility

According to the component method, the rotational response of a joint is based on the mechanical properties of its different constitutive components. By decomposing the joint into relevant components, it is possible to compute the mechanical properties of any joint. However, as specified in corresponding section, some components are assumed to be included in the deformations of the beam and, consequently, there are not contributing in the flexibility of the joint. Those components are beam flange in tension and beam flange in compression.

The initial stiffness $S_{j,ini}$ is derived from the elastic stiffnesses of the components presented in table 3.6. The load-deformation relationship of extensional spring, which represent elastic behaviour of each component, is given by:

$$F_i = k_i \cdot E \cdot \Delta_i \tag{3.17}$$

in which:

- F_i is the force in the spring i;
- k_i is the stiffness coefficient of the component i (cfr. table 3.6);
- E is the Young modulus;
- Δ_i is the deformation of the spring i;

Then, a spring model is used to combine the component elastic stiffnesses of components as illustrated in figure 3.31.

[16] As a reminder, the stiffness considered is that of Model 1 proposed by Jaspart, as the force transmitted through the bolt holes is, at this stage, unknown.

[17] The Jaspart model is also considered in this context.

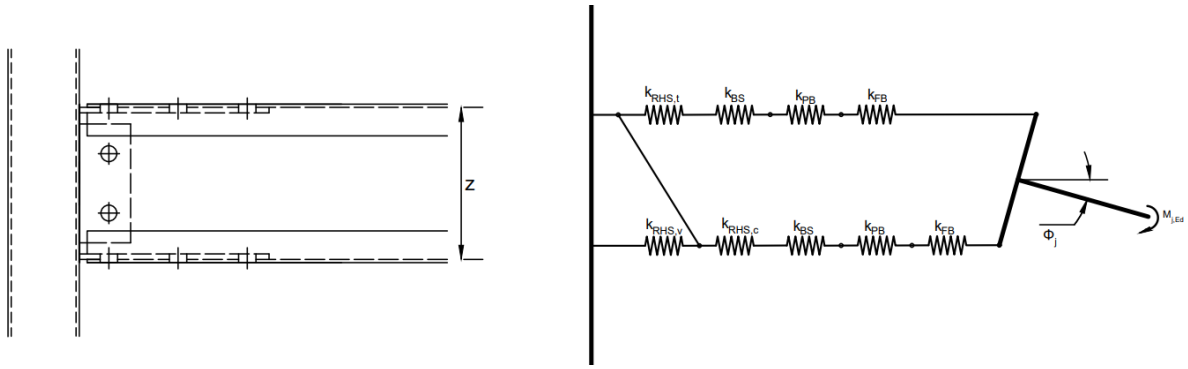

Figure 3.31: Spring model

All springs are desposed in series in a such way that the force in each spring is equal to F. The moment M_{Ed} acting on the spring model is equal to $F \cdot z$, where z is the distance between the shear plan of top and bottom bolts connecting Plate 1 and 2 to the beam flanges. The rotation ϕ in the joint is obtained by summing the ratio between each spring displacement and z. Thus,

$$S_{j,ini} = \frac{M_{Ed}}{\phi} = \frac{F \cdot z}{\frac{\sum_i \Delta_i}{z}} \tag{3.18}$$

Using equation 3.17, it follows:

$$S_{j,ini} = \frac{F \cdot z^2}{\frac{F}{E} \cdot \sum_i \frac{1}{k_i}} = \frac{E \cdot z^2}{\sum_i \frac{1}{k_i}} = E \cdot z^2 \cdot k_{eq} \tag{3.19}$$

By disposing the components spring in series, their equivalent stiffness is given by:

$$\frac{1}{k_{eq}} = \frac{1}{k_{BS}} + \frac{1}{k_{PB}} + \frac{1}{k_{FB}} + \frac{1}{k_t} + \frac{1}{k_c} + \frac{1}{k_{t,c}} + \frac{1}{k_{c,c}} + \frac{1}{k_{v,c}}$$

$$\frac{1}{k_{eq}} = \frac{1}{2.86} + \frac{1}{1.1} + \frac{1}{0.39} + \frac{1}{\infty} + \frac{1}{\infty} + \frac{1}{2.7} + \frac{1}{2.7} + \frac{1}{3}$$

$$k_{eq} = 0.2 \text{ mm}$$

Injecting this equivalent stiffness in equation 3.19 gives a rotational stiffness of the joint equal to 1581 kN.m/rad.

In accordance with the provisions of the Eurocode, the joint can be classified as semi-rigid, as it satisfies the following condition:

$$S_{j,\text{ini}} \leq 8 \cdot \left(\frac{EI}{L}\right)_{\text{Roof beam}} = \frac{8 \cdot 3.76 \cdot 10^8}{10^6} = 3008 \text{ kNm/rad}$$

This classification is made under the assumption that the overall structure behaves as a rigid frame[18].

[18] In Chapter 4, it will be rigorously established that the structure is classified as rigid irrespective of the type of joint employed.

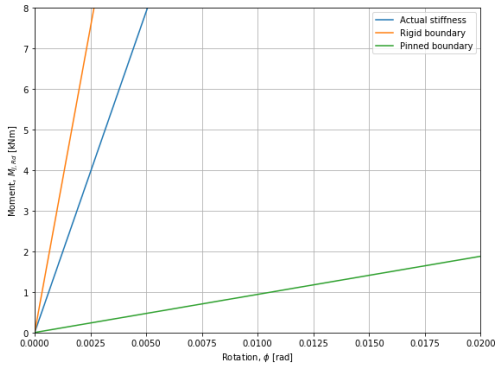

Figure 3.32: *Option 1-A* classification based on rotational stiffness

From the perspective of deformation capacity, the selected assembly is considered ductile, as the governing component in the design process, namely, the plastification of the wall chord, exhibits ductile behaviour. The design assumptions involving the static theorem are therefore satisfied.

3.5 Option 1-b

An other configuration has been imagined where M12 bolts have been used in order to have two bolts per bolt row. This ensure a better stiffness than the configuration with simple bolt rows. Moreover, by employing two rows of bolts, the width of the plates is increased, thereby maximising their resistance to both tension and compression. However, this configuration also results in a significant reduction in the overall length of the plates. This would be advantageous for the stacking of these connector elements.

The conception retained in the aim of reaching rigid joint is illustrated in figure 3.33 and 3.34.

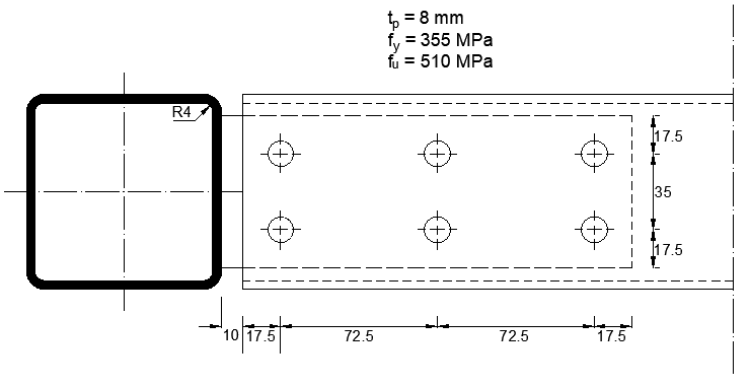

Figure 3.33: Beam flange to plate connection

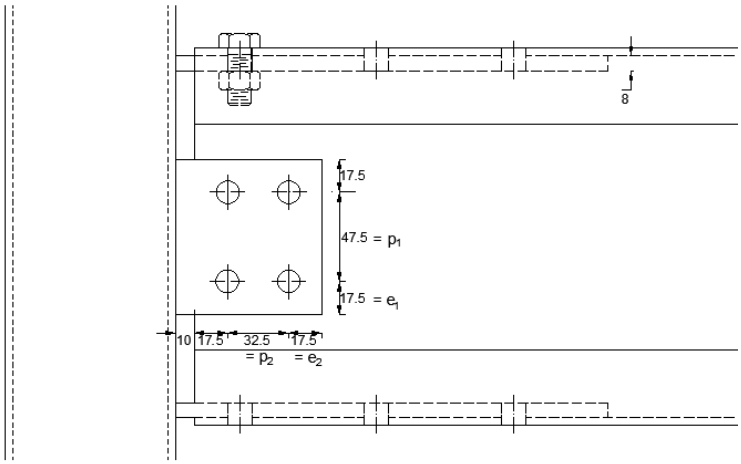

Figure 3.34: Beam web to plate connection

The component method is also used to extract the resistance of every component. The final result are given in table 5.23. In Annex A, every detail are given to demonstrate these results.

Component	**Resistance [kN]**
Bolt in shear (beam flange)	202.3
Plate 1 and 2 in bearing	575.5
Beam flange in bearing	203.5
Plate 1 in tension	161.6
Plate 2 in compression	198.8
Block tearing-Plate 1	498.1
Block tearing-Beam flange	166.4
Sleeve face in tension	56.8
Sleeve face in compression	56.8
Sleeve face in shear	72.3

Table 3.7: Computed Results for Bending-Resisting Components

The resistance of the joint is equal to 10.9 kN.m. This resistance is lower than that of the roof beam, as indicated by the study of DEGOTTE; nevertheless, the joint is classified as a fully-strength joint, because this moment capacity surpasses the column's plastic resistance

The assembly thus exhibits a mode of ductile failure, as the dimensioning component remains the chord plastification of the sleeve, which, as a reminder, is ductile in nature.

The other components in the shear resistance of the joint are given in the table below.

Components	Resistance [kN]
Bolt in shear beam web	134.9
Plate 3 in bearing	340.5
Beam web in bearing	165.9
Plate 3 in shear	106.5
Block tearing plate 3	135.0

Table 3.8: Resistances of components involved in the shear resistance of the joint

The stiffness coefficient corresponding to each component are given in table 3.9.

Components	Stiffness [mm]
Bolt in shear (beam flange)	2.06
Plate 1 and 2 in bearing	1.36
Beam flange in bearing	0.48
Plate 1 in tension	∞
Plate 2 in compression	∞
Sleeve face in tension	8.98
Sleeve face in compression	8.98
Sleeve face in shear	3.04

Table 3.9: Stiffness coefficient results

Based on the analytical model outlined in Section 3.4.14, the rotational stiffness of the joint is calculated to be 2000 kN·m/rad. This value classifies the joint as semi-rigid, in accordance with standard stiffness classification, as depicted in the figure below.

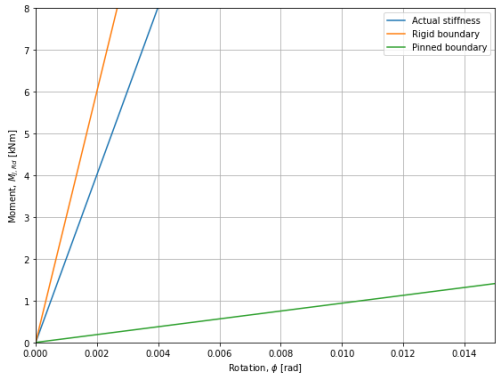

Figure 3.35: *Option 1-B* classification based on rotational stiffness

3.6 Option 2

The latest configuration reflects an assembly technique that simplifies the mounting process. Instead of using individual plates, a channel section is used which enable a continuous weld with the steel sleeve, see Figure 3.38.

This assembly configuration will be tested using a single row of bolts, as the presence of the oblique fillet may complicate the positioning of a double row. Nonetheless, it is entirely feasible to employ M12 bolts in a double-row arrangement. However, for the purposes of this study, *Option 2* will be exclusively tested with a single row of bolts in order to avoid any potential issues associated with the fillet transition. In this context, M12 bolts are initially tested to provide maximum shear resistance over a short length. The specifications and characteristics of the tested assembly are presented in the various views shown below.

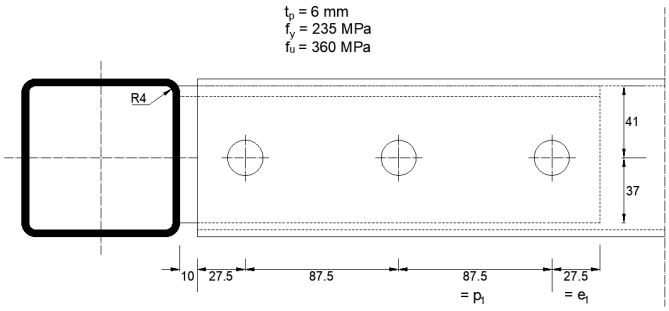

Figure 3.36: Beam flange/ support flange connexion : Constructive dispositions

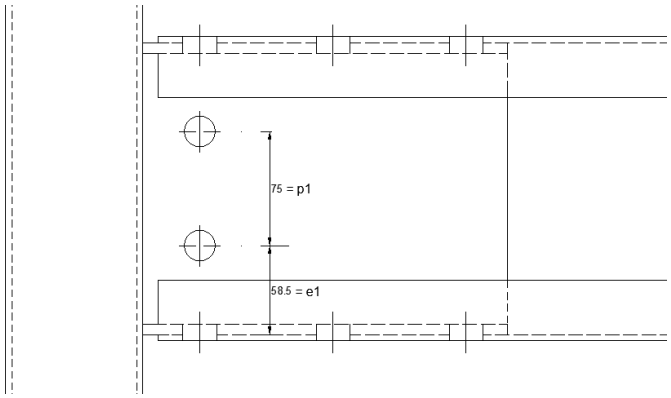

Figure 3.37: Beam flange/ support flange connexion : Constructive dispositions

Figure 3.38: Channel section configuration welded on RHS steel sleeve

Components	Resistance [kN]
Bolt in shear (beam flange)	294.0
Plate 1 and 2 in bearing	250.6
Beam flange in bearing	167.0
Plate 1 in tension	193.8
Plate 2 in compression	202.6
Block tearing in Plate 1	176.8
Block tearing in beam flange	161.6
Plate 1 - Chord plastification (tension)	65.6
Plate 2 - Chord plastification (compression)	65.6
Sleeve face in shear	72.29

Table 3.10: Resistances of components involved in overall bending resistance of the joint

The resistance in flexion of this joint configuration is equal to 12.6 kN.m. Although this resistance remains lower than that of the beam subjected to strong axis bending, it is still greater than that of the column. Therefore, the assembly can be classified as fully-strength joint. And, the failure mode of this joint assembly is controlled by ductile component behaviour.

The four other components in the shear resistance of the joint are given in the table below.

Components	Resistance [kN]
Bolt in shear beam web	196.0
Plate 3 in bearing	192.4
Beam web in bearing	132.5
Plate 3 in shear	141.6

Table 3.11: Resistances of components involved in the shear resistance of the joint

The stiffness coefficient corresponding to each component are given in table 5.23 and were found based on EN NBN 1993-1-8:2024.

Components	Stiffness [mm]
Bolt in shear (beam flange)	2.86
Plate 1 and 2 in bearing	0.59
Beam flange in bearing	0.39
Plate 1 in tension	∞
Plate 2 in compression	∞
Plate 1 - chord plastification (tension)	8.98
Plate 2 - chord plastification (compression)	8.98
Sleeve face in shear	3.04

The rotational stiffness of the joint is calculated to be 1497.6 kNm/rad. As illustrated in the figure below, the joint is classified as semi-rigid, in accordance with standard joint classification criteria.

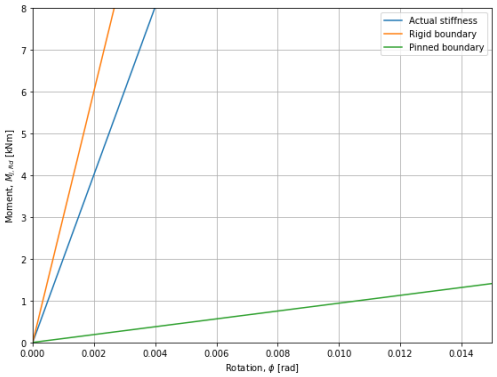

Figure 3.39: *Option 2* classification based on rotational stiffness

3.7 Comparative Analysis of Configurations

In terms of classification, the three configurations provide fully-strength joints and semi-rigid joints exhibiting ductile behaviour. Nevertheless, none of these assemblies can ensure a resistance exceeding that of the beam, as desired by DEGOTTE. Regarding strength, the joint will only fail after the column has collapsed. The beam will be the last component to fail, assuming that other associated phenomena—such as lateral-torsional buckling, local buckling, or similar effects—are disregarded.

From a structural resistance perspective, all three assemblies are limited by the strength of the sleeve face. However, it is noteworthy that certain components exhibit greater stiffness and resistance in *Option 2*, despite the support thickness being only 6 mm and made of S235-grade steel. In comparison, the first two configurations employ isolated flat plates with a thickness of 8 mm and a higher-strength S355-grade steel. Consequently, the material-performance ratio

is more favourable in *Option 2*. Furthermore, this configuration presents advantages in terms of assembly, as welding the C-profile support to the column is simpler and more practical. In contrast, connecting three individual flat plates to the steel sleve requires more handling and operational effort than welding a single C-profile to the sleeve.

Moreover, from a production and utilisation perspective, it would be considerably more advantageous to manufacture a single, unified item rather than multiple separate plates.

In conclusion, *Option 2* appears to be the most compelling choice from several perspectives.

Chapter 4 — Influence of the selected joints solutions on the structural response

4.1 Introduction

In the previous chapter, it was demonstrated that *Option 2* represents the most promising joint configuration. Although the overall resistance of the joint cannot reach that of the beam itself, all components were calibrated with this objective in mind, i.e., $F_{Rd} > 160\,\text{kN}$. As a result, some components exhibit unnecessarily high resistance compared to others, leading to an uneven distribution of internal resistances across the joint. This imbalance is illustrated in Figure 4.1. In this graph, the unity check represents the ratio between the target resistance of 160 kN and the actual resistance achieved within each component.

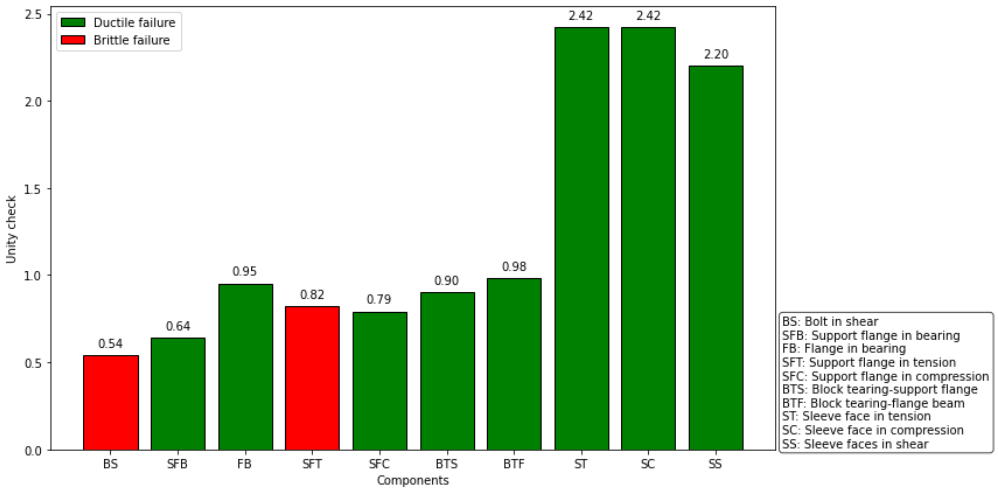

Figure 4.1: Unity check for each component involved in the resistance of *Option 2* joint

This chapter aims to refine the design of the joint in order to achieve a more balanced load distribution among its components, while still ensuring that the assembly can resist the applied moment transfer between the beam and the column. In doing so, it will also be examined how the rotational stiffness of the joint influences the global behaviour of the structure.

It is important to recognize that improving the uniformity of component utilization affects not only the joint's resistance but also its stiffness, which in turn impacts the overall structural response.

Consequently, joint design becomes an iterative process in which both strength and stiffness must be optimized in parallel, as changes to one can significantly influence the other.

The central objective of this chapter is to develop a joint configuration that satisfies two criteria: *optimal resistance* and *optimal stiffness*. These terms are defined more precisely as follows.

A joint with *optimal resistance* is one in which the total moment capacity, $M_{j,Rd}$[1], is nearly reached, and each component is utilized close to its individual capacity. This uniform engagement of components is difficult to achieve, particularly because different components contribute unequally to stiffness and resistance. Another challenge is to ensure that the joint remains ductile in order to validate several assumptions outlined in the previous chapter.

On the other hand, *optimal stiffness* refers to the stiffness value that results in the most favourable structural response. This can be interpreted in several ways. For example:

- One of the aims of a semi-rigid connection is to improve the distribution of bending moments between connected elements, specifically, to reduce the moment in the beam and increase it in the column compared to a pinned connection, leading to a more efficient structural behaviour. Alternatively, in the case of a rigid connection, where the column is stronger due to its need to resist a significant combination of bending moment and axial force (M+N).
- The rotational stiffness also affects the failure modes of the structure. Depending on its magnitude, the overall system may behave more rigidly or more flexibly, with significant implications for structural safety and design. This aspect will be examined in greater detail later in the chapter.

While other evaluation criteria may be relevant, this chapter will focus on the aspects outlined above, as they provide the most direct insight into the structural performance and design optimization of the joint.

The structural frame analysis was performed using the FineLg finite element software, developed jointly by the *Greisch engineering office* and the *University of Liège*. In this study, two types of analyses were conducted: a linear buckling analysis and a geometrically and materially non-linear analysis.

It is worth recalling that other structural analysis methods could also be used, depending on the desired level of precision and modeling complexity:

- **First-order linear elastic analysis** : This is the most basic method, assuming linear elastic material behaviour and small displacements.

[1] $M_{j,Rd}$ or $2/3M_{j,Rd}$, depending on the idealization adopted for $S_{j,ini}$. This will be discussed in detail in a later section.

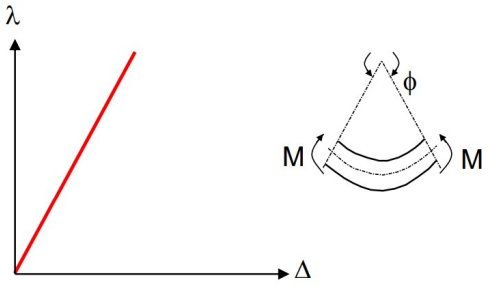

Figure 4.2: First-order linear elastic analysis [9]

- **Linear buckling analysis** : Used to determine the elastic critical load and assess structural stability. This method is particularly relevant for structural classification and is further explained in Section 4.3.

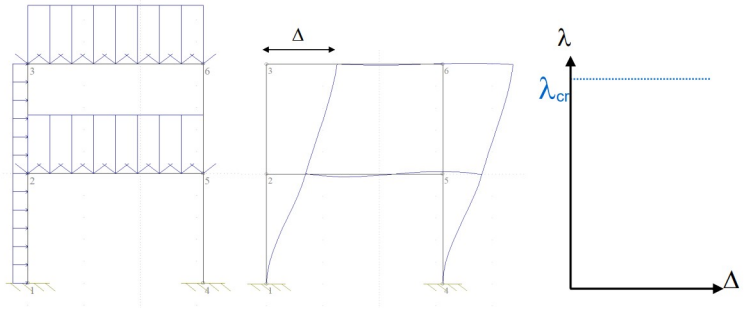

Figure 4.3: Linear buckling analysis [9]

- **Second-order elastic analysis** : This analysis takes into account geometric nonlinearity by solving equilibrium on the deformed configuration, incorporating both $P-\Delta$ and $P-\delta$ effects [2], while assuming the material remains linearly elastic.

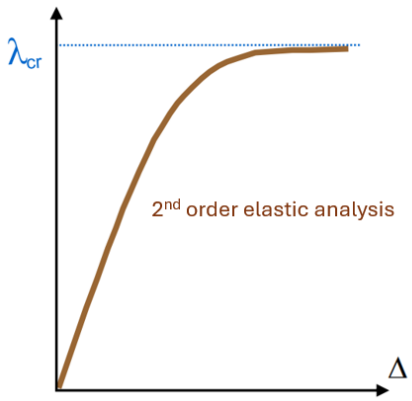

Figure 4.4: Second-order elastic analysis [9]

- **First-order rigid-plastic analysis**: In this idealized approach, elements are considered

[2] $P-\Delta$ represents the global deformations of the structure under loading, whereas $P-\delta$ accounts for the local deformations of the members.

perfectly rigid up to the formation of a plastic mechanism. It is typically used for ultimate limit state evaluations.

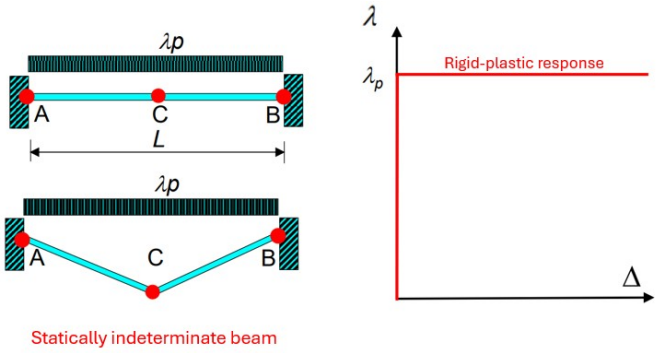

Figure 4.5: First-order rigid-plastic analysis [9]

- **Second-order elasto-plastic analysis**: This comprehensive method considers both material and geometric nonlinearities. It includes the effects of stiffness degradation due to plastic hinge formation, offering a realistic simulation of structural performance up to failure.

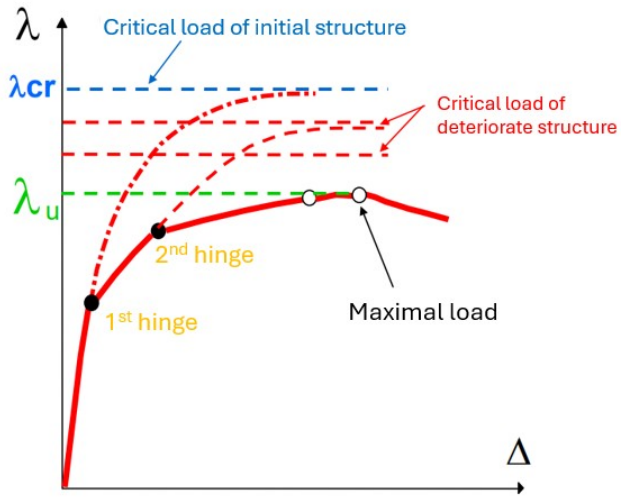

Figure 4.6: Second-order elasto-plastic analysis [9]

The selection of the appropriate frame analysis method depends on three key factors

- Structure class. A 1^{st} order analysis can be carried out if the structure is classified as rigid, i.e $\alpha_{cr} > 10$ for elastic analysis and $\alpha_{cr} > 15$ for plastic analysis.[3] If the structure is classified as flexible, i.e. i.e $\alpha_{cr} < 10$ for elastic analysis and $\alpha_{cr} < 15$ for plastic analysis, a second order analysis is recommended.
- Classification of transversal sections respect to the capacity of the section to develop plasticity or not. This criteria leads to the choice of an elastic or plastic analysis and verification.

[3]The critical multiplier, denoted as α_{cr}, is defined as the ratio of the critical load to the applied load. This parameter is crucial in stability analysis, as it indicates the factor by which the applied load must be multiplied to reach the critical load at which instability occurs. A more detailed discussion of this concept can be found in Section 4.3

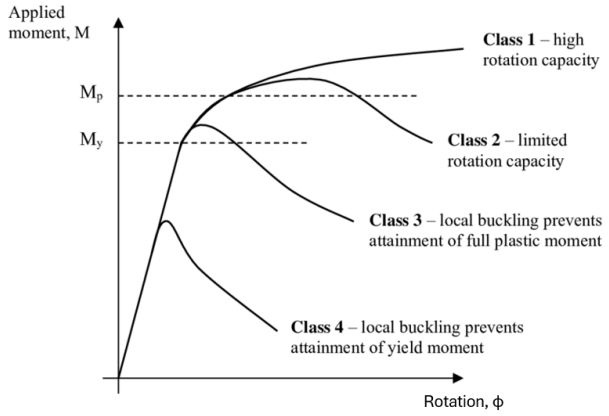

Figure 4.7: Classification of sections under bending

- The software tools and the practical experience of the engineer.

Given that Finelg is capable of performing non-linear analyses that account for both geometrical and material non-linearities, a complete second order analysis is made. Concurrently with this analysis, a linear buckling analysis is also performed to examine the impact of the connection on both local and global instabilities within the structure.

4.2 Structure modelling in FineLg

Before presenting the two types of analysis carried out, it is essential to highlight the key characteristics of the structure and the loads to which it is subjected. As the primary objective of this master thesis is to design an innovative bolted connection for demountable modular structures, the remaining structural aspects will be outlined only briefly in the following sections. The reasoning leading to the load cases will be omitted in this report, in order to maintain the focus of this work on the beam-to-column connection.

The model, illustrated in Figure 4.8, consists of four modules: two at the base level and two at the first floor. Since not all parameters related to the floor system have been defined at this stage, only a two-dimensional analysis will be conducted. This analysis is performed in the direction of the main beam span. It is evident that the overall structural behaviour is inherently three-dimensional, due to the stiffness of the floor system, secondary beams, and other out-of-plane elements. However, a two-dimensional analysis can still provide valuable insight into the structural response.

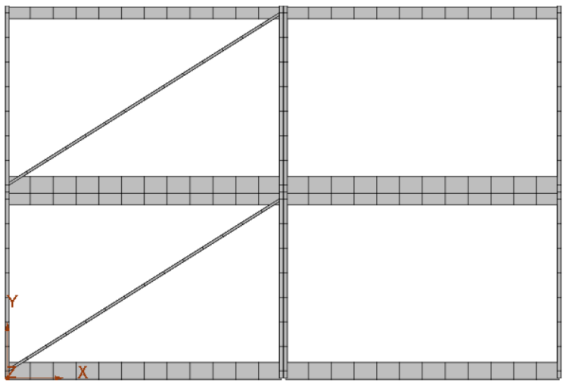

Figure 4.8: FineLg 2D model

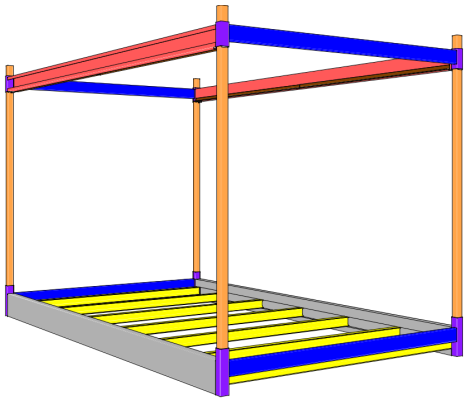

Figure 4.9: 3D view of the modular structure (DEGOTTE)

4.2.1 Structure constitutive members

The demountable modular structures developed by DEGOTTE are based on a rectangular steel framework composed of the following elements:

- The vertical load-bearing elements consist of SHS 80×5 steel columns. Their geometric and mechanical properties are summarized in the table below. The columns are cold-formed and manufactured from S235 structural steel.

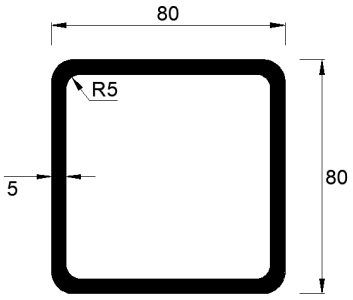

Figure 4.10: SHS80x5 Column cross section

(a) Geometry

Profil	b [mm]	t [mm]	ro [mm]	ri [mm]	A [mm^2]	A_v [mm^2]
SHS 80 / 5	80	5	7.5	5	1473	737

(b) Inertia properties

Profil	I [$\times 10^6$ mm^4]	W_{el} [$\times 10^3$ mm^3]	W_{pl} [$\times 10^3$ mm^3]
SHS 80 / 5	1.366	34.15	41.13

(c) Mechanical resistance and properties

Profil	$N_{pl,Rd}$ [kN]	$V_{pl,Rd}$ [kN]	$M_{el,Rd}$ [kNm]	$M_{pl,Rd}$ [kNm]	Curve	Classe
SHS 80 / 5	346.2	99.94	8.03	9.66	a	1

Table 4.1: Column cross section properties

- Floor beams utilize C310 G-shaped cross-sections, also fabricated from S235 structural steel, selected for their suitability in supporting the modular floor system.

Section	**Steel**	A_g mm^2	I_y mm^4	I_t mm^4	I_w mm^4	$W_{y,el}$ mm^3	$W_{y,pl}$ mm^3	$W_{y,eff}$ mm^3	$M_{c,y,Rd}$ kNm
CR310A	S235	2845	$3.45 \cdot 10^7$	15530	$2.124 \cdot 10^{11}$	$2.2 \cdot 10^5$	$2.83 \cdot 10^5$	$2.27 \cdot 10^5$	66.6

Table 4.2: Geometrical properties of floor beams

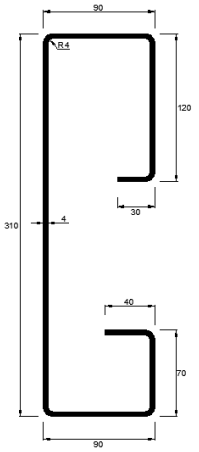

Figure 4.11: Floor beam cross section

- The roof beams are composed of C200 cold-formed C-shaped steel profiles, fabricated from S235 grade steel. Key geometric and mechanical properties of the section are provided in Table 4.3, with a detailed illustration shown in Figure 4.12.

Section	**Steel**	A_g mm^2	I_y mm^4	I_t mm^4	I_w mm^4	$W_{y,el}$ mm^3	$W_{y,pl}$ mm^3	$W_{y,eff}$ mm^3	$M_{c,y,Rd}$ kNm
CR200A	S235	1776	$1.07 \cdot 10^7$	9470	$2.26 \cdot 10^{10}$	107400	125720	114768	29.6

Table 4.3: Geometrical properties of roof beams

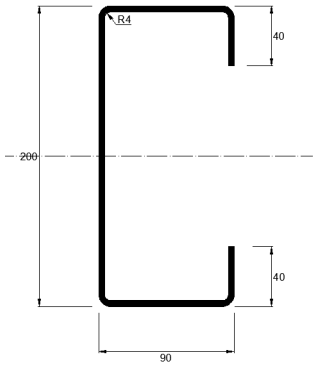

Figure 4.12: Roof beam cross section

- Bracing elements are composed of flat steel plates with dimensions 50 × 10 mm.

4.2.2 Connections

Connections are key elements contributing in the global analysis of the structure and also for local analysis of its constitutive members.

At the ground floor, columns are simply supported, i.e. all translations fixed and free rotations.

The type of beam-to-column joints used are the C-shaped support corresponding to *Option 2* presented in Section 3.6. This solution is elaborated for the case of a connection with the roof beam; however, the developments related to the component method demonstrate that this option can also be adopted for the floor beams described in the preceding section. Indeed, these floor beams possess the same thickness and wall width as the roof beams. Moreover, it is observed that the block tearing phenomenon would be significantly reduced in the case of floor beams, as they feature longer stiffeners. In summary, adopting the same type of connection (*Option 2*) for CR200A and CR310A beams constitutes a substantial advantage for the proposed solution. All beam-to-column connections would be identical throughout the structure, with their height adjusted according to the connected beam.

As an initial assumption, the rotational stiffness of 1500 kNm/rad, determined in Chapter 3 for *Option 2*, is retained for this iteration and will be subject to further optimization at a later stage. This rotational stiffness is applied exclusively to the roof beam-to-column connections. Considering the increased height of the floor beams, the corresponding floor joints are assigned a higher rotational stiffness of 3700 kNm/rad. A schematic representation of the rotational stiffness distribution implemented in the FineLg model is presented in Figure 4.13. All these joints are idealized as indefinitely elastic. This assumption must be verified for the optimized joint.

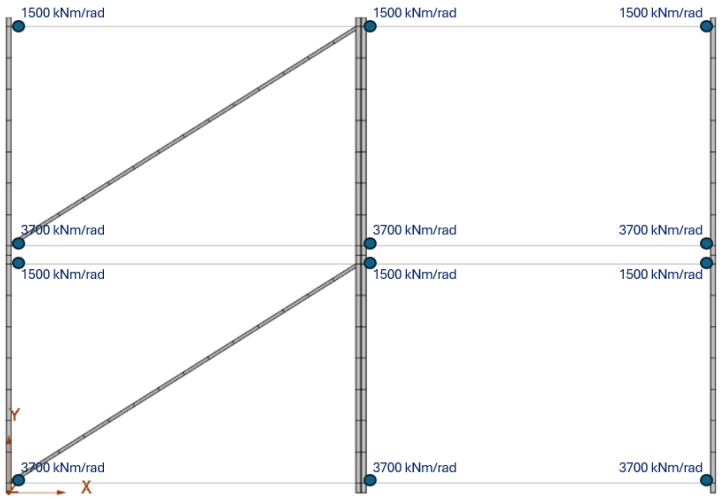

Figure 4.13: Rotational stiffness of beam to column connections

The connections between the upper and lower modules provide full translational restraint while allowing free rotational movement.

4.2.3 Loads

Several load cases were analyzed in order to identify the most critical scenario. The different loads applied in the model are summarized in the table below.

Loads on beam	kN/m
1st floor- Floor beam	13.45
1st floor- Roof beam	1.61
2nd floor- Floor beam	13.45
2nd floor- Roof beam	8.55

Table 4.4: Design loads applied to the different beam elements

The applied wind load is equal to 0.89 kN/m. All of these loads were defined by the team of doctoral researchers involved in the project, based on discussions and technical meetings held with DEGOTTE.

It is equally important to emphasize that the aforementioned loads are designed loads according to the ultimate limit state (ULS). Later in this chapter, when verifying structural elements under the serviceability limit state (SLS), a ratio term between SLS and ULS will be introduced to simplify the structural modeling. This ratio is specifically determined for each structural component, as they are subjected to different load combinations. The SLS/ULS ratio is established as 0.675 and 0.64 for floor beams and roof beams, respectively. Furthermore, it will subsequently be demonstrated that these are the only structural elements requiring verification under SLS conditions.

4.3 Linear Buckling Analysis

The Linear buckling Analysis LBA addresses instability problems through bifurcation analysis[4]. The study assumes a perfectly elastic, idealized structure under ideal loading. However, real structures often include geometric and material imperfections, such as residual stresses or construction deviations. Despite these limitations, determining critical load multipliers α_{cr} remains essential for understanding second-order structural behaviour. This analysis provides foundational insight into stability under non-linear effects. The impact of this analysis will be discussed in the GMNIA analysis.

4.3.1 Euler's Column illustration

LBA analysis is usually introduced by the classical example of the stability of a perfectly straight, simply column with length ℓ and flexural rigidity EI, subjected to an axial compressive force αP applied at one of its ends, see Fig. 4.14-a. This idealised case, developed in reference [10], provides a fundamental reference for understanding structure instability by bifurcation.

[4]In civil engineering, bifurcation refers to a sudden change in the equilibrium path of a structure under increasing load. It marks the point at which the structure may follow an alternative deformation mode, often associated with instability.

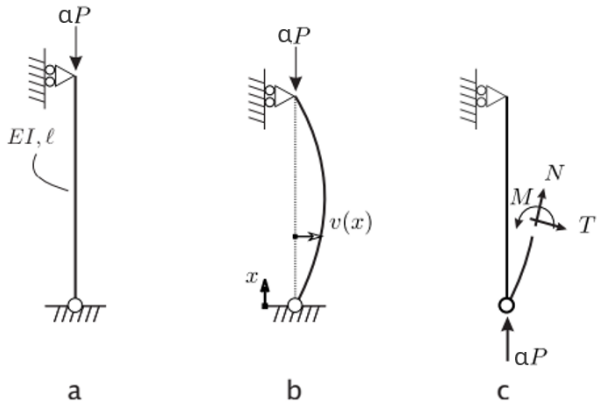

Figure 4.14: Example of Euler instability [10]

A load multiplier α is introduced to scale the applied force to represent a load that can gradually increase. When $\alpha = 0$, no force acts on the column, and the applied load increases progressively as α increases. Given that the column is assumed to be perfectly straight, perfectly vertical, and subjected to a load precisely aligned with its axis, no lateral displacement is expected under these ideal conditions. However, let us consider the possibility that, at some point, the column may undergo a transverse deformation $v(x)$, as illustrated in Figure 4.14-b. A global equilibrium shows that the base point only faces a vertical reaction equals to αP. In fact, the horizontal reactions are identically equal to zero as no horizontal load is applied on the member. A local equilibrium gives the bending moment distribution along the member as:

$$M(x) = \alpha P\, v(x) \tag{4.1}$$

In case of low rotation, the relationship between the bending moment and the curvature is given by $M = -EIv''$ which leads to the governing equation of this column as:

$$EIv''(x) + \alpha P\, v(x) = 0 \tag{4.2}$$

where the boundary conditions are $v(0) = v(l) = 0$.
The governing equation is a second-order, linear, homogeneous differential equation with constant coefficients. A key feature of bifurcation instability lies in this homogeneity, as it implies that the equation admits the trivial solution $v = 0$. This solution represents a perfectly straight column under axial load, showing no lateral deformation. However, for certain specific values of the load multiplier α, the differential equation admits non-trivial solutions in addition to the trivial one $v = 0$. These particular values indicate critical conditions under which the column may experience lateral deflection, signalling a bifurcation of the equilibrium.
The only solution of the governing differential equation 4.2 that satisfy the first limit condition $v(0) = 0$ is

$$v(x) = A\, sin\left(\sqrt{\frac{\alpha P}{EI}}x\right) \tag{4.3}$$

and injecting the second limit condition $v(l) = 0$ leads to the Euler's critical load P_{cr}.

$$P_{cr} = k^2 \frac{\pi^2 EI}{l^2} \tag{4.4}$$

with P_{cr} equals to $\alpha_{cr}P$ and $k \in R_0$.
From the equation above we can see that Non-trivial solutions to the problem only exist when the load multiplier α assumes specific values α_{cr}, which form an infinite set. Injecting the solution in the deformation equation defined at equation 4.3, it is found that

$$v(x) = A\ sin\frac{k\pi}{l}x \tag{4.5}$$

In terms of deformation shape, either the member does not deform at all which corresponds to the trivial solution $v = 0$ or the member deforms according to a sinusoidal shape given by equation 4.5 at various value of α_{cr}. The fact that the deformation is idealized by a continuous function highlights the infinite number of degrees of freedom associated with the column. Additionally, the amplitude of deformation is determined up to an arbitrary constant, denoted A. Any solution that is a multiple A of a fundamental solution is also a solution to the equation. This is the reason why a LBA analysis refers to mode of instability and not the magnitude. As the member has an infinite degrees of freedom, it has also an infinite mode of instability. Thereby, there are n modes and critical multipliers for a structure with n degrees of freedom.

4.3.2 LBA in FineLg

In case of linear instability, the EULER stability criterion is given by

$$(\underline{K}_0 + \lambda \underline{K}_\sigma)\{u_c\} = 0 \tag{4.6}$$

where $\underline{K}_0$ is the linear stiffness matrix;
$\underline{K}_\sigma$ the initial stress matrix;
$\{u_c\}$ the buckling mode (eigenvector).

In FineLg, three algorithms are used to find the eigenvalue [11]:

- the power method;
- the secant method;
- the subpace iteration method.

In the model, the power method has been chosen because it offers the most eigenvalues comparing

with the two other algorithm. Given that the structure possesses bracings, a global instability mode requests huge quantity of energy and by so high instability mode.

4.3.3 Results

Based on the inputs presented in Section 4.2, the first observed instability mode is local, with a critical load factor of $\alpha_{cr} = 10.2$. As illustrated in Figure 4.16, this mode is characterized by the buckling of the ground floor columns only. The upper storey columns remain stable, as they are subjected to relatively low loading.

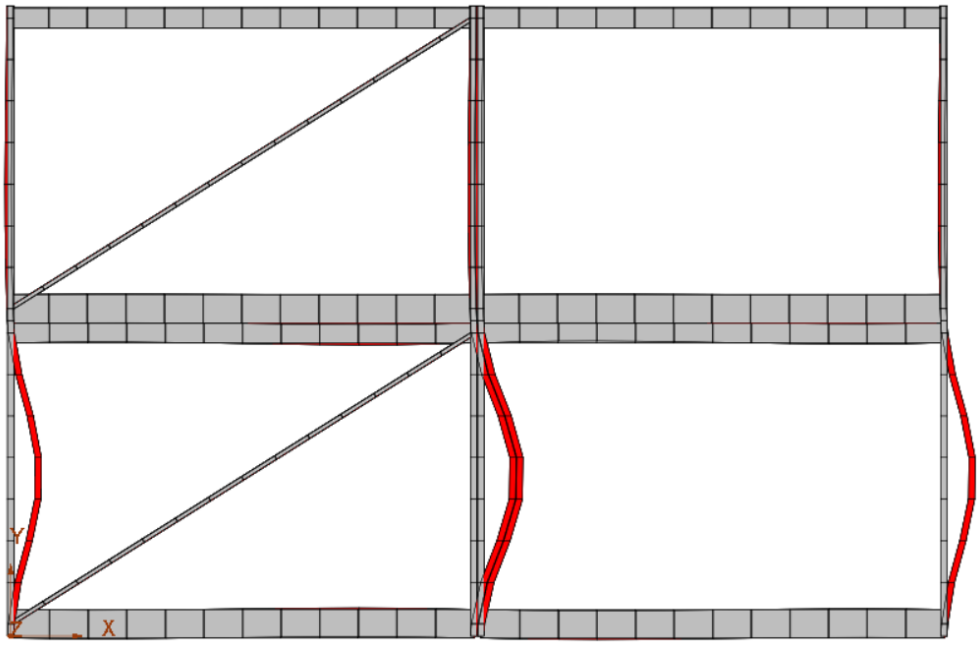

Figure 4.15: First mode of instability

To classify a structure as rigid or flexible structure, a global instability mode is needed. The number of mode has been increased till facing a global one. A global instability is reached at mode 33 where a lateral displacement of the structure is met. The critical multiplier $\alpha_{cr,global}$ corresponding to this mode is 100. Consequently, the structure is a classified as rigid structure given that $\alpha_{cr,global} > 10$.

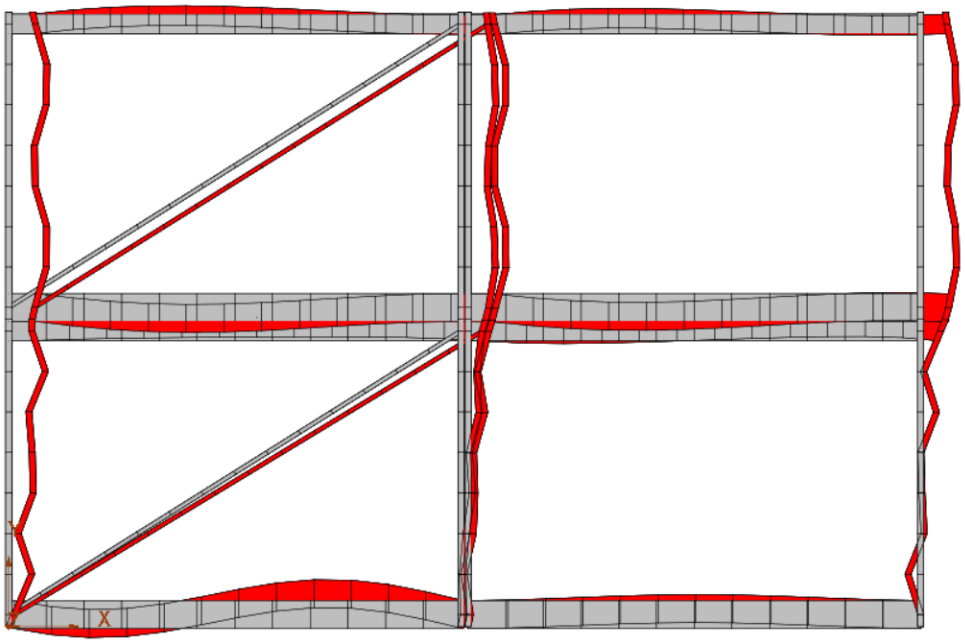

Figure 4.16: Mode 38 representing first global instability mode

This critical multiplier is certainly high due to the fact that the structure is braced. Bracing provides additional stiffness and stability to the structure. These elements resist deformation by working in tension and compression, depending on the direction of the load. The fact that $\alpha_{cr,global}$ is high demonstrate, somehow, the efficiency of bracing system chosen for the structure.

4.4 Geometrically and materially non-linear analysis

The second analysis executed in the FineLg model is a Geometrically and Materially Non-linear Analysis with imperfections (GMNIA). FineLg is able to make a real non-linear analysis considering structure imperfection, local imperfection, local deformations and global deformations in the second order analysis. The numerical methods implemented in FINELG allow for the tracking of a structure's response under progressively increasing external loads, capturing its behaviour up to, and even beyond, the point of collapse or instability.

4.4.1 GMNIA in FineLg

Geometrical non-linearities are accounted for within the finite element framework using one of several available formulations: the total Lagrangian, the updated Lagrangian, or the corotational approach [11]. Each of these methods provides a way to capture large displacement and large rotation effects, depending on the specific nature of the structural problem being analysed.

As for material non-linearity, the program incorporates an incremental plasticity theory based on the assumption of small strains. This approach enables the simulation of complex inelastic behaviour under loading. A variety of constitutive models are supported within the software,

including classical laws such as elastic-perfectly plastic, bilinear, trilinear, and more advanced ones like the Ramberg–Osgood model. These models are essential for accurately representing the stress–strain relationships of different materials under non-linear loading conditions.
Ramberg–Osgood law, shown in Figure 4.17, has been applied on beams, columns and bracings which are cold-formed members. Indeed, according to Eurocode EN 1993-1-14:2025, which addresses finite element modelling, the material law to be used for cold-formed steel is specified as the Ramberg–Osgood constitutive model. Beyond the fact that this law is recommended by the Eurocode, several studies have demonstrated the accuracy of this modelling approach when compared to experimental results[13].

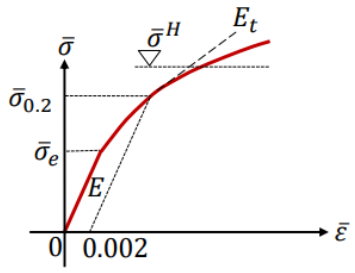

Figure 4.17: Ramberg–Osgood law (FineLg user manual)

During the cold-forming process of such sections, the material at the corners undergoes strain hardening, which locally increases the yield strength. However, accounting for this effect in a beam model is challenging, since only a single material law is typically assigned to the entire cross-section. Several studies, has shown that this effect can generally be neglected if residual stresses are also disregarded. This is due to the fact that the two phenomena tend to have opposing influences on structural stability and may, to some extent, cancel each other out. Consequently, residual stresses are not incorporated into the GMNIA model.

Non-linear structural analysis is generally performed using an incremental approach. In FineLg, the following definitions have been established [11]:

- During a load step, the system to be solved is:

$$K_T\{du\} = \{dP\} \tag{4.7}$$

- During an equilibrium correction, the system becomes:

$$K_T\{du\} = \{RES\} \tag{4.8}$$

The correction process is halted when the residual vector {RES} becomes sufficiently small, indicating that the structure has reached equilibrium under the applied external loading.

Various strategies exist to progress between successive steps. A common method involves applying incremental loads; however, this can lead to convergence difficulties when the applied load approaches a peak value. An alternative is displacement control, which alleviates this issue but introduces similar challenges when displacements reach their maximum. A possible improvement lies in combining both techniques. Nevertheless, a more robust and widely adopted approach is the arc-length method [11]. This technique maintains equilibrium by advancing along a spherical path in the load-displacement space, ensuring intersection with the equilibrium curve regardless of the nature of the response increment. Selecting arc-length method allowed the use of an automatic loading which compute automatically the radius of the new step.

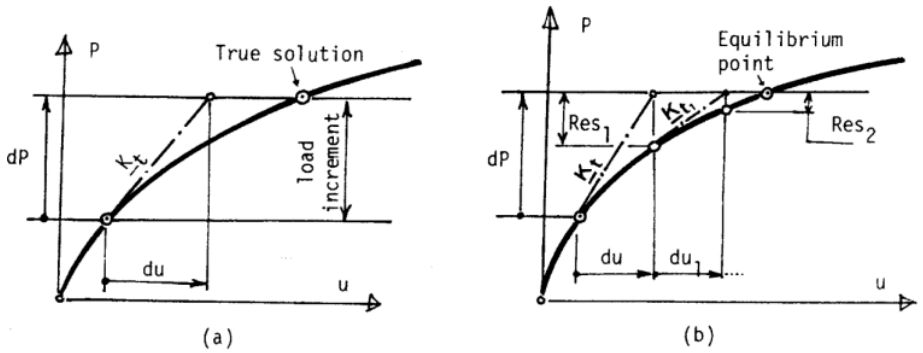

Figure 4.18: Load step (a) with equilibrium corrections (b)

4.4.2 Results

With the inputs presented in Section 4.2, the MNT diagram below have been extracted.

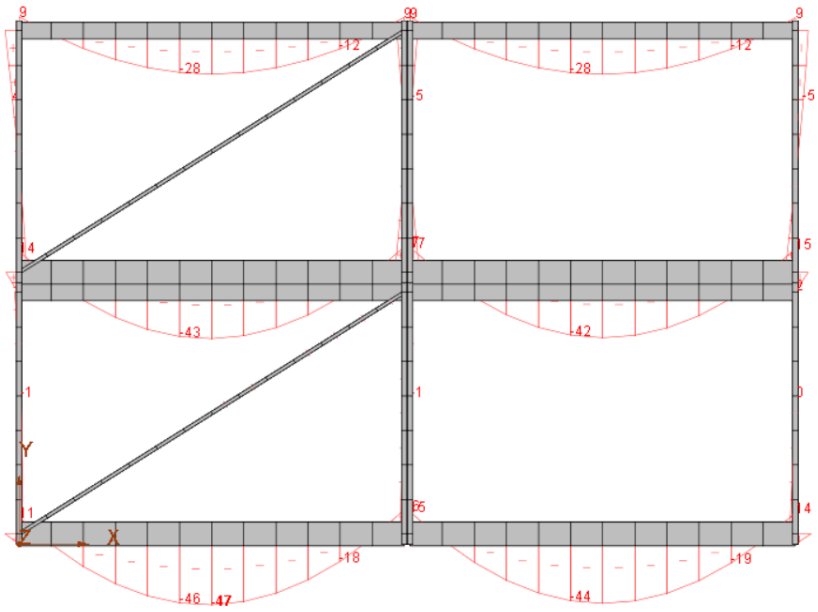

Figure 4.19: Bending moment diagram at ULS

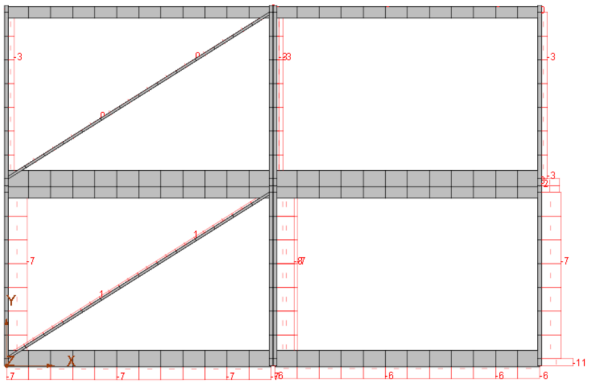

Figure 4.20: Axial force diagram at ULS

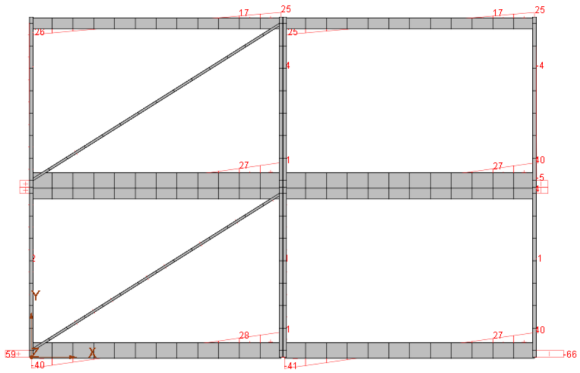

Figure 4.21: Shear force diagram at ULS

In a statically indeterminate structure, the distribution of internal forces depends on the relative stiffness of the connected members. In such systems, it is well established that stiffer elements attract more force. This phenomenon is clearly observed in Figure 4.19, where at the second level, a significant portion of the bending moment is attracted by the roof beam, while the top-floor columns carry relatively little. This is expected, as the flexural stiffness of the roof beam is substantially greater than that of the columns.

$$\left(\frac{EI}{L}\right)_{\text{C-shaped, Roof beam}} = \frac{210000 \cdot 1.074 \cdot 10^7}{6000} = 3.76 \cdot 10^8 \text{ N}.mm^2 \tag{4.9}$$

$$\left(\frac{EI}{L}\right)_{\text{SHS80x5, Column}} = \frac{210000 \cdot 1.366 \cdot 10^6}{4000} = 7.1 \cdot 10^7 \text{ N}.mm^2 \tag{4.10}$$

From these expressions, it is evident that the flexural stiffness of the roof beam is approximately five times higher than that of the SHS80x5 columns, justifying the observed redistribution of bending moments. This observation is equally applicable to floor beams.

To verify that the model has properly converged, it is essential to examine the variation of internal forces within an element throughout the load increments. In this model, convergence is evident as plastification is observed in the beams following the Ramberg-Osgood law. This plastification occurs prior to the buckling of one of the columns in the lower floor. The figure below illustrates the evolution of the load multiplier as a function of the rotation in one of the roof beams.

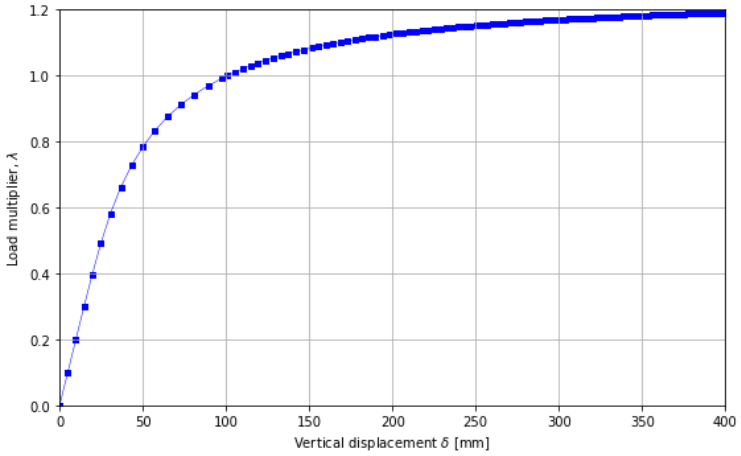

Figure 4.22: Load multiplier λ in function of vertical displacement δ at the roof beam midspan

4.5 Results and discussion

Based on the two analyses carried out, LBA and GMNIA, two key observations can be made:

- The LBA model indicates that the structure behaves as a rigid frame. In this context, the beam-to-column joints are transversely non-displaceable.
- The GMNIA model, on the other hand, provides insight into the internal force distribution within the structure. In particular, regarding the bending moment distribution, it is evident that due to the relatively low flexural stiffness of the columns, the moment is not significantly transferred to them.

As a result, the semi-rigid nature of the joints is not adequately reflected through the moment distribution. To assess the influence of the rotational stiffness of the joints on the structural behaviour, two extreme cases are considered.

First, the structure is analysed assuming pinned connections at each beam-to-column joint. This configuration corresponds to the initial design approach adopted by DEGOTTE. In such a case, it is expected that bending moments will increase in the beams and decrease in the columns. It is also expected that instability modes will develop earlier.

Secondly, fully rigid joints are considered. Under this assumption, the opposite behaviour is anticipated: bending moments are expected to decrease in the beams and increase in the columns. Moreover, the critical loads leading to either local or global instabilities are expected to be higher than those observed in the previously tested semi-rigid configuration.

After evaluating these two extreme cases, it becomes easier to identify the optimal range within which the rotational stiffness of the connection should lie.

4.5.1 Case 1: Rigid joint

Based on Equation 4.9, the rotational stiffness values implemented in FineLg to simulate rigid joints are given by:

$$S_{j,ini,rigid,\text{Roof beam}} = 10 \cdot \left(\frac{EI}{L}\right)_{\text{Roof beam}} = \frac{10 \cdot 3.76 \cdot 10^8}{10^6} = 3759 \text{ kNm/rad} \tag{4.11}$$

$$S_{j,ini,rigid,\text{Floor beam}} = 10 \cdot \left(\frac{EI}{L}\right)_{\text{Floor beam}} = \frac{10 \cdot (210000 \cdot 3.45 \cdot 10^7/6000)}{10^6} = 12075 \text{ kNm/rad} \tag{4.12}$$

As a reminder, a joint is classified as a *rigid joint* when its rotational stiffness exceeds eight times the flexural stiffness of the connected beam, in the context of a rigid frame. In Section 4.3.3, it is demonstrated that under *Option 2* joint conditions, the structure exhibits behaviour consistent with that of a rigid frame. Given that a rigid joint possesses substantially higher rotational stiffness, this effect is further amplified. Specifically, for a rigid connection modelled with a rotational stiffness of $10 \cdot (EI/L)_{\text{beam}}$,[5] the critical load multiplier indicating global structural instability increases from 100 to 105. The critical load multiplier associated with local instability increases from 10.2 to 10.6. This increase is consistent with expectations, as a rigid connection effectively reduces the buckling length of the underlying columns, thereby enhancing their stability. The results obtained are illustrated in the figures below.

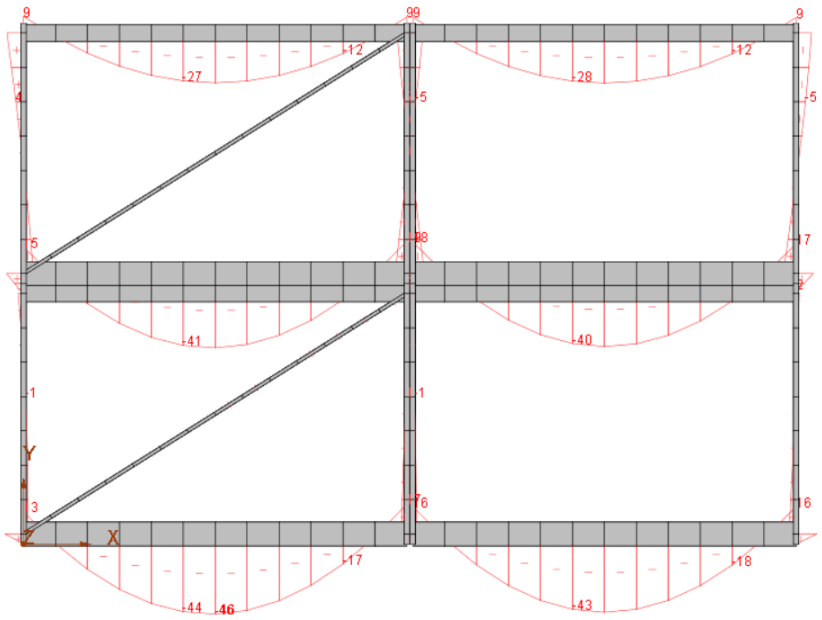

Figure 4.23: Moment distribution with rigid beam-to-column joints

[5] A factor of $10 \cdot (EI/L)_{\text{beam}}$ is used instead of the minimum $8 \cdot (EI/L)_{\text{beam}}$ to ensure that the stiffness clearly exceeds the threshold for rigid joint classification. Assuming a rotational stiffness more than ten times greater than that of the beam is unnecessary and may lead to convergence difficulties in the numerical analysis.

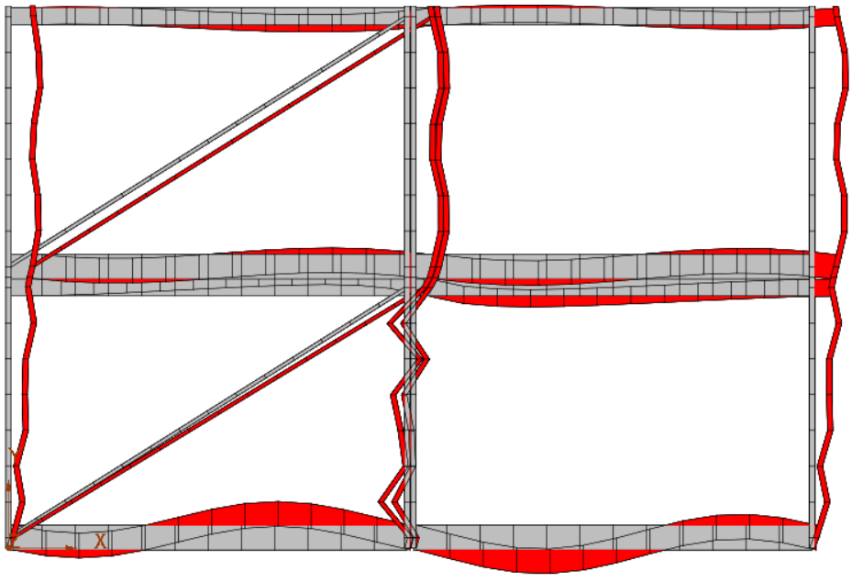

Figure 4.24: Mode 38 representing first global instability mode under rigid joints

In the case of rigid joints, the bending moment transmitted through the top roof joint reaches approximately 9.5 kNm. In comparison, for a *Option 2* joint with a rotational stiffness of 1500 kNm, the moment was about 9.2 kNm. This indicates a relatively small difference, despite the rotational stiffness being more than doubled. This observation further highlights that the significant disparity between the flexural stiffnesses of the beam and the column has a non-negligible influence on the distribution of moments between these members. The maximum bending moment in the roof beams remained nearly constant, with a value of approximately 28 kNm, compared to that observed for the *option 2* joints. Ce moment est très proche de la résistance plastique de la poutre de toiture, qui est de 29.6kNm.

It can therefore be concluded that a flexural stiffness greater than that of *Option 2*, i.e., 1500 kNm/rad, yields moment distributions that are nearly identical to those observed in the case of rigid connections. Similarly, it is noted that the critical buckling load is slightly improved in the rigid case.

4.5.2 Case 2: Pinned joint

In practical terms, for a pinned joint, no rotational stiffness is typically considered. However, for the purposes of numerical analysis, it is approximated as $0.010 \cdot \left(\frac{EI}{L}\right)_{\text{beam}}$[6]. By applying a similar approach to the beam-column joints at both the roof and floor levels, the following expression is obtained:

$$S_{j,ini,pinned} = 0.01 \cdot \left(\frac{EI}{L}\right)_{beam} = \frac{0.01 \cdot 3.76 \cdot 10^8}{10^6} = 3.76 \text{ kNm/rad} \tag{4.13}$$

[6] As in the rigid case, the factor of 0.5 specified by the Eurocode is replaced by 0.01 to ensure that an insignificant stiffness is considered.

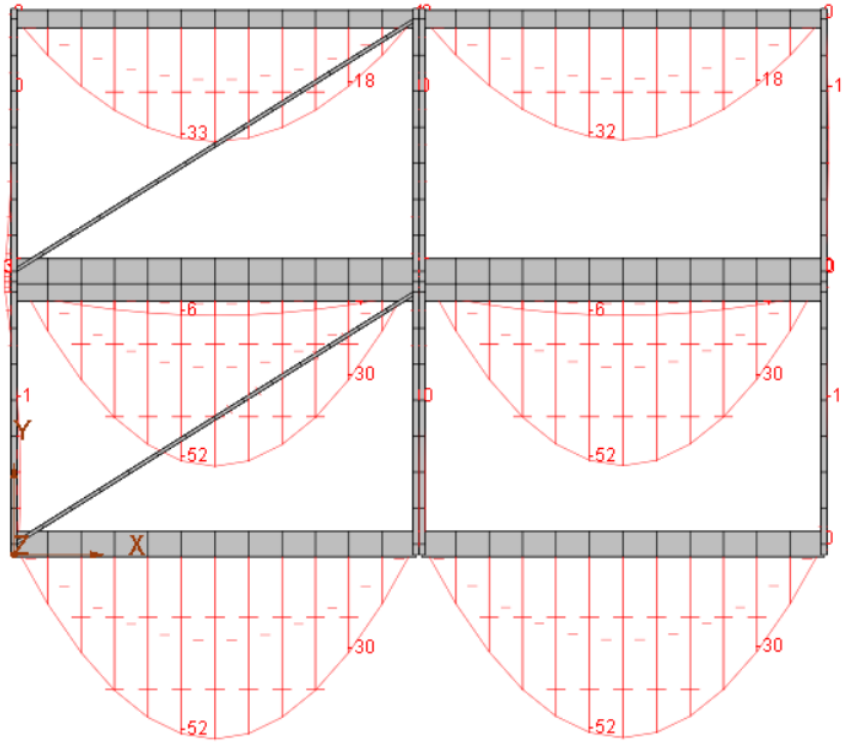

Figure 4.25: Moment distribution with pinned beam-to-column joints

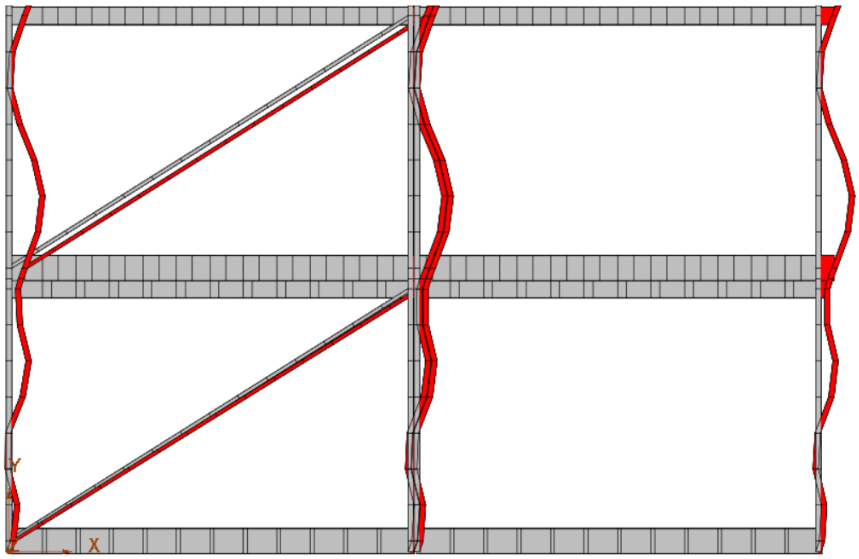

Figure 4.26: Mode 14 representing first global instability mode under rigid joints

The moment transmitted through the roof joint is currently 0.5 kNm, which is considered acceptable, as achieving a perfect hinge with $M_{j,Ed} = 0$ kNm in practice is difficult. Another observation is that the maximum bending moment in the beams is higher for the pinned connection, which aligns with expectations. The difference is relatively small, only 5 kNm, between a rigid and pinned case, which can be explained by the fact that the flexural stiffness of the column is five times greater than that of the beams, as previously mentioned.

4.5.3 Optimisation

This brief comparison between the rigid and pinned cases allows for a clear understanding of the required resistance range that the joint must accommodate. Furthermore, it highlights the critical range within which the rotational stiffness should be optimized. Indeed, since the optimization targets a semi-rigid joint[7], it is anticipated that the moment range developed within the joint should fall between 0.5 kNm and 9.5 kNm, representing the extreme cases discussed in the preceding sections. These loads are relatively low, which presents challenges in achieving an appropriate stiffness while maintaining a resistance that is close to these values.

During this optimization process, it will be verified that the bending moment acting on the joint does not exceed its elastic limit, i.e., $\frac{2}{3}M_{j,Rd}$, to validate the assumption that the initial stiffness of the joint in the model, $S_{j,ini}$, remains accurate. If this condition is not satisfied, it becomes necessary to reduce this initial stiffness by a factor of two. While decreasing the stiffness would permit a plastic verification of the joint, it would simultaneously lead to an increase in the bending moments within the beams. However, as demonstrated in the rigid case, which represents the ideal scenario for moment distribution in the beam, it is observed that the maximum bending moment already approaches the plastic resistance of the roof beam. Therefore, stiffness is a critical factor, justifying the need to keep the joint in its elastic range to preserve its initial stiffness and ensure structural efficiency.

In the initial optimization phase, the first assembly considered is *Option 2*, as outlined in the introduction of this chapter. Upon analysing the moment diagram presented in Figure 4.19, it is evident that the roof joint has exceeded its elastic behaviour. Specifically, the joint moment is 9 kNm, whereas the elastic moment is $2/3 \cdot M_{j,Rd} = 8.4$ kNm. Consequently, the initial modelling assumption that the joint stiffness equals $S_{j,ini}$ is incorrect and must be adjusted to $S_{j,ini}/2$, as recommended by Eurocode 3. Implementing this modification reduces the transverse moment acting on the joint to 8.8 kNm, which is now below the plastic resistance of the joint ($M_{j,Rd} =$ 12.6 kNm). Furthermore, the moment applied to the roof beam remains below its plastic resistance. This adjusted stiffness of $S_{j,ini}/2 = 748$ kNm/rad suggests that a stiffness within this range could yield favourable results.

The second optimization phase will focus on calibrating the components to achieve a target stiffness of 700 *kNm/rad*. This will be accomplished by rebalancing the resistances of the various components, as referenced in the introduction of this chapter (see Figure 4.1). Regarding the target plastic resistance, it is important to recognize that if this ideal stiffness were to be reduced by half due to joint plastification, the moment in the roof beam would exceed its plastic resistance. The applied moment on this beam is 29.8 kNm for a joint stiffness modeled as $S_{j,ini}/2 = 350$ kNm/rad. Therefore, it would be more advantageous to target a joint resistance that allows the connection to remain elastic, thereby enabling modeling with an initial stiffness equal to $S_{j,ini}$. This approach ensures that the maximum moment in the roof beam remains below its plastic resistance,

[7] A rigid joint would be costly, while a pinned joint offers a greater buckling length for the column, as demonstrated in its first instability mode in Section 4.5.2.

as concluded during the first optimization phase. Finally, the target plastic resistance of the joint is determined such that:

$$M_{j,Ed} \leq \frac{2}{3} M_{j,Rd}$$
$$M_{j,Rd} \geq \frac{3}{2} M_{j,Ed} = 13.2 \text{ kNm}$$

where $M_{j,Ed}$ is set to 8.8 kNm, corresponding to the moment observed during the first optimization phase for a stiffness $S_{j,ini} = 748$ kNm/rad.

Following these two phases, the target assembly should exhibit an initial stiffness $S_{j,ini}$ of 748 kNm/rad along with a plastic resistance exceeding 13.2 kNm.

An Excel-based spreadsheet tool was developed as part of this thesis to facilitate the calibration of joint resistance and joint rotational stiffness. By adjusting both the geometry and the material properties of the roof joint components, an optimized configuration was obtained, providing a joint plastic resistance of 13.7 kNm and a rotational stiffness of 620 kNm/rad. As illustrated in the following figures, the corresponding assembly configuration for these parameters will be designated as assembly configuration *Option 2-1*.

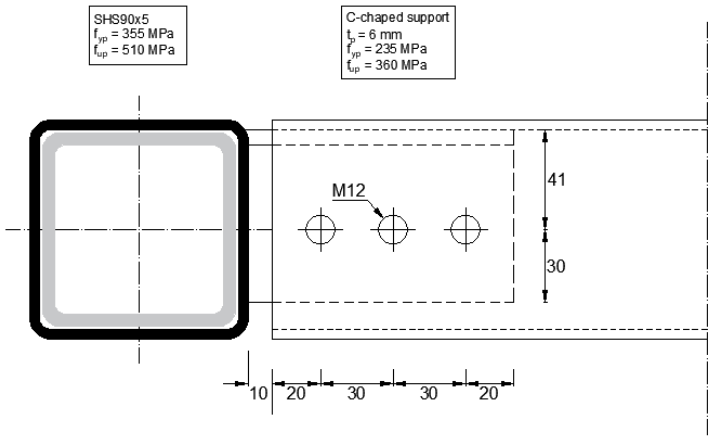

Figure 4.27: Plan view of roof joint – Beam flange to support flange connection

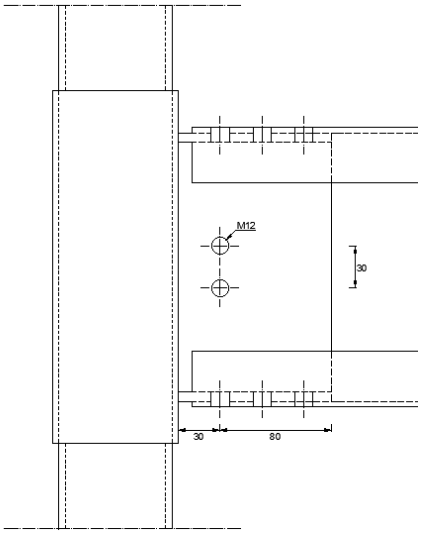

Figure 4.28: Elevation view of roof joint – Beam web to support web connection

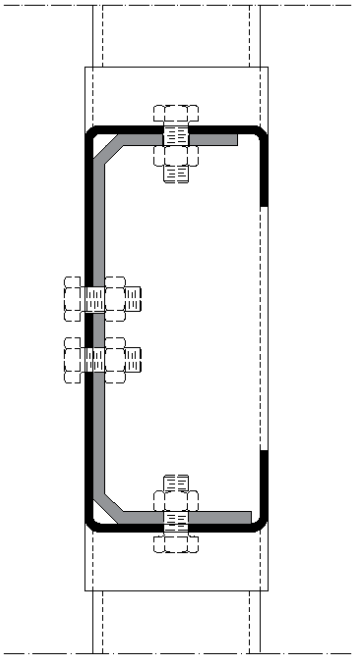

Figure 4.29: *Option 2-1* side view for the roof joint

The corresponding properties, in terms of resistance and stiffness, are given in the table below.

Component	**Resistance [kN]**	**Stiffness [mm]**
Bolt in shear (beam flange)	101.2	1.03
Plate 1 and 2 in bearing	106.9	0.38
Beam flange in bearing	71.2	0.25
Plate 1 in tension	182.9	∞
Plate 2 in compression	182.9	∞
Block tearing plate 1	88	-
Block tearing beam flange	115.7	-
Sleeve face in tension	87.4	0.43
Sleeve face in compression	87.4	0.43
Column face in shear	109.2	3.04
Bolt in shear beam web	67.4	-
Plate 3 in bearing	99.7	-
Beam web in bearing	66.5	-
Plate 3 in shear	141.6	-

Table 4.5: *Option 2-1* joint type results for roof beams

Regarding the floor beams, the same solution presented in Figure 4.27 is maintained, with the exception of the beam height which varies. A plastic moment of 21.52 kNm is attained, with a rotational stiffness of 1530 kNm/rad. Following this adaptation, the results presented below are obtained.

Component	Resistance [kN]	Stiffness [mm]
Bolt in shear (beam flange)	101.2	1.03
Plate 1 and 2 in bearing	106.9	0.38
Beam flange in bearing	71.2	0.25
Plate 1 in tension	182.9	∞
Plate 2 in compression	182.9	∞
Block tearing plate 1	88	-
Block tearing beam flange	115.7	-
Sleeve face in tension	87.4	0.43
Sleeve face in compression	87.4	0.43
Column face in shear	109.2	3.04
Bolt in shear beam web	67.4	-
Plate 3 in bearing	99.7	-
Beam web in bearing	66.5	-
Plate 3 in shear	231.2	-

Table 4.6: *Option 2-1* joint type results for floor beams

Incorporating the characteristics of this joint into the FineLg model yields a critical load multiplier of 9.13 for the first buckling mode, which remains a local mode associated with the instability of the first-level columns. The global buckling mode appears at mode 27, with a corresponding critical multiplier $\alpha_{cr,global}$ equal to 92. The distribution of the bending moment is illustrated in the following figure.

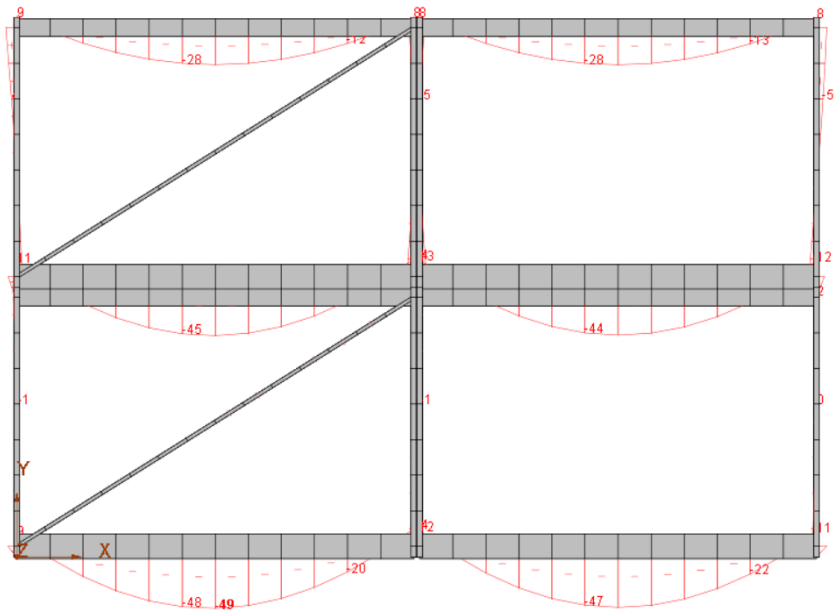

Figure 4.30: Moment diagram with *Option 2-2* joints

The moment developed in the joint is 8.7 kNm, which remains below the elastic resistance threshold that would necessitate a reduction of $S_{j,ini}$ in the model, i.e., $2/3\,M_{j,Rd} = 9\,\text{kNm} \geq 8.7\,\text{kNm}$. Therefore, it is valid to model the joint's rotational stiffness as equal to $S_{j,ini}$. Following

the same rationale, it is also observed that the floor beam joints remain within the elastic domain, as the maximum encountered moment of 14 kNm is less than two-thirds of 21.52 kNm. In conclusion, the assumption regarding the initial stiffness equivalent to $S_{j,ini}$ remains valid for the entire structural system.

The roof joint operates at approximately 97% of its elastic capacity, demonstrating efficient structural optimization. Similarly, the floor joint functions at nearly 98% of its elastic capacity, indicating comparable optimization effectiveness. The accompanying diagram illustrates the relationship between component resistance capacities and the roof joint's experienced moment. Analysis of this figure reveals that the governing failure mechanism - beam flange in bearing - dominates the connection's behaviour. This failure mode ensures ductile performance of the assembly, thereby validating the application of the static theorem employed in the design calculations. The observed behaviour confirms the theoretical assumptions regarding plastic redistribution within the connection system..

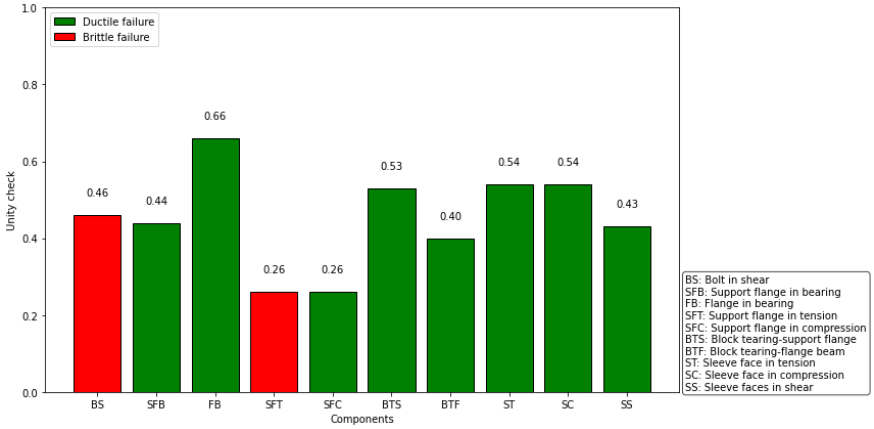

Figure 4.31: Resistance capacity of each component in comparison with experienced moment joint.

At ULS, the maximum bending moment in the roof beam is 29.4 kNm, while its plastic resistance capacity is 29.6 kNm. The floor beam, on the other hand, is subjected to a maximum moment of 49 kNm, which remains below its plastic resistance capacity of 66.6 kNm. Regarding the columns, it is similarly observed that they adequately resist the applied loads, as illustrated in Figure 4.34. The load multiplier exceeds the unitary value corresponding to the ULS load cases for each element in the structure, as shown in the graphs below.

At SLS, a vertical displacement exceeding $L/300 = 20\,\text{mm}$ is observed at mid-span of the roof beam. However, as demonstrated by the rigid joint case examined in Section 4.5.1, the maximum deflection of the beam with rigid connections is 35 mm [8]. Consequently, if even this ideal scenario fails to satisfy SLS requirements for the beam, then no semi-rigid connection configuration can

[8] As mentioned in Section 4.2.3, the deflections under SLS are obtained for a load multiplier equal to the SLS loads divided by the ULS loads. This approach is adopted to work with a single model while minimizing the number of load cases.

ensure compliance with this verification criterion. Indeed, reducing the joint stiffness would increase the sagging moment in the beam and consequently amplify the observed deflection.

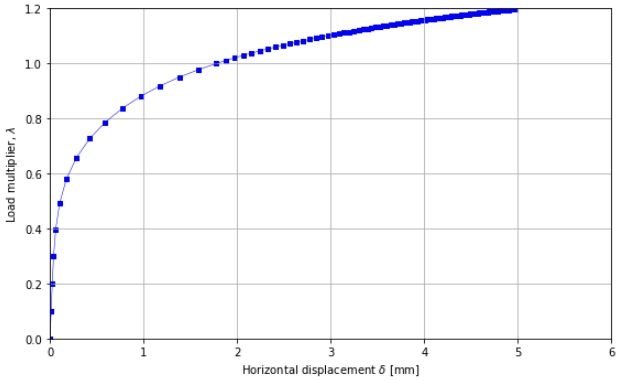

Figure 4.32: Load multiplier in function of vertical displacement at the roof beam midspan

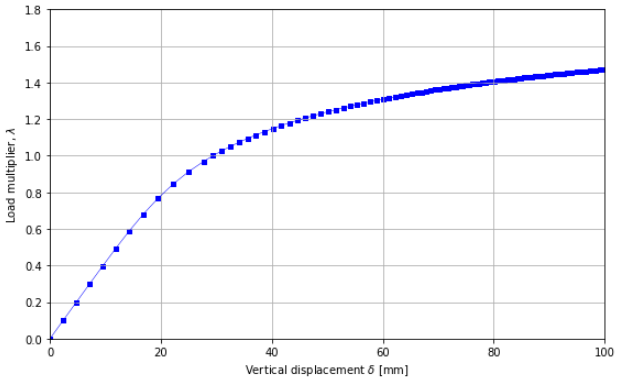

Figure 4.33: Load multiplier in function of vertical displacement at the floor beam midspan

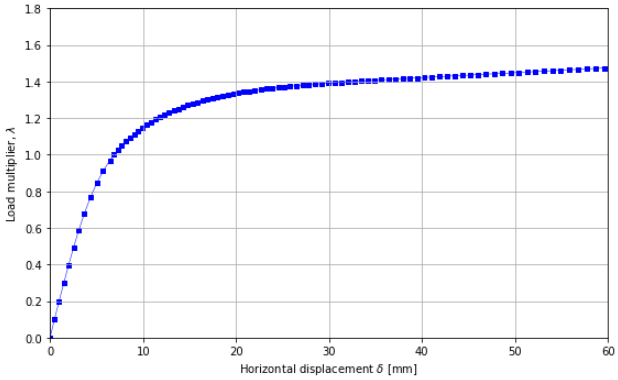

Figure 4.34: Load multiplier in function of horizontal displacement at bottom edge column

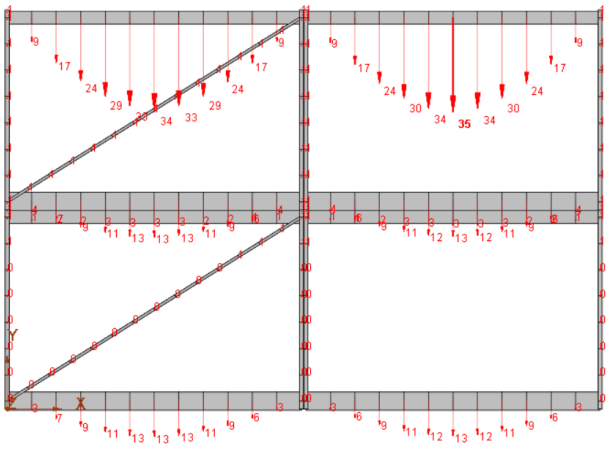

Figure 4.35: Vertical deflection under rigid joints

Following these verifications, the roof beam fails to satisfy the Serviceability Limit States requirements regardless of the connection type implemented. Consequently, its properties must be enhanced to comply with the maximum allowable deflection of 20 mm.

To address this issue, the roof beams (CR200A) in the upper module could be replaced with floor beams (CR310A). Regarding the roof beam in the lower module, there is no structural justification for increasing its properties except for the purpose of standardizing beam elements throughout the structure.

If this measure is adopted, the recently presented assembly, *Option 2-1*, would remain suitable. Indeed, since the CR200 beam would be replaced by a CR310 beam, the resistance would increase to 66 kNm, which is sufficient for ULS verification. Specifically, the floor beam supports a greater load than the roof beam; therefore, given that ULS requirements were satisfied in the previous configuration, they would similarly be met in this new arrangement. The moment in the roof beam would increase slightly due to the enhanced flexural stiffness of the replacement beam, but its plastic resistance remains adequate to accommodate this marginal increase. Regarding the connection, the moment would decrease because the CR300 beam would attract more load than the CR200 beam. In parallel with this physical reasoning, the roof beam of the upper module, initially a CR200, was replaced with a CR310 beam in the FineLg model. The numerical results are consistent with the explanation provided above.In summary, all ULS verifications are satisfied.

The SLS requirements for the proposed configuration are satisfactorily met, as evidenced by the subsequent figure. All vertical deflections in the beams remain below the prescribed limit of 20 mm. The horizontal forces are significantly small due to the structure's rigidity in non-transversally displaceable nodes, as demonstrated earlier.

In conclusion, the initial structural design employing CR200A roof beams for the upper module fails to satisfy the SLS requirements. Consequently, a modification substituting these beams with CR300A sections would be necessary and would demonstrate validity for both ULS and SLS conditions. In this scenario, Assembly Option 2 would prove suitable. However, further optimization for this modified configuration remains possible. Such optimization falls beyond

the scope of the present work, as this study primarily proposes a replacement solution without comprehensive knowledge of budgetary constraints or other practical considerations.

In the following two sections, the influence of assembly choice on the local and global behaviour of the structure initially designed by DEGOTTE will be examined. In both studies, no structural modifications are made in order to provide an analysis based on the real case of the structure. Only various assembly configurations will be tested to enable conclusions to be drawn regarding which types of assemblies would be particularly advantageous to implement.

4.5.4 Influence of Joint Rotational Stiffness on Column Buckling Length

In all types of joints studied in this lecture, the first buckling mode of the structure is typically governed by the instability of the bottom columns. According to the Eurocodes, this column buckling behaviour is strongly influenced by the rotational stiffness of the joints. To investigate this phenomenon, a parametric study is conducted to assess the effect of joint rotational stiffness on the effective buckling length of a column. This analysis is carried out using the LBA model, from which the critical load factor α_{cr} corresponding to the first mode is extracted for different joint configurations.

Given that α_{cr} represents the ratio between the critical buckling load and the applied axial load, it is possible to deduce the buckling length of a column. Specifically, the critical load computed by FineLg is given by:

$$N_{cr} = \alpha_{cr} \cdot N_{Ed} \tag{4.14}$$

where α_{cr} is the eigenvalue obtained from the LBA model, and N_{Ed} is the axial compressive force acting in the column under applied loading. In the current configuration, the compressive force in each bottom column is equal to 70.8 kN.

Rewriting Euler's critical load formula (as defined in Equation 4.4) leads to:

$$N_{cr} = \frac{\pi^2 EI}{L_{fl}^2} \tag{4.15}$$

where L_{fl} is the effective buckling length, defined as $k \cdot L$ with k being the effective length factor. By equating Equations 4.14 and 4.15, the corresponding buckling length can be expressed as:

$$L_{fl} = \sqrt{\frac{\pi^2 \cdot EI}{\alpha_{cr} \cdot N_{Ed}}} \tag{4.16}$$

This approach, applied to various joint types presented in this chapter, confirms that the rotational stiffness of the joints influences the buckling length of the bottom columns. However, this effect is significant only within certain ranges of rotational stiffness. A graphical representation of the

buckling length as a function of joint rotational stiffness is shown in Figure 4.36. The graph illustrates the following joint types under investigation:

- The *Option 2* joint, designed to attain resistance superior to that of the roof beam (CR200A) when coupled with a C-shaped support (see Section 3.6);
- *Option 2-1*, which represents the optimal solution selected for this research;
- *Option 2-2*, an intermediate joint configuration providing rotational stiffness approximating pinned connection behavior;
- *Option 2-3*, an intermediate joint exhibiting rotational stiffness values intermediate between *Option 2-2* and *Option 2*;
- A pinned joint is incorporated to establish the lower bound of rotational stiffness (see Section 4.5.2);
- Correspondingly, a rigid joint is included to represent the upper bound of rotational stiffness (refer to Section 4.5.1).

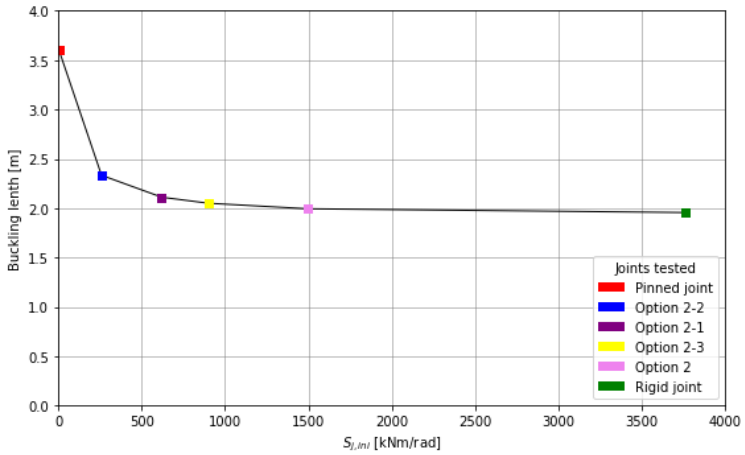

Figure 4.36: Variation of the buckling length in function of the rotational stiffness

In theory, the greater the rigidity of a joint, the shorter the effective buckling length of the connected column. Conversely, lower rotational stiffness results in a longer buckling length. In this particular structure, an atypical behaviour is observed: near the pinned-joint condition, the buckling length initially decreases significantly before stabilizing around a rotational stiffness of 1500 kNm/rad. It becomes evident that *Option 2-1* offers an optimal buckling length relative to its rotational stiffness. *Option 2* may be considered economically inefficient, as its gain in buckling resistance is limited despite having twice the rotational stiffness of *Option 2-1*.

Figure 4.36 clearly illustrates that pinned joints are highly detrimental to minimizing the column's buckling length and should be avoided in this structural configuration. Although, from a moment distribution perspective, a pinned connection may initially appear advantageous due to the limited moment transfer between the beam and the column despite a nominally rigid connection, this graph demonstrates that, in addition to assessing the influence of joint rigidity on moment distribution, a buckling length analysis provides critical insight into the optimal stiffness range to target.

Consequently, a comprehensive evaluation of both factors is essential for ensuring an optimal solution.

The numerical results presented in Figure 4.36 can be compared with those obtained through an analytical approach. The numerical results account for the global structural stiffness contributions as well as an accurate representation of the actual instability mode. In contrast, the analytical approach is based on the assumption that all columns in the structure buckle simultaneously, as illustrated in Figure 4.37. However, as demonstrated by the first buckling mode in FineLg, only the ground-floor columns experience buckling. This phenomenon can be attributed to the fact that these columns bear a significantly higher axial load compared to the columns on the upper floor, making them more susceptible to instability under compressive forces.

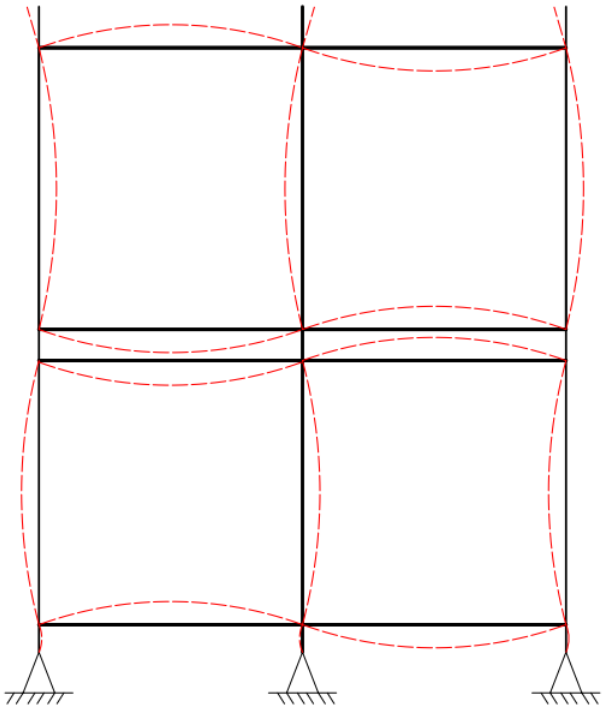

Figure 4.37: Assumption on the instability mode for an Analytical approach

The results of this approach are obtained in accordance with Eurocode 3, using formulations that incorporate the flexural stiffness of the connections. The two edge columns on the ground floor are the first to experience instability. Indeed, while all ground-floor columns are subjected to the same axial load in a first order analysis, the central columns are stabilized by the additional stiffness provided by the beams on both sides. It should be noted that the central column actually consists of two separate columns, each belonging to an adjacent module. From an energy perspective, these two columns buckle in the same direction, inducing single curvature bending in the floor slab[9]. The edge column is analyzed using the analytical approach prescribed by the Eurocode.

By performing the following derivation, the analytical buckling length is obtained for each of

[9]For clarity in the illustration, the central column in Figure 4.37 is depicted as a single line, though it is actually composed of two columns belonging to the left and right modules.

the previously enumerated connection configurations. Given that the structure is characterized by non-sway nodes, the effective length factor (or buckling coefficient) for the edge column can be determined using the following expression:

$$k_{fl} = \frac{\ell_{fl}}{L_c} = \left[\frac{1 + 0.145\,(\eta_1 + \eta_2) - 0.265\eta_1\eta_2}{2 - 0.364\,(\eta_1 + \eta_2) - 0.247\eta_1\eta_2}\right] \tag{4.17}$$

where η_1 and η_2 are respectively given vy

$$\eta_1 = \frac{K_c + K_{c1}}{K_c + K_{c1} + K_{b,floor} + K_{b,roof}} \tag{4.18}$$

$$\eta_2 = \frac{K_c + K_{c2}}{K_c + K_{c2} + K_{b,floor}} \tag{4.19}$$

The stiffness values of the various elements are defined as follows:

- $K_c = I_c/L_c$ Stiffness of the studied column;
- $K_{c1} = I_{c1}/L_{c1}$ Stiffness of the upper floor column;
- $K_{b,floor} = \frac{\rho I_{b,floor}}{4L_b} \frac{1}{1+\frac{\rho E I_{b,floor}}{S_{j,ini} L_b}}$ Stiffness of the floor beam (C310A);
- $K_{b,roof} = \frac{\rho I_{b,roof}}{4L_b} \frac{1}{1+\frac{\rho E I_{b,roof}}{S_{j,ini} L_b}}$ Stiffness of the roof beam (C200A);
- $K_{c2} = I_{c2}/L_{c2}$ Stiffness of the column segment located beneath the ground floor beam;

In the column buckling mode, the contribution of both beams is accounted for. As illustrated in Figure 4.37, the instability mode demonstrates that the spacing between the roof beam (of ground floor module) and the floor beam (of first floor module) is sufficiently small to be considered as a fixed point. Therefore, these two beams contribute to the stiffness at the top of the studied column.

By substituting the properties of the columns and beams in terms of moments of inertia and element lengths, the resulting values are presented in Figure 4.38 for varying stiffness parameters.

As illustrated in Figure 4.38, which compares the analytical and numerical approaches, it is evident that the analytical method underestimates the overall structural stiffness. However, the results also demonstrate that the analytical approach developed in the Eurocode remains conservative, as it yields larger buckling lengths than those observed in reality. If column design is based on this method, the resulting structural resistance will be underestimated, yet on the safe side for engineering purposes. However, the variation of the buckling length as a function of the rotational stiffness of the joint remains similar in both approaches. In both cases, a significant reduction in the buckling length is observed for scenarios approaching a pinned joint. Furthermore, it is noteworthy that, in both methods, the improvement in stability provided by joints with stiffness values exceeding 1500 kNm/rad is marginal.

It is essential to clarify that the joint stiffness values specified in the graph above belong to a predefined family of configurations, as indicated in the figure caption. By “family of joints,” we mean that the stiffness implemented in the model varies depending on whether a roof beam or a

floor beam is connected.[10]

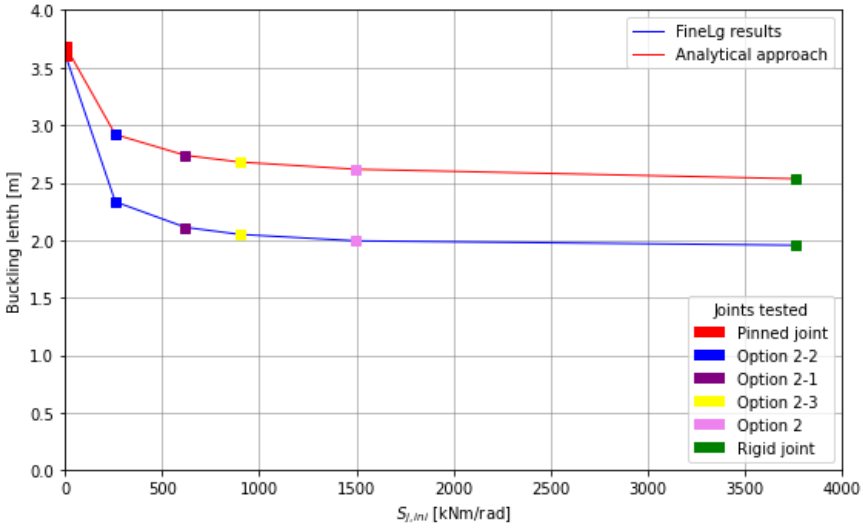

Figure 4.38: Comparison of Analytical and Numerical Results

In conclusion, the assembly configuration *Option2-1* appears to be the most optimal from a structural standpoint, particularly in terms of stiffness and the critical buckling length of the exterior columns.

4.5.5 Influence of Joint Stiffness on moment distribution

In parallel with the recent study, it is pertinent to examine the evolution of the transferred moment in a joint as a function of the selected joint type. The graph below illustrates both the moment transferred by the roof joint and the floor joint. The tested joint configurations correspond to those mentioned in the preceding section.

Given that the moment resisted by the connection is transferred to the column, thereby simultaneously reducing the load on the connected beam, it is evident that the proposed solution *Option 2-1* appears to be the most optimal. This conclusion holds despite the fact that the SLS of the structure are not validated, as previously established. Nevertheless, the graph presented in Figure 4.39 clearly demonstrates that if the initial structural configuration designed by Degotte—specifically, the roof beams composed of CR200A profiles—were to be maintained, the *Option 2-1* connection would remain the most favorable configuration. This optimality is observed both in terms of moment distribution and with respect to the column buckling lengths.

[10]It has previously been noted that the stiffness of floor beam joints is calculated by adjusting the height of the connecting element.

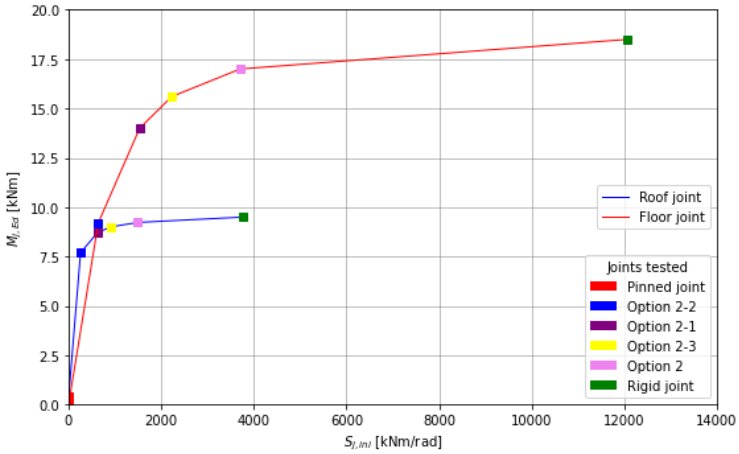

Figure 4.39: Moment in joints as function of rotational stiffness

In the presented graph, the rigid connection transfers the maximum moment to the column. However, the financial investment required to achieve such a rigid joint would be substantial. Conversely, a pinned connection, or at least an approximation thereof, would undoubtedly be more cost-effective but would subject the beam to bending moments exceeding its plastic moment resistance.

In conclusion, as demonstrated in the second phase of the optimization process, the influence of joint assembly on the buckling length of columns and presently examining its impact on the moment transfer between beams and columns, it becomes evident that the *Option 2-1* solution is significantly optimized. The sole limitation concerns the roof beam CR200A, which fails to satisfy the SLS requirements.

4.5.6 Sustainability adaptation

Since DEGOTTE operates in the rental sector, it is essential to retain the flexibility to repurpose modular units at the end of a lease agreement in order to offer them to new clients. That is the reason why it is important to ensure a maximum cycle of utilization of the joint designed. Deformations in the joints must be limited and there by a new design is required.

Si la solution *Option 2-1* advenait à être conservée, sur base de résistance énuméré dans les tableau 4.5 et 4.6, la résistance minimale correspond au beam flange in bearing. Pour limiter les déformations en pression diamétrale, NBN EN1993-1-8:2024 suggère d'adopter quelques modifications dans le calcul de cette composante.

$$F_{b,\mathrm{Rd,red}} = \frac{k_m \alpha_{b,\mathrm{red}} f_u dt}{\gamma_{M2}} \tag{4.20}$$

where the reduction factor $\alpha_{b,\mathrm{red}}$ shall be determined in accordance with Annex A.15.2. describing the Primoz model explained in chapter 3. In computational applications, a limiting deformation of $d/6$ is imposed otherwise, $\alpha_{b,\mathrm{red}} = min(\alpha_b; 2)$.

When examining the bearing behaviour of the Primoz model's plate, it becomes evident that

the bearing force acting on the flange does not induce deformations exceeding 2 mm. It should be noted that the optimal configuration (*Option 2-1*) incorporates M12 bolts, for which this deformation limit is set at 2 mm. As clearly demonstrated in the graphs below, this deformation threshold is not exceeded, neither in the edge bolts nor in the internal bolts. The force transmitted through each bolt hole amounts to 15.6 kN[11], knowing that the moment transferred by the connection reaches 8.7 kNm.

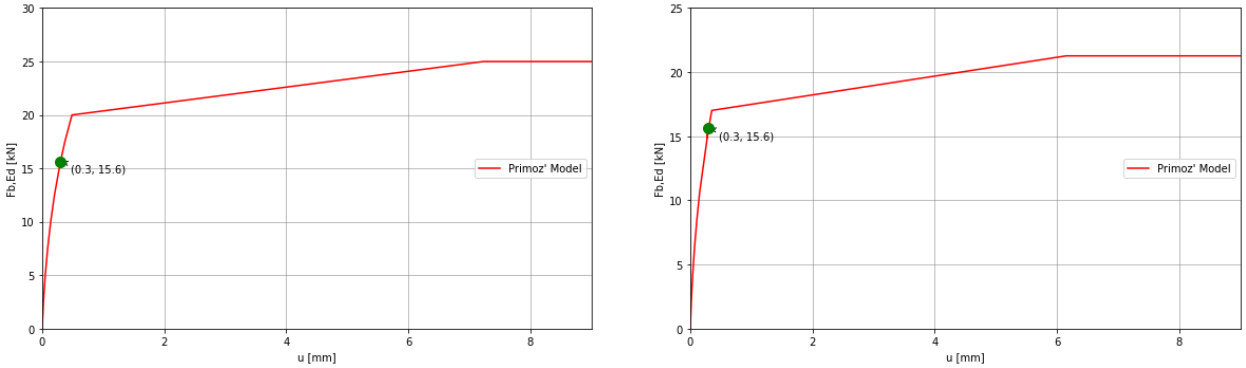

(a) Deformations at inner bolt hole

(b) Deformation at end bolt hole

Figure 4.40: Deformations at bolt holes under $M_{j,Ed} = 8.7kNm$ for *Option 2-1* configuration

[11]The hypothesis of load equidistribution among fastener holes is justified by the connection's demonstrated ductility.

Chapter 5 — Conclusion

The primary objective of this research was to develop an innovative joint solution compatible with the modular structural system designed by DEGOTTE. The component method was implemented and thoroughly detailed to provide complete mechanical characterization of the proposed connection system. This approach enabled systematic evaluation of the joint's structural behaviour while maintaining compatibility with modular construction requirements.

Chapter 3 conducted a systematic evaluation of three beam-to-column joint configurations for modular steel construction, assessing their structural performance against DEGOTTE's design criteria. The analysis revealed that all configurations—Options 1-A, 1-B, and 2—exhibited moment resistances below the target value of 29.6 kNm, with failure governed by chord plastification of the SHS90/4 sleeve. Rotational stiffness measurements classified the joints as semi-rigid according to Eurocode 3 limits. All options demonstrated sufficient ductility for plastic redistribution. While each configuration exceeded the column's bending resistance (9.3 kNm), Option 2 proved superior due to its optimized material-performance ratio (6mm S235 vs. 8mm S355), simplified assembly (single C-profile welding), enhanced production efficiency, and higher moment resistance. The study concludes that achieving the target resistance would necessitate modifications such as upgrading to S355 steel and increasing wall thickness to 6mm (requiring SHS100/8 profiles). Despite not meeting the full plastic capacity of the beam, Option 2 represents the most balanced solution, offering optimal structural performance, constructibility, and manufacturing efficiency.

Chapter 4 explored the influence of joint solutions on structural response, focusing on optimizing resistance and stiffness for *Option 2*. Through iterative analysis, *Option 2-1* emerged as the optimal configuration, balancing rotational stiffness (620 kNm/rad) and plastic resistance (13.7 kNm). Linear buckling and non-linear analyses revealed that rigid joints marginally improved stability but were economically inefficient, while pinned joints increased beam moments and buckling lengths. The study highlighted the need to replace CR200A roof beams with CR310A sections to meet serviceability limits. Analytical and numerical comparisons confirmed Option 2-1 as structurally efficient, minimizing column buckling lengths and ensuring elastic joint behaviour. Sustainability considerations validated limited deformations, making *Option 2-1* a viable solution for demountable modular structures.

This research developed an optimized semi-rigid and full-strength joint solution for DEGOTTE's modular system using component-based analysis. *Option 2-1* emerged as optimal, achieving 13.7 kNm resistance and 620 kNm/rad stiffness while maintaining constructability and material

efficiency. Structural analyses confirmed its effectiveness in controlling buckling behavior and meeting serviceability requirements when paired with CR310A as roof beams. Although not reaching full plastic capacity, the solution satisfies key modular construction demands through balanced performance. The study recommends implementing *Option 2-1* as a technically and economically viable connection system.

Bibliography

1. Université de liège, Département MSM., C.I.C.M., Saint-Remy-les-Chevreuse, *Frame design inclunding joint behaviour Volume 1*, January 1997.

2. T. Yin, Z. Wang, K. Zheng, and S. Lu, A New Method for Design of the Semi-Rigid Steel Frame—The Integration of Joint Inverse Design and Structural Design, Buildings, vol. 12, no. 7, p. 938, 2022, doi: 10.3390/buildings12070938.

3. J.-P. Jaspart and K. Weynand., *Design of Joints in Steel and Composite Structures: Eurocode 3: Design of Steel Structures Part 1-8: Design of Joints / Eurocode 4: Design of Composite Steel and Concrete Structures*, 2016.

4. European Committee for Standardization (CEN), Bureau de Normalisation (NBN), *Eurocode 3: Design of steel structures—Part 1-8: Design of joints (NBN EN 1993-1-8:2024)*, 2024.

5. European Committee for Standardization (CEN), *Eurocode 3: Design of steel structures – Part 1-8: Design of joints (EN 1993-1-8:2005 + AC:2009)*, 2005.

6. F. DREZE, Degotte, *Plan d'exécution – Projet Moms 2*, 2024.

7. MOŽE, Primož and PICULIN, Sara, *Analytical prediction of load-deformation behaviour for bearing at bolt holes*, 2024 vol. 60, p. 105968. https://doi.org/10.1016/j.istruc.2024.105968

8. J. Conde, L. Silva, A.F. Santos, M.S. Lemma, T. Tankova,A model for the initial stiffness of the face plate component, 2023 https://doi.org/10.1016/j.engstruct.2023.116836

9. J-F. Demonceau, *Structures métalliques et mixte acier-béton, GCIV0644-1, 2023-2024.*

10. V. Denël, *Analyse des tructures II, GCIV0607-2, 2023-2024.*

11. Greisch, UEE-ULG, *Chap01: Introduction*, 2024

12. European Committee for Standardization (CEN), *Eurocode 3 — Design of steel structures — Part 1-14: Design assisted by finite element analysis*, 2024.

13. European Committee for Standardization (CEN), Bureau de Normalisation (NBN), *Eurocode 3: Design of steel structures—Part 1-8: Design of joints (NBN EN 1993-1-8:2023)$_A$nnexC : Designofnominallypinnedconnections*, 2023.

Annex A : Option 1-B Design

This configuration employs M12 bolts to enhance joint rigidity, utilizing two parallel rows of three bolts for the flange connection (Fig. 5.1). The corresponding web connection assembly is detailed in Figure 5.2.

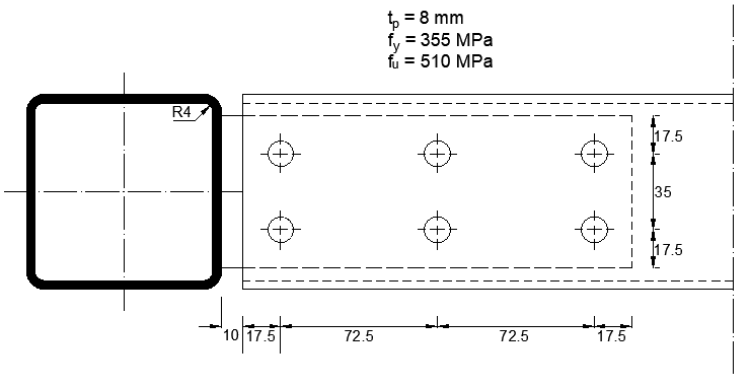

Figure 5.1: Beam flange/ Plate 1 and 2 connexion

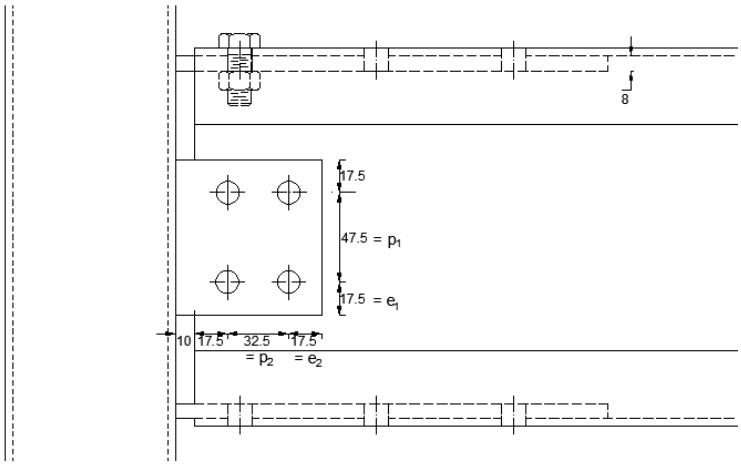

Figure 5.2: Beam web/ Plate 3 connexion

Bolts in shear - Beam flange / Plate 1 and 2

a) Resistance

The shear resistance of a single M12 bolt is calculated using the following expression:

$$F_{v,Rd} = \frac{\alpha_v \cdot f_{ub} \cdot A_s}{\gamma_{M2}}$$

Where: - $\alpha_v = 0.5$, as recommended for grade 10.9 bolts. This class corresponds to an ultimate tensile strength of $f_{ub} = 1000$MPa. - A_s is the tensile stress area of the bolt, taken in the threaded portion, with a value of 84.3 mm^2. - $\gamma_{M2} = 1.25$, the partial safety factor for bolt resistance, as specified in the NBN EN standards.

Substituting the values into the equation gives:

$$F_{v,Rd} = \frac{0.5 \cdot 1000 \cdot 84.3}{1.25 \cdot 1000} = 33.72\text{kN}$$

The total shear resistance of the connection is then calculated by:

$$F_{tot,Rd} = n \cdot m \cdot F_{v,Rd}$$

Where: - $n = 6$, the number of bolts involved in shear, - $m = 1$, the number of shear planes in the connection (see figure 2).

Hence:

$$F_{v,Rd,tot} = 6 \cdot 1 \cdot 33.72 = 202.32\text{kN}$$

b) Stiffness

For bolt rows in bearing-type connections:

$$k_\text{v} = \frac{8 \cdot n_\text{b} \cdot d^2 \cdot f_\text{ub}}{E \cdot d_\text{M16}}$$

$$k_\text{v} = \frac{8 \cdot 6 \cdot 12 \cdot 1000}{210000 \cdot 16} = 2.06 \text{ mm}$$

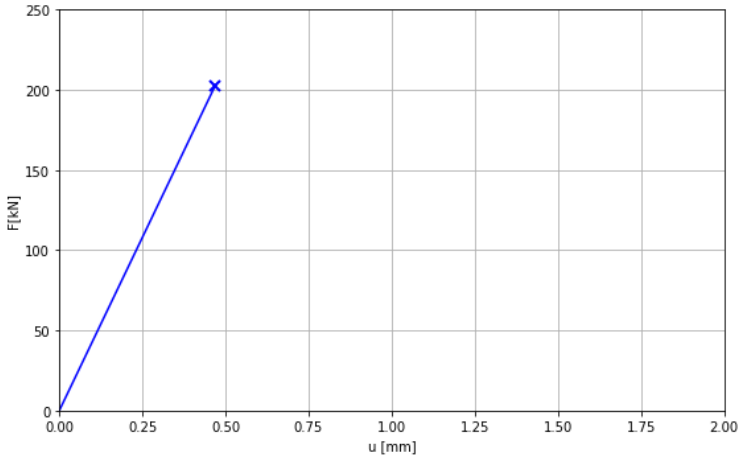

Figure 5.3: Bolt in shear Load-Deformation behaviour

Plate 1 and 2 in bearing

The edge distance in the direction of loading is $e_1 = 17.5$ mm, and the horizontal spacing between bolt rows is $p_1 = 72.5$ mm. The resistance is calculated as follows:

- **Material coefficient**: $k_m = 1$ (Plate 3 is made of S355 steel).
- **End bolts**:

$$\alpha_{\text{b, end}} = \min\left(\frac{e_1}{d_0}, 3 \cdot \frac{f_{\text{ub}}}{f_u}, 3\right) = \min\left(\frac{17.5}{13}, 3 \cdot \frac{1000}{490}, 3\right) = 1.35$$

$$F_{b,Rd,\text{ end}} = 2 \cdot \frac{k_m \cdot \alpha_{\text{b, end}} \cdot f_u \cdot d \cdot t}{\gamma_{\text{M2}}} = 2 \cdot \frac{1 \cdot 1.35 \cdot 510 \cdot 12 \cdot 8}{1.25 \cdot 1000} = 105.7\text{kN}$$

- **Inner bolts**:

$$\alpha_{\text{b,inner}} = \min\left(\frac{p_1}{d_0} - 0.5, 3 \cdot \frac{f_{\text{ub}}}{f_u}, 3\right) = \min\left(\frac{72.5}{13} - 0.5, 3 \cdot \frac{1000}{510}, 3\right) = 3$$

$$F_{b,Rd,\text{ inner}} = 4 \cdot \frac{k_m \cdot \alpha_{\text{b, inner}} \cdot f_u \cdot d \cdot t}{\gamma_{\text{M2}}} = 4 \cdot \frac{1 \cdot 3 \cdot 510 \cdot 12 \cdot 8}{1.25 \cdot 1000} = 469\text{kN}$$

Among the six bolts, four are classified as inner and the other two as end bolts (refer to Figure 5.4).

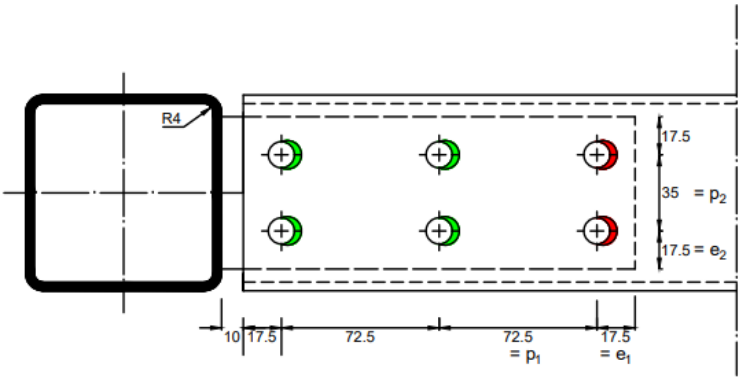

Figure 5.4: Plate 1 and 2 in bearing : Inner bolt (in green) and End bolt (in red)

Thus, the total bearing resistance is:

$$F_{b,Rd,tat} = F_{b,Rd,end} + F_{b,Rd,\text{ inner}}$$

$$F_{b,Rd,tat} = 105.7 + 469 = 574.7\text{kN}$$

b) Stiffness

Linear behaviour proposed by Professor Jaspart

$$k_\text{b} = \frac{12 \cdot n_\text{b} \cdot k_\text{d} \cdot k_\text{t} \cdot d \cdot f_\text{u}}{E} = \frac{12 \cdot 6 \cdot 0.86 \cdot 0.75 \cdot 12 \cdot 510}{210000} = 1.35\ mm$$

Where:

- $n_\text{b} = 6$, is the number of bolts ;
- $k_d = min(k_{d1}, k_{d2}) = min(0.86; 1.25) = 0.86$;
- $k_{d1} = min(0.25 \cdot \frac{e_1}{d} + 0.5; 1.25) = min(0.25 \cdot \frac{17.5}{20} + 0.5; 1.25) = 0.86$;
- $k_{d2} = min(0.25 \cdot \frac{p_1}{d} + 0.375; 1.25) = min(0.25 \cdot \frac{72.5}{20} + 0.375; 1.25) = 1.25$;
- $k_t = min(1.5 \cdot \frac{t_j}{d_{M16}}; 2.5) = min(1.5 \cdot \frac{8}{16}; 2.5) = 0.75$
  with t_j, the thickness of the steel plate on which the bolt bears.

The load deformation law is illustrated in figure 5.19.

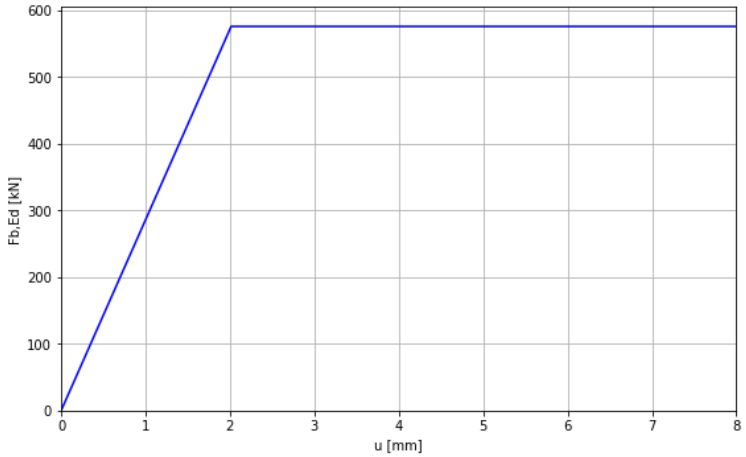

Figure 5.5: Plate in bearing Load-deformation behaviour

Non-linear behaviour proposed Primož Može

The second model offers results presented in tables and graphs below.

$F_{b,Ed}$ [kN]	0.00	5.27	10.55	15.82	21.09	26.36	31.64	36.91	42.18
$\sigma_{b,Ed}$ [-]	0.00	0.11	0.22	0.32	0.43	0.54	0.65	0.75	0.86
u [-]	0.00	0.00	0.00	0.00	0.01	0.01	0.01	0.02	0.02
S_b	0.00	88.88	75.39	65.80	58.22	51.92	46.54	41.85	37.71
k_b	0.00	1.73	1.46	1.28	1.13	1.01	0.90	0.81	0.73
u [mm]	0.00	0.01	0.03	0.06	0.09	0.12	0.17	0.22	0.27

Table 5.1: Characterstic points of the embedment curve for one end bolt hole

$F_{b,Ed}$ [kN]	0.00	11.75	23.50	35.25	47.00	58.75	70.50	82.25	94.00
$\sigma_{b,Ed}$ [-]	0.00	0.24	0.48	0.72	0.96	1.20	1.44	1.68	1.92
u [-]	0.00	0.00	0.01	0.02	0.03	0.04	0.07	0.10	0.15
S_b	0.00	72.96	55.21	43.26	34.32	27.30	21.64	17.02	13.22
k_b	0.00	1.42	1.07	0.84	0.67	0.53	0.42	0.33	0.26
u [mm]	0.00	0.04	0.10	0.20	0.34	0.53	0.80	1.18	1.74

Table 5.2: Characterstic points of the embedment curve for one inner bolt hole

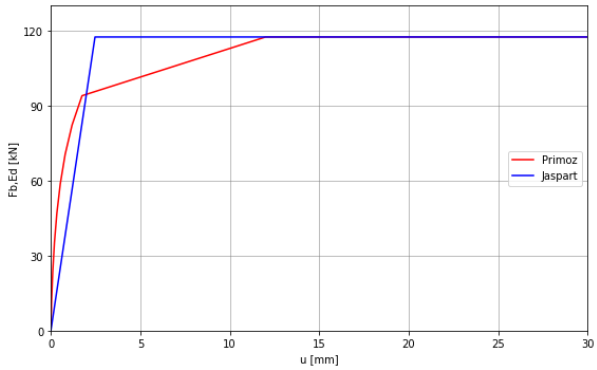

(a) Jaspart and Primoz model comparison at the inner bolt

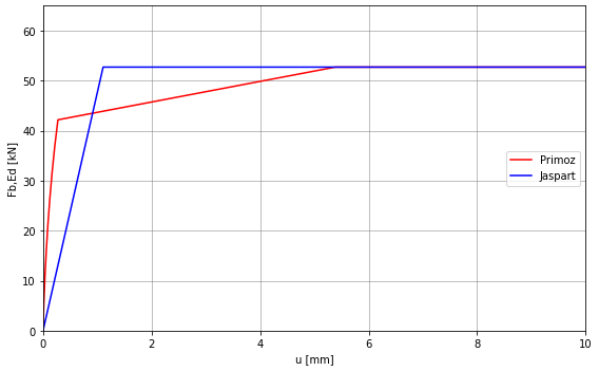

(b) Jaspart and Primoz model comparison at the end bolt

Figure 5.6: Comparison between Jaspart's model and Primoz's model for one bolt hole

Beam flange in bearing

a) Resistance

The edge distance in the direction of loading is $e_1 = 17.5$ mm, and the horizontal spacing between bolt rows is $p_1 = 72.5$ mm. The resistance is calculated as follows:

- **Material coefficient**: $k_m = 1$ (Beam flange made of S235 steel).
- **End bolts**:

$$\alpha_{\text{b, end}} = \min\left(\frac{e_1}{d_0}, 3 \cdot \frac{f_{\text{ub}}}{f_u}, 3\right) = \min\left(\frac{17.5}{13}, 3 \cdot \frac{1000}{490}, 3\right) = 1.35$$

$$F_{b,Rd,\text{ end}} = 2 \cdot \frac{k_m \cdot \alpha_{\text{b, end}} \cdot f_u \cdot d \cdot t}{\gamma_{\text{M2}}} = 2 \cdot \frac{1 \cdot 1.35 \cdot 360 \cdot 12 \cdot 4}{1.25 \cdot 1000} = 37.3\text{kN}$$

- **Inner bolts**:

$$\alpha_{\text{b,inner}} = \min\left(\frac{p_1}{d_0} - 0.5, 3 \cdot \frac{f_{\text{ub}}}{f_u}, 3\right) = \min\left(\frac{72.5}{13} - 0.5, 3 \cdot \frac{1000}{490}, 3\right) = 3$$

$$F_{b,Rd,\text{ inner}} = 2 \cdot \frac{k_m \cdot \alpha_{\text{b, inner}} \cdot f_u \cdot d \cdot t}{\gamma_{\text{M2}}} = 4 \cdot \frac{1 \cdot 3 \cdot 360 \cdot 12 \cdot 4}{1.25 \cdot 1000} = 165.9\text{kN}$$

Among the six bolts, four are classified as inner and the other two as end bolts (refer to Figure 5.7).

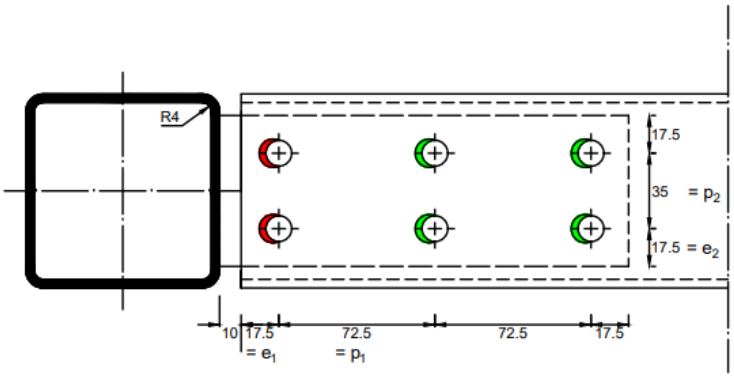

Figure 5.7: Beam flange in bearing : Inner bolts (in red) and End bolt (in green)

Thus, the total bearing resistance is:

$$F_{b,Rd,tot} = F_{b,Rd,end} + F_{b,Rd,\text{ inner}}$$

$$F_{b,Rd,tot} = 37.3 + 165.9 = 203.2\text{kN}$$

b) Stiffness

Linear behaviour proposed by Professor Jaspart

$$k_\text{b} = \frac{12 \cdot n_\text{b} \cdot k_\text{d} \cdot k_\text{t} \cdot d \cdot f_\text{u}}{E} = \frac{12 \cdot 6 \cdot 0.86 \cdot 0.375 \cdot 12 \cdot 360}{210000} = 0.48\ mm$$

Where:

- $n_\text{b} = 6$, is the number of bolts ;
- $k_d = min(k_{d1}, k_{d2}) = min(0.86; 1.25) = 0.86$;
- $k_{d1} = min(0.25 \cdot \frac{e_1}{d} + 0.5; 1.25) = min(0.25 \cdot \frac{17.5}{20} + 0.5; 1.25) = 0.86;$
- $k_{d2} = min(0.25 \cdot \frac{p_1}{d} + 0.375; 1.25) = min(0.25 \cdot \frac{72.5}{20} + 0.375; 1.25) = 1.25;$
- $k_t = min(1.5 \cdot \frac{t_j}{d_{M16}}; 2.5) = min(1.5 \cdot \frac{4}{16}; 2.5) = 0.375$
  with t_j, the thickness of the steel plate on which the bolt bears.

The load deformation law is illustrated in figure 5.19.

Figure 5.8: Load-deformation behaviour for one bolt hole

Non-linear behaviour proposed Primož Može

The second model offers results presented in tables and graphs below.

$F_{b,Ed}$ [kN]	0.00	4.15	8.29	12.44	16.59	20.74	24.88	29.03	33.18
$\sigma_{b,Ed}$ [-]	0.00	0.24	0.48	0.72	0.96	1.20	1.44	1.68	1.92
u [-]	0.00	0.00	0.01	0.02	0.03	0.04	0.07	0.10	0.15
S_b	0.00	72.96	55.21	43.26	34.32	27.30	21.64	17.02	13.22
k_b	0.00	1.50	1.14	0.89	0.71	0.56	0.45	0.35	0.27
u [mm]	0.00	0.04	0.10	0.20	0.34	0.53	0.80	1.18	1.74

Table 5.3: Characterstic points of the embedment curve for one inner bolt hole

$F_{b,Ed}$ [kN]	0.00	1.86	3.72	5.58	7.44	9.30	11.17	13.03	14.89
$\sigma_{b,Ed}$ [-]	0.00	0.11	0.22	0.32	0.43	0.54	0.65	0.75	0.86
u [-]	0.00	0.00	0.00	0.00	0.01	0.01	0.01	0.02	0.02
S_b	0.00	88.88	75.39	65.80	58.22	51.92	46.54	41.85	37.71
k_b	0.00	1.83	1.55	1.35	1.20	1.07	0.96	0.86	0.78
u [mm]	0.00	0.01	0.03	0.06	0.09	0.12	0.17	0.22	0.27

Table 5.4: Characterstic points of the embedment curve for one end bolt hole

A comparison of the first and second model is shown in figure 5.20.

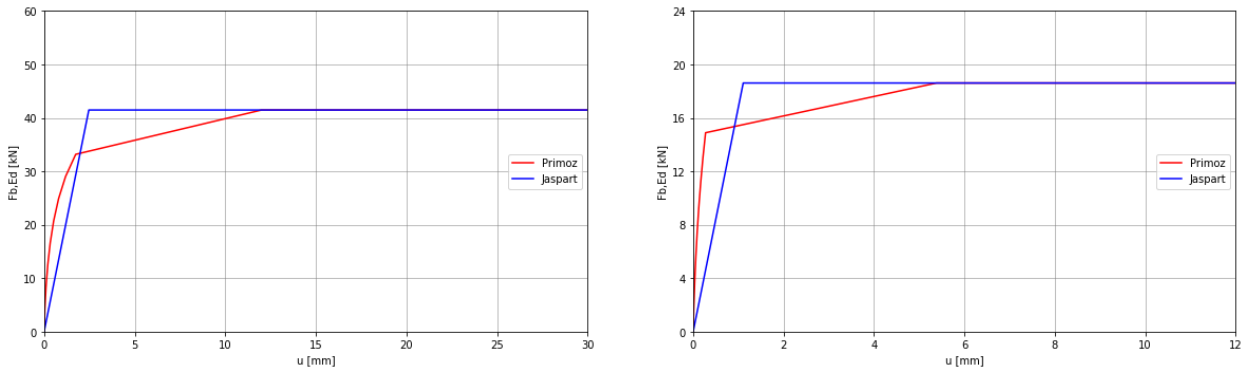

(a) Comparison at the inner bolt

(b) Comparison at the end bolt

Figure 5.9: Comparison between Jaspart's model and Primoz's model for one bolt hole

Plate 1 in tension

a) Resistance

The tensile resistance of the plate is evaluated by considering both the gross and net section capacities. The governing resistance is taken as the lower of the two.

- **Gross Section Resistance:**

  The tensile resistance of the gross cross-section is calculated as:

$$N_{pl,Rd} = \frac{A_p \cdot f_y}{\gamma_{M0}} = \frac{8 \cdot 70 \cdot 355}{1.0 \cdot 1000} = 198.8\,\text{kN}$$

- **Net Section Resistance:**
  The tensile resistance of the net section, accounting for the bolt hole deduction, is given by:

$$N_{u,Rd} = \frac{0.9 \cdot (A_p - d_0 \cdot t) \cdot f_u}{\gamma_{M0}} = \frac{0.9 \cdot (8 \cdot 70 - 2 \cdot 13 \cdot 8) \cdot 510}{1.0 \cdot 1000} = 161.6\,\text{kN}$$

Since the net section resistance is lower, it governs the design. This indicates a brittle failure mode, as rupture occurs through the reduced cross-section near the bolt hole.

b) Stiffness

The stiffness coefficient is infinity. (cfr. to section 3.4.4)

$$k_t = \infty$$

Plate 2 in Compression

a) Resistance

The design resistance in compression is evaluated in accordance with EN 1993-1-1 of the Eurocode. Since the plate is laterally stabilized through its connection to the beam flange, global instability is not expected to occur. Nevertheless, the plate is classified as Class 3. As a result, the design check is limited to the section capacity, given by the following expression:

$$N_{pl,Rd} = \frac{A_p \cdot f_{y,fp}}{\gamma_{M0}} \tag{5.1}$$

where A_p is the cross-sectional area of the plate, $f_{y,fp}$ is the yield strength of the fin plate material, and γ_{M1} is the partial safety factor for resistance of cross-sections. Hence,

$$N_{pl,Rd} = \frac{70 \cdot 8 \cdot 355}{1.0 \cdot 1000} = 198.8\,\text{kN}$$

b) Stiffness

The stiffness coefficient is infinity. (cfr. to section 3.4.4)

$$k_c = \infty$$

Block tearing - Plate 1

Considering a plate under uniform tension with two bolt rows aligned with the loading direction, the stress distribution is assumed uniform across the net section[1], as demonstrated in Figure 5.10.

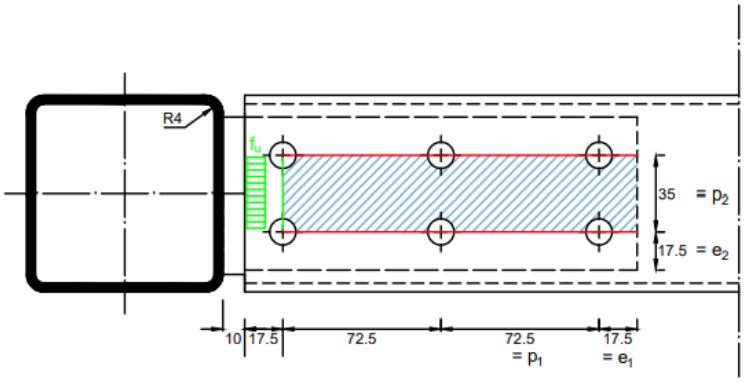

Figure 5.10: Plate 1 - Block tearing

The net area subjected to tension is:

$$A_{nt} = (p_2 - d_0) \cdot t_p = (35 - 13) \cdot 8 = 176\,\text{mm}^2$$

The areas subjected to shear, at the gross and net sections respectively, are:

$$A_{gv} = 2 \cdot (e_1 + 2 \cdot p_1) \cdot t_p = 2 \cdot (17.5 + 2 \cdot 72.5) \cdot 8 = 2600\,\text{mm}^2$$

$$A_{nv} = 2 \cdot (e_1 + 2 \cdot p_1 - 2.5 \cdot d_0) \cdot t_p = 2 \cdot (17.5 + 2 \cdot 72.5 - 2.5 \cdot 13) \cdot 8 = 2080\,\text{mm}^2$$

The design value of the block tearing resistance is then computed as:

$$V_{eff,1,Rd} = \frac{A_{nt} \cdot f_u + \min\left(\frac{A_{gv} \cdot f_y}{\sqrt{3}}, \frac{A_{nv} \cdot f_u}{\sqrt{3}}\right)}{\gamma_{M2}}$$

$$V_{eff,1,Rd} = \frac{176 \cdot 490 + \min\left(\frac{2600 \cdot 355}{\sqrt{3}}, \frac{2080 \cdot 510}{\sqrt{3}}\right)}{1.25 \cdot 1000} = 498.1\,\text{kN}$$

Block tearing - Beam flange

The same verification is proceed for this component.

[1]This assumption holds when: (1) bolt rows are symmetrically positioned at mid-width, and (2) both bearing resistance and bolt shear capacity are verified to prevent localized failure modes.

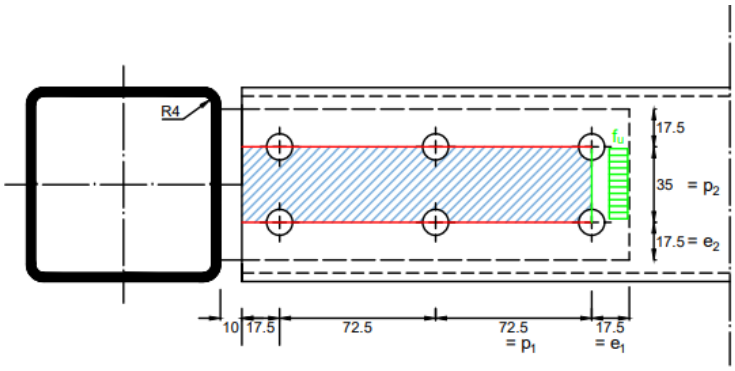

Figure 5.11: Beam flange - Block tearing

The net area subjected to tension is:

$$A_{nt} = (p_2 - d_0) \cdot t_p = (35 - 13) \cdot 4 = 88\,\text{mm}^2$$

The areas subjected to shear, at the gross and net sections respectively, are:

$$A_{gv} = 2 \cdot (e_1 + 2 \cdot p_1) \cdot t_p = 2 \cdot (17.5 + 2 \cdot 72.5) \cdot 4 = 1300\,\text{mm}^2$$

$$A_{nv} = 2 \cdot (e_1 + 2 \cdot p_1 - 2.5 \cdot d_0) \cdot t_p = 2 \cdot (17.5 + 2 \cdot 72.5 - 2.5 \cdot 13) \cdot 4 = 1040\,\text{mm}^2$$

The design value of the block tearing resistance is then computed as:

$$V_{eff,1,Rd} = \frac{A_{nt} \cdot f_u + \min\left(\frac{A_{gv} \cdot f_y}{\sqrt{3}}, \frac{A_{nv} \cdot f_u}{\sqrt{3}}\right)}{\gamma_{M2}}$$

$$V_{eff,1,Rd} = \frac{88 \cdot 360 + \min\left(\frac{1300 \cdot 235}{\sqrt{3}}, \frac{1040 \cdot 360}{\sqrt{3}}\right)}{1.25 \cdot 1000} = 166.4\,\text{kN}$$

Column wall Chord plastification and chord punching shear

a) Resistance

Using equation 3.9, where only the width ratio change from the first configuration. It becomes, β, given by the ratio between the plate width and the connected RHS width, $\frac{b_p}{b_0} = \frac{70}{90} = 0.78$. The obtained resistances are

- **Top support flange in tension** :

$$N_{1,t,\text{Rd}} = \frac{2.3 \cdot 235 \cdot 4^2 \cdot \left(1 + 3 \cdot 0.78^2\right) \cdot 11.25^{0,35} \cdot 1}{1.0 \cdot 1000} = 57\,kN$$

- **Bottom support flange compressions** :

$$N_{1,c,\mathrm{Rd}} = \frac{2.3 \cdot 235 \cdot 4^2 \cdot \left(1 + 3 \cdot 0.848^2\right) \cdot 11.25^{0,35} \cdot 1}{1.0 \cdot 1000} = 57\,kN$$

b) Stiffness

$$K_{D,fixed} = \frac{E}{1-\nu^2}\frac{t^3}{n^3} = \frac{210000}{1-0.33^2}\frac{4^3}{2^3} = 1.9 \text{ kN/m}$$

where

ν is the poisson coefficient related to steel, 0.33

t the thickness of the face, 4mm

n the distance of the horizontal plate to the edge of the RHS face, 2mm

The corresponding stiffness coefficient equals to 9 mm.

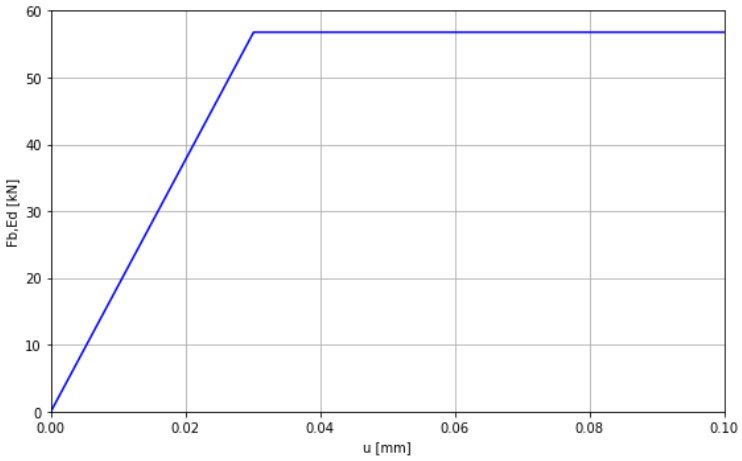

Figure 5.12: Column face stiffness

Column face in shear

a) Resistance

The design resistance in shear for the two panels of the column is 72.3kN. (cfr. section 3.4.8)

b) Stiffness

Idem. (cfr. section 3.4.8)

Bolts in Shear – Beam Web / Plate 3

Figure 5.13 illustrates Plate 3, which features two rows of two M12 bolts. Bolts of class 10.9 are employed, ensuring consistency with those used in flange connections. Plate 3 possesses similar

mechanical properties to Plates 1 and 2.

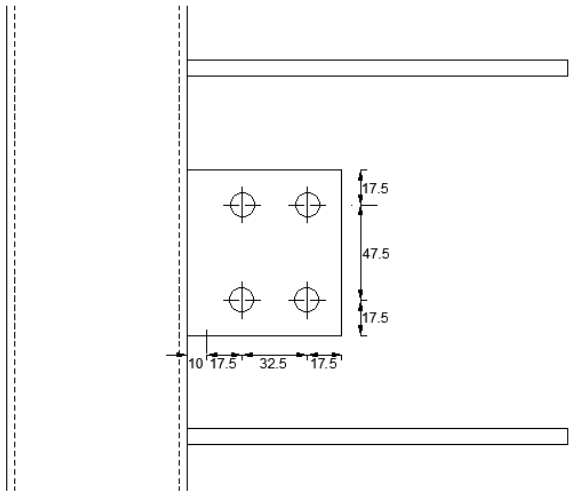

Figure 5.13: Plate 3 geometry

The shear resistance of a single bolt has been determined in Section 5 as $F_{v,Rd} = 33.72\,\text{kN}$. Considering one shear plane and four bolts engaged in shear, the total shear resistance is:

$$F_{\text{tot},v,Rd} = n \cdot m \cdot F_{v,Rd} = 4 \cdot 1 \cdot 33.72 = 134.9\,\text{kN}$$

Plate 3 in Bearing

The edge distance in the direction of loading is $e_1 = 17.5\,\text{mm}$, and the vertical spacing between bolt rows is $p_1 = 47.5\,\text{mm}$. The resistance is calculated as follows:

- Material coefficient: $k_m = 1$ (Plate 3 is made of S355 steel).
- **End bolts:**

$$\alpha_{\text{b,end}} = \min\left(\frac{e_1}{d_0}, 3 \cdot \frac{f_{\text{ub}}}{f_u}, 3\right) = \min\left(\frac{17.5}{13}, 3 \cdot \frac{1000}{490}, 3\right) = 1.35$$

$$F_{b,Rd,\text{end}} = 2 \cdot \frac{k_m \cdot \alpha_{\text{b,end}} \cdot f_u \cdot d \cdot t}{\gamma_{\text{M2}}} = 2 \cdot \frac{1 \cdot 1.35 \cdot 510 \cdot 12 \cdot 8}{1.25 \cdot 1000} = 105.7\,\text{kN}$$

- **Inner bolts:**

$$\alpha_{\text{b,inner}} = \min\left(\frac{p_1}{d_0} - 0.5, 3 \cdot \frac{f_{\text{ub}}}{f_u}, 3\right) = \min\left(\frac{47.5}{13} - 0.5, 3 \cdot \frac{1000}{490}, 3\right) = 3$$

$$F_{b,Rd,\text{inner}} = 2 \cdot \frac{k_m \cdot \alpha_{\text{b,inner}} \cdot f_u \cdot d \cdot t}{\gamma_{\text{M2}}} = 2 \cdot \frac{1 \cdot 3 \cdot 510 \cdot 12 \cdot 8}{1.25 \cdot 1000} = 235.0\,\text{kN}$$

Among the four bolts, two are classified as inner and the other two as end bolts (refer to Figure 5.14).

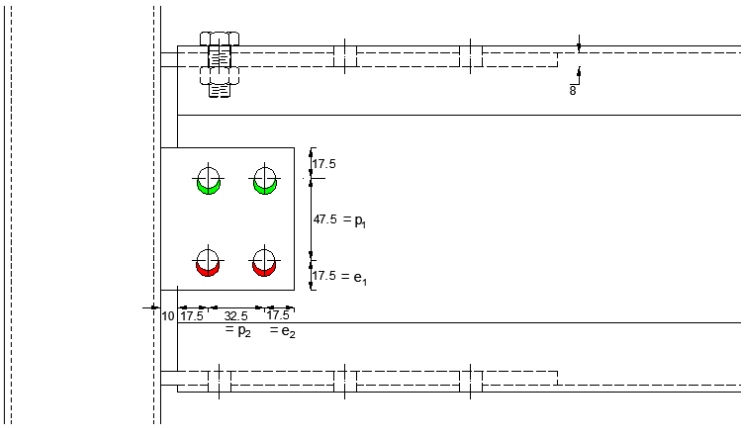

Figure 5.14: Plate 3 in bearing : Inner bolt (in green) and End bolt (in red)

Thus, the total bearing resistance is:

$$F_{b,Rd,\text{tot}} = F_{b,Rd,\text{end}} + F_{b,Rd,\text{inner}} = 105.7 + 235 = 340.7\,\text{kN}$$

Beam Web in Bearing

As illustrated in Figure 5.15, the edge distance is $e_1 = 75\,\text{mm}$. Knowing that the beam is made of S235 steel. The bearing resistance is computed as:

- $k_m = 1$ (S235 steel).
- **End bolts:**

$$\alpha_{\text{b,end}} = \min\left(\frac{e_1}{d_0}, 3\cdot\frac{f_{\text{ub}}}{f_u}, 3\right) = \min\left(\frac{76.25}{13}, 3\cdot\frac{1000}{360}, 3\right) = 3$$

$$F_{b,Rd,\text{end}} = 2\cdot\frac{1\cdot 3\cdot 360\cdot 12\cdot 4}{1.25\cdot 1000} = 82.9\,\text{kN}$$

- **Inner bolts:**

$$\alpha_{\text{b,inner}} = \min\left(\frac{p_1}{d_0} - 0.5, 3\cdot\frac{f_{\text{ub}}}{f_u}, 3\right) = \min\left(\frac{47.5}{13} - 0.5, 3\cdot\frac{1000}{360}, 3\right) = 3$$

$$F_{b,Rd,\text{inner}} = 2\cdot\frac{1\cdot 3\cdot 360\cdot 12\cdot 4}{1.25\cdot 1000} = 82.9\,\text{kN}$$

Thus, the total bearing resistance of the beam web is:

$$F_{b,Rd,\text{tot}} = 82.9 + 82.9 = 165.8\,\text{kN}$$

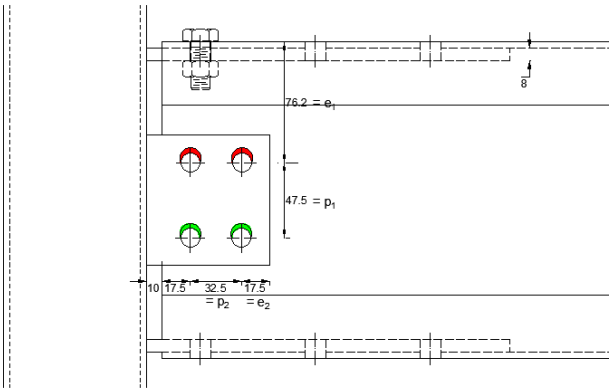

Figure 5.15: Beam web in bearing : Inner bolt (in green) and end bolt (in red)

Plate 3 in Shear

According to the NBN 1993 1-8:2024 recommendations, the design shear resistance of the fin plate should be taken as the smallest of the following design resistance values: the gross section in shear, the net section in shear, and block tearing.

- **Gross section in shear** :

$$V_{v,p,Rd} = \frac{A_{v,fp} \cdot f_{y,fp}}{1.27 \cdot \sqrt{3} \cdot \gamma_{M0}} \tag{5.2}$$

$$V_{v,p,Rd} = \frac{82.5 \cdot 8 \cdot 355}{1.27 \cdot \sqrt{3} \cdot 1.0 \cdot 1000} = 106.5\,\text{kN}$$

- **Net section in shear** :

$$V_{u,fp,Rd} = \frac{A_{v,net,fp} \cdot f_{u,fp}}{\sqrt{3} \cdot \gamma_{M2}} \tag{5.3}$$

$$V_{u,fp,Rd} = \frac{(82.5 - 2 \cdot 13) \cdot 8 \cdot 510}{\sqrt{3} \cdot 1.25 \cdot 1000} = 106.5\,\text{kN}$$

- **Block tearing** : In the presence of shear, block tearing may occur.
  The net tension area is:

$$A_{nt} = (e_2 + p_2 - 1.5 \cdot d_0) \cdot t_p = (17.5 + 32.5 - 1.5 \cdot 13) \cdot 8 = 244\,\text{mm}^2$$

  The gross and net shear areas are:

$$A_{gv} = (e_1 + p_1) \cdot t_p = (17.5 + 47.5) \cdot 8 = 520\,\text{mm}^2$$

$$A_{nv} = (e_1 + p_1 - 1.5 \cdot d_0) \cdot t_p = (17.5 + 47.5 - 1.5 \cdot 13) \cdot 8 = 364\,\text{mm}^2$$

  Considering a non-uniform distribution of tension in the tensile area, the design block tearing resistance is given by:

$$V_{eff,1,Rd} = \frac{0.5 \cdot A_{nt} \cdot f_u + \min\left(\frac{A_{gv} \cdot f_y}{\sqrt{3}}, \frac{A_{nv} \cdot f_u}{\sqrt{3}}\right)}{\gamma_{M2}} = 135\,\text{kN}$$

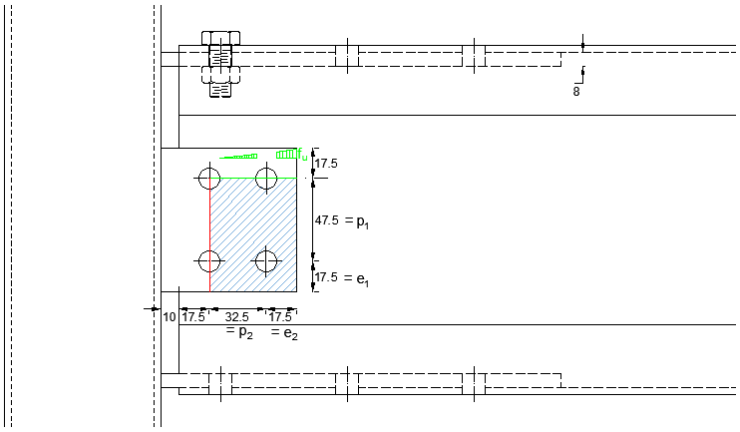

Figure 5.16: Plate 3 - Block tearing

Annex B : Option 2 Design

Bolts in shear - Beam flange / Joint flange

As the bolts configuration is similar to one choosen for Option 1-A, the resistance remains the same, 294 kN. (cfr to section 3.4.1)
Idem for the stiffness.

Support flange in bearing

a) Resistance

The bearing resistance of the plates is determined using the Belgian Standard, NBN EN 1993-1-8:2024. The resistance is given by the following equation:

$$F_{\mathrm{b,Rd}} = \frac{k_{\mathrm{m}} \alpha_{\mathrm{b}} f_{\mathrm{u}} dt}{\gamma_{\mathrm{M2}}}$$

Where:

- For end fasteners:

$$\alpha_{\mathrm{b,end\ bolt}} = \min\left(\frac{e_1}{d_0}; 3 \cdot \frac{f_{\mathrm{ub}}}{f_{\mathrm{u}}}; 3\right) = \min\left(\frac{27.5}{20+2}; 3 \cdot \frac{1000}{490}; 3\right) = 1.25$$

- For inner fasteners:

$$\alpha_{\mathrm{b,inner\ bolt}} = \min\left(\frac{p_1}{d_0} - \frac{1}{2}; 3 \cdot \frac{f_{\mathrm{ub}}}{f_{\mathrm{u}}}; 3\right) = \min\left(\frac{87.5}{20+2} - 0.5; 3 \cdot \frac{1000}{490}; 3\right) = 3$$

- $k_m = 1$, as the elastic resistance of the plates is 355 MPa, so that $f_y \leq 460\,\mathrm{MPa}$. The ultimate resistance f_u of the plates is 510 MPa.

In Figure 5.17, the geometry of Plates 1 and 2 is presented, from which e_1 and p_1 can be extracted. In this configuration, there are two internal bolts (in green) and one external bolt (in red), as illustrated in Figure 5.18.

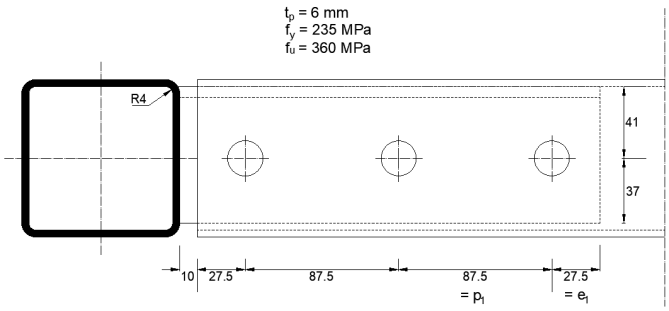

Figure 5.17: Beam flange/ support flange connexion : Constructive dispositions

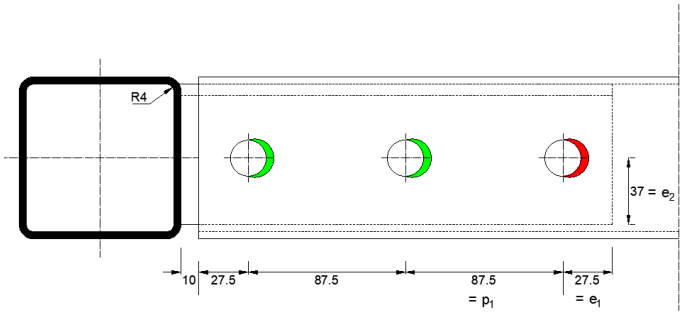

Figure 5.18: Support flange in bearing : Inner bolt (in green) and End bolt (in red)

Using Equation 3.5, the resistance of the inner and external bolts can be calculated as follows:

- For the inner bolts:

$$F_{b,\text{Rd,inner bolt}} = 2 \cdot \frac{k_m \cdot \alpha_{\text{b,inner bolt}} \cdot f_u \cdot d \cdot t}{\gamma_{\text{M2}}} = 2 \cdot \frac{1 \cdot 3 \cdot 360 \cdot 20 \cdot 6}{1.25 \cdot 1000} = 207.3\,\text{kN}$$

- For the end bolt:

$$F_{b,\text{Rd,end bolt}} = 1 \cdot \frac{k_m \cdot \alpha_{\text{b,end bolt}} \cdot f_u \cdot d \cdot t}{\gamma_{\text{M2}}} = 1 \cdot \frac{1 \cdot 1.25 \cdot 360 \cdot 20 \cdot 6}{1.25 \cdot 1000} = 43.2\,\text{kN}$$

Therefore, the total bearing resistance of support top and bottom flanges is:

$$F_{\text{b,Rd,tot}} = F_{b,\text{Rd,inner bolt}} + F_{b,\text{Rd,end bolt}}$$

$$F_{\text{b,Rd,tot}} = 207.3 + 43.2 = 250.5\,\text{kN}$$

b) Stiffness

Linear behaviour proposed by Professor Jaspart

$$k_{\text{b}} = \frac{12 \cdot n_{\text{b}} \cdot k_{\text{d}} \cdot k_{\text{t}} \cdot d \cdot f_{\text{u}}}{E} = \frac{12 \cdot 3 \cdot 0.84 \cdot 0.56 \cdot 20 \cdot 360}{210000} = 0.58\ mm$$

Where:

- $n_b = 3$, is the number of bolts ;
- $k_d = min(k_{d1}, k_{d2}) = min(0.84; 1.25) = 0.84$;
- $k_{d1} = min(0.25 \cdot \frac{e_1}{d} + 0.5; 1.25) = min(0.25 \cdot \frac{27.5}{20} + 0.5; 1.25) = 0.84$;
- $k_{d2} = min(0.25 \cdot \frac{p_1}{d} + 0.375; 1.25) = min(0.25 \cdot \frac{87.5}{20} + 0.375; 1.25) = 1.25$;
- $k_t = min(1.5 \cdot \frac{t_j}{d_{M16}}; 2.5) = min(1.5 \cdot \frac{6}{16}; 2.5) = 0.56$
  with t_j, the thickness of the steel plate on which the bolt bears.

The load deformation law is illustrated in figure 5.19.

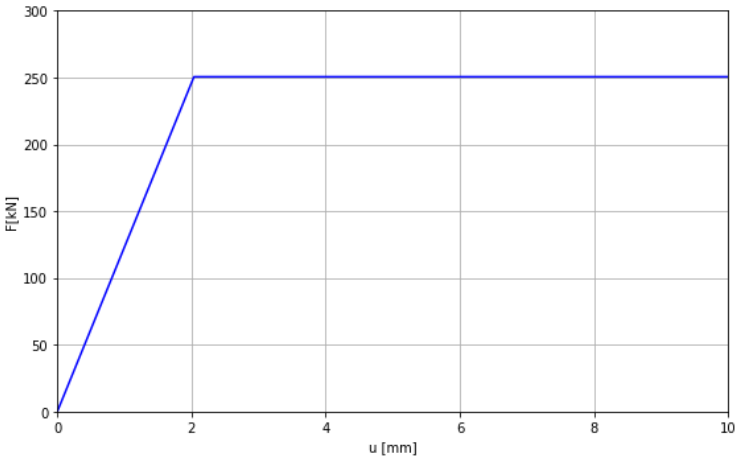

Figure 5.19: Load-deformation behaviour for one bolt hole

Non-linear behaviour proposed Primož Može

The second model offers results presented in tables and graphs below.

$F_{b,Ed}$ [kN]	0.00	10.37	20.74	31.10	41.47	51.84	62.21	72.58	82.94
$\sigma_{b,Ed}$ [-]	0.00	0.24	0.48	0.72	0.96	1.20	1.44	1.68	1.92
u [-]	0.00	0.00	0.01	0.02	0.03	0.04	0.07	0.10	0.15
S_b	0.00	72.96	55.21	43.26	34.32	27.30	21.64	17.02	13.22
k_b	0.00	0.75	0.57	0.44	0.35	0.28	0.22	0.18	0.14
u [mm]	0.00	0.07	0.17	0.33	0.56	0.88	1.33	1.97	2.91

Table 5.5: Characterstic points of the embedment curve for one inner bolt hole

$F_{b,Ed}$ [kN]	0.00	4.32	8.64	12.96	17.28	21.60	25.92	30.24	34.56
$\sigma_{b,Ed}$ [-]	0.00	0.10	0.20	0.30	0.40	0.50	0.60	0.70	0.80
u [-]	0.00	0.00	0.00	0.00	0.01	0.01	0.01	0.02	0.02
S_b	0.00	90.12	77.01	67.65	60.23	54.05	48.75	44.12	40.02
k_b	0.00	0.93	0.79	0.70	0.62	0.56	0.50	0.45	0.41
u [mm]	0.00	0.02	0.05	0.09	0.13	0.19	0.25	0.32	0.40

Table 5.6: Characterstic points of the embedment curve for one end bolt hole

A comparison of the first and second model is shown in figure 5.20.

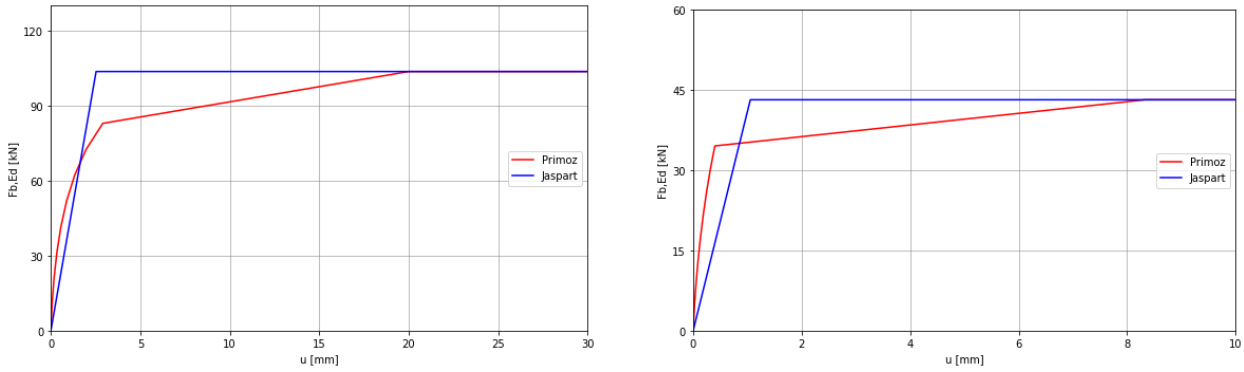

(a) Comparison at the inner bolt

(b) Comparison at the end bolt

Figure 5.20: Comparison between Jaspart's model and Primoz's model for one bolt hole

Beam flange in bearing

Cfr. to section 3.4.3

Support Support in tension (or Plate 1 in tension)

a) Resistance

Once the bolts resist the applied shear forces, a tensile force is induced in Plate 1. The tensile resistance of the plate is evaluated by considering both the gross and net section capacities. The governing resistance is taken as the lower of the two.

- **Gross Section Resistance:**
  The tensile resistance of the gross cross-section is calculated as :

$$N_{pl,Rd} = \frac{A_p \cdot f_y}{\gamma_{M0}} = \frac{862 \cdot 235}{1.0 \cdot 1000} = 202.6\,\text{kN}$$

  where the area subjected to tension As corresponds to an equivalent cleat Leg, as illustrated in figure 5.21

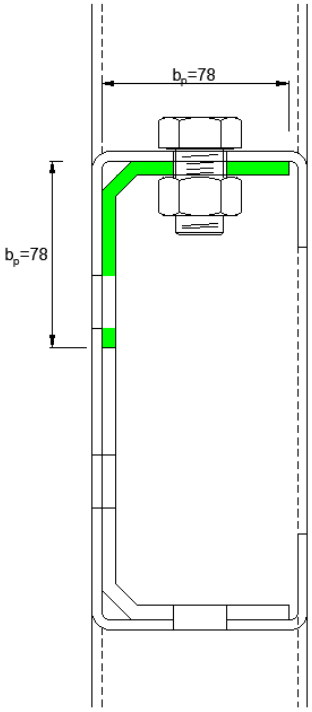

Figure 5.21: Area subjected to tension

- **Net Section Resistance:**
  The tensile resistance of the net section, accounting for the bolt hole deduction, is given by:

$$N_{u,Rd} = \frac{0.9 \cdot (A_p - 2 \cdot d_0 \cdot t) \cdot f_u}{\gamma_{M0}} = \frac{0.9 \cdot (862 - 2 \cdot 22 \cdot 6) \cdot 360}{1.0 \cdot 1000} = 193.8\,\text{kN}$$

Since the net section resistance is lower, it governs the design. This indicates a brittle failure mode, as rupture occurs through the reduced cross-section near the bolt hole.

b) Stiffness

According to the Eurocode 3 Part 1-8, the stiffness coefficient of a plate under tension should be considered infinite.

$$k_t = \infty$$

Plate 2 in Compression

a) Resistance

The design resistance in compression is evaluated in accordance with EN 1993-1-1 of the Eurocode. Since the support is a compact member, global instability is not expected to occur. Nevertheless, the plate is classified as Class 3. As a result, the design check is limited to the section capacity,

given by the following expression:

$$N_{pl,Rd} = \frac{A_p \cdot f_{y,fp}}{\gamma_{M0}} \tag{5.4}$$

where A_p[2] is the cross-sectional area of the plate, $f_{y,fp}$ is the yield strength of the fin plate material, and γ_{M1} is the partial safety factor for resistance of cross-sections. Hence,

$$N_{pl,Rd} = \frac{862 \cdot 235}{1.0 \cdot 1000} = 202.6\,\text{kN}$$

b) Stiffness

Once again, Eurocode 3 Part 1-8 assumes an infinitely stiff coefficient for plates in compression.

$$k_c = \infty$$

Block tearing - Support flange

Due to the tensile forces acting on the support top flange[3], the possibility of block tearing must also be evaluated. Beyond checking the support flange in bearing, a separate verification is required to ensure that the latest does not fail by block tearing.

According to Belgian standards, block tearing is decomposed into two simultaneous failure modes: tension and shear. Given that the support flange is subjected to uniform tension, it is assumed that the tension is uniformly distributed over the tension area, as illustrated in Figure 5.22.

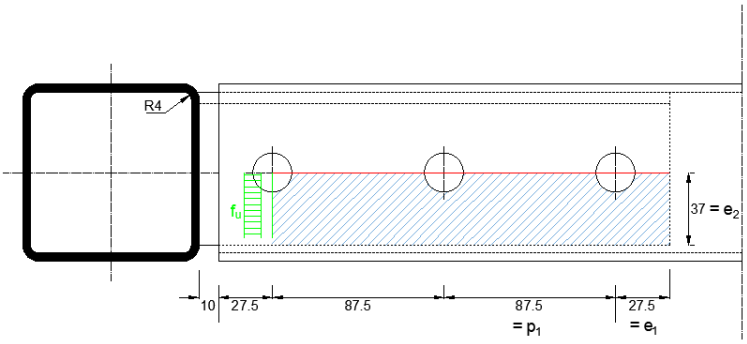

Figure 5.22: Support flange - Block tearing

The net tension area is calculated using an equivalent cleat section, where the stiffener leg

[2]where A_p represents the effective area in bearing, conservatively taken as the gross cross-sectional area in tension due to uncertainties in load diffusion length through the web of the supporting element.

[3]The risk of block tearing for the top flange is motivated by the fact that the support section is not twice symmetrical. The support web make one side stiffer than the other. Block tearing can develop at the weak side.

(initially 40 mm) is effectively reduced to $\frac{b-d_0}{2}$. Eurocode recommends using an "equivalent equal-leg angle with leg length equal to the smaller leg".
This adjustment reflects the conservative assumption that, under tension, stress diffusion occurs along a length up to that of the connected leg. Thus, the net area in tension is:

$$A_{nt} = \left(e_2 - \frac{d_0}{2}\right) \cdot t_{fp}$$

$$A_{nt} = \left(37 - \frac{22}{2}\right) \cdot 6 = 156$$

The gross and net shear areas are respectively :

$$A_{gv} = (e_1 + 2 \cdot p_1) \cdot t_f = (27.5 + 2 \cdot 87.5) \cdot 6 = 1215\,\text{mm}^2$$

$$A_{nv} = (e_1 + 2 \cdot p_1 - 2.5 \cdot d_0) \cdot t_f = (27.5 + 2 \cdot 87.5 - 2.5 \cdot 22) \cdot 6 = 885\,\text{mm}^2$$

Assuming uniform stress distribution in the tension area, the block tearing resistance is:

$$V_{eff,1,Rd} = \frac{A_{nt} \cdot f_u + \min\left(\frac{A_{gv} \cdot f_y}{\sqrt{3}}, \frac{A_{nv} \cdot f_u}{\sqrt{3}}\right)}{\gamma_{M2}}$$

$$V_{eff,1,Rd} = \frac{156 \cdot 360 + \min\left(\frac{1215 \cdot 235}{\sqrt{3}}, \frac{885 \cdot 360}{\sqrt{3}}\right)}{1.25 \cdot 1000} = 176.8\,\text{kN}$$

Block tearing - Beam flange

This component configuration is identical to one presented in section 3.4.6. The resistance obtained is 161.7 kN.

Column wall Chord plastification and chord punching shear

Using equation 3.9, where only the width ratio change from the first configuration. It becomes, β, given by the ratio between the plate width and the connected RHS width, $\frac{b_p}{b_0} = \frac{74}{90} = 0.87$. The obtained resistances are

- **Top support flange in tension** :

$$N_{1,t,\text{Rd}} = \frac{2.3 \cdot 235 \cdot 4^2 \cdot \left(1 + 3 \cdot 0.87^2\right) \cdot 11.25^{0,35} \cdot 1}{1.0 \cdot 1000} = 65.6\,kN$$

- **Bottom support flange compressions** :

$$N_{1,c,\text{Rd}} = \frac{2.3 \cdot 235 \cdot 4^2 \cdot \left(1 + 3 \cdot 0.87^2\right) \cdot 11.25^{0,35} \cdot 1}{1.0 \cdot 1000} = 65.6\,kN$$

b) Stiffness

$$K_{D,fixed} = \frac{E}{1-\nu^2}\frac{t^3}{n^3} = \frac{210000}{1-0.33^2}\frac{4^3}{2^3} = 1.9 \text{ kN/m}$$

where

ν is the poisson coefficient related to steel, 0.33

t the thickness of the face, 4mm

n the distance of the horizontal plate to the edge of the RHS face, 2mm

The corresponding stiffness coefficient equals to 9 mm.

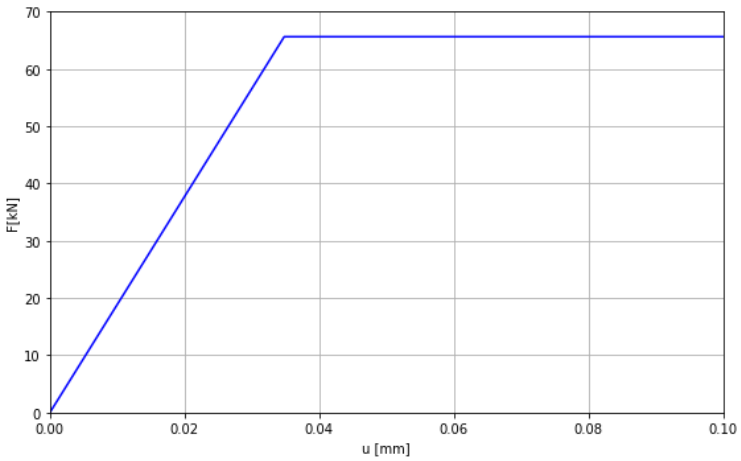

Figure 5.23: Column face stiffness N+

Column face in shear

The design resistance in shear for the two panels of the column is 72.3kN. (cfr. to section 3.4.8)

Bolts in shear - Beam web / Support web

As specified in section 3.4.9, the shear resistance of two is equal to 192 kN.

Support web in bearing

The methodology for evaluating the bearing resistance follows that described in Section 3.4.2. The edge distance in the direction of loading is $e_1 = 58.5\,\text{mm}$, and the vertical spacing between bolt rows is $p_1 = 75\,\text{mm}$. The resistance is calculated as follows:

- Material coefficient: $k_m = 1$ (Plate 3 is made of S355 steel).
- **End bolts:**

$$\alpha_{\text{b,end}} = \min\left(\frac{e_1}{d_0}, 3\cdot\frac{f_{\text{ub}}}{f_u}, 3\right) = \min\left(\frac{58.5}{22}, 3\cdot\frac{1000}{490}, 3\right) = 2.65$$

$$F_{b,Rd,\text{end}} = \frac{k_m \cdot \alpha_{\text{b,end}} \cdot f_u \cdot d \cdot t}{\gamma_{\text{M2}}}$$

$$F_{b,Rd,\text{end}} = \frac{1 \cdot 2.65 \cdot 360 \cdot 20 \cdot 6}{1.25 \cdot 1000} = 91.6\,\text{kN}$$

- **Inner bolts:**

$$\alpha_{\text{b,inner}} = \min\left(\frac{p_1}{d_0} - 0.5, 3 \cdot \frac{f_{\text{ub}}}{f_u}, 3\right) = \min\left(\frac{75}{22} - 0.5, 3 \cdot \frac{1000}{490}, 3\right) = 2.9$$

$$F_{b,Rd,\text{inner}} = \frac{k_m \cdot \alpha_{\text{b,inner}} \cdot f_u \cdot d \cdot t}{\gamma_{\text{M2}}}$$

$$F_{b,Rd,\text{inner}} = \frac{1 \cdot 2.9 \cdot 360 \cdot 20 \cdot 6}{1.25 \cdot 1000} = 100.2\,\text{kN}$$

Among the two bolts,one is classified as inner bolt and the other as end bolt (refer to Figure 5.24).

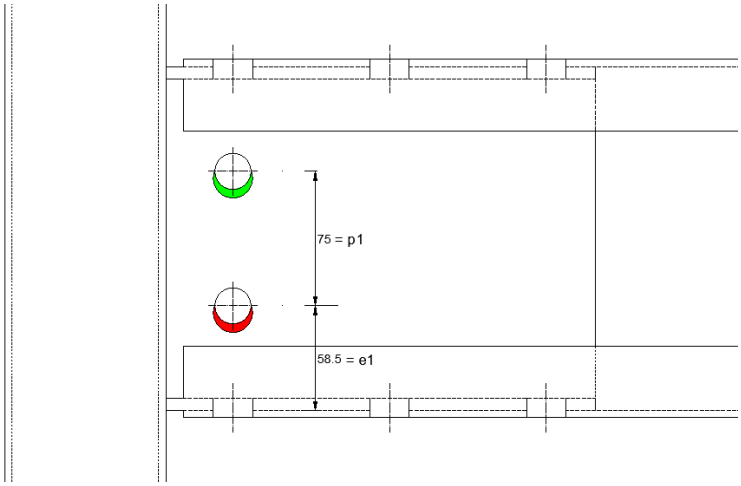

Figure 5.24: Support web in bearing : Inner bolt (in green) and End bolt (in red)

Thus, the total bearing resistance is:

$$F_{b,Rd,\text{tot}} = F_{b,Rd,\text{end}} + F_{b,Rd,\text{inner}} = 91.6 + 100.2 = 191.8\,\text{kN}$$

Beam web in bearing

The bearing resistance of the beam web is given in section 3.4.11 and is equal to 132.5 kN.

Support web in shear

The beam web resistance in shear is given by:

- At gross section:

$$V_{v,p,Rd} = \frac{A_{v,fp} \cdot f_{y,fp}}{\sqrt{3} \cdot \gamma_{M0}}$$

$$V_{v,p,Rd} = \frac{1044 \cdot 235}{\sqrt{3} \cdot 1.0 \cdot 1000} = 141.6\,\text{kN}$$

- At net section:

$$V_{v,p,Rd} = \frac{A_{v,net,fp} \cdot f_{u,fp}}{\sqrt{3} \cdot \gamma_{M0}}$$

$$V_{v,p,Rd} = \frac{780 \cdot 360}{\sqrt{3} \cdot 1.0 \cdot 1000} = 162\,\text{kN}$$

The gross section governs this component.

List of Figures

List of Tables